INVESTIGATING THE ROLE OF LEUCINE-RICH REPEAT KINASE 2 (LRRK2) IN THE INNATE IMMUNE SYSTEM

KATE HURLEY

Thesis submitted to the University of Ottawa
in partial fulfillment of the requirements for the
MSc degree in Microbiology and Immunology

Department of Biochemistry, Microbiology, and Immunology
Faculty of Medicine
University of Ottawa

PREFACE
CONTRIBUTION OF COLLABORATORS

Dr. Michael Schlossmacher's laboratory (University of Ottawa) provided the *Lrrk2*^{G2019S} and *Lrrk2*^{D1994S} mice for the experiments.

APPROVALS

The experimental protocols were approved by the University of Ottawa Animal Care Committee and include the protocols BMI-3486 and BMI-1638. A Biohazardous Materials Use Certificate was obtained from the University of Ottawa Office of Risk Management – Occupational Health and Safety.

ABSTRACT

Myeloid cells, such as monocytes and neutrophils, are generated in the bone marrow (BM) and are an important part of the innate immune system. Leucine-rich repeat kinase 2 (LRRK2) is a large, multi-domain protein that is expressed at high levels in the BM and myeloid cells. Agonistic mutations in the gene coding for LRRK2 promote better clearance of pathogens but have been identified as risk factors for inflammatory diseases, suggesting that LRRK2 may play a role in modulating the cell biology of innate immune cells. We aimed to decipher the cellular and molecular mechanisms impacted by enhanced LRRK2 kinase activity in a mouse typhoid model. Our results indicate that the agonistic *p.G2019S* mutation of *Lrrk2* results in better clearance of *Salmonella* typhimurium (ST) in the BM, in comparison to wildtype mice. We also demonstrated that the *p.G2019S* mutation promotes maintenance of BM cell numbers following infection with ST. To further determine which BM cell types were most involved in the enhanced clearance of ST, we isolated bone marrow-derived macrophages (BMDMs) and dendritic cells (BMDCs), monocytes, and neutrophils from adult mice. Following *in vitro* infection with ST, neutrophils, but not BMDMs, BMDCs, or monocytes harbouring the $Lrrk2^{G2019S}$ mutation, demonstrated a significant reduction in the bacterial burden of ST, relative to wildtype cells. Furthermore, our results indicate that neutrophils from $Lrrk2^{G2019S}$ mice demonstrate increased transcription of genes involved in the production of reactive oxygen species (ROS), along with higher levels of ROS following infection with ST, compared to wildtype neutrophils. Principally, the results of this project will provide new insights into the understanding of the impact of the agonistic $Lrrk2^{G2019S}$ mutation on the innate immune response to infection with ST.

ACKNOWLEDGEMENTS

First and foremost, I would like to thank my supervisor, Dr. Subash Sad, for providing me with the opportunity to pursue my Master's degree in his laboratory. I am sincerely grateful for his immense guidance and support throughout my research project. His invaluable advice, insight, and knowledge have greatly contributed to my research and my overall experience throughout graduate school.

I extend my gratitude to my thesis advisory committee members, Dr. Michael Schlossmacher and Dr. Lisheng Wang, for their valuable advice and support. Special thanks to the Schlossmacher laboratory for their pivotal role and assistance with my project.

A heartfelt thanks to all members of the Sad laboratory, especially Avni Bhan, Sahil Yadav, Rayan El Hamra, Willem Brandt, Osama Mahdi, Dikchha Rijal, and Ardeshir Ariana, for their readiness to help with my experiments and their unwavering support over the years. Your encouragement, discussions, and advice have truly made this journey a pleasant one.

Finally, I would like to thank my parents, siblings, and close friends. Without their continuous love, support, and encouragement, this would not have been possible.

TABLE OF CONTENTS

LIST OF ABBREVIATIONS

AIM2	absent in melanoma 2
ALR	AIM2-like receptors
APC	antigen presenting cell
ARE	antioxidant response element
ASC	apoptosis-associated speck-like protein containing a CARD
BM	bone marrow
BMDC	bone marrow-derived dendritic cell
BMDM	bone marrow-derived macrophage
CARD	caspase recruitment domain
CD	Crohn's disease
CFU	colony forming unit
CGD	chronic granulomatous disease
CLP	common lymphoid progenitor
CLR	C-type lectin receptors
CMP	common myeloid progenitor
COR	C-terminal of Roc domain
CSF	colony-stimulating factor
DC	dendritic cell
DPI	days post-infection
DUOX	dual oxidase
ELISA	enzyme-linked immunosorbent assay
GM-CSF	granulocyte-macrophage colony-stimulating factor
GMP	granulocyte-monocyte progenitor
GS	*Lrrk2*^{G2019S} mice
GWAS	genome-wide association studies
H_2DCFDA	2',7'-dichlorodihydrofluorescein diacetate
H_2O_2	hydrogen peroxide
HSC	hematopoietic stem cell
HSPC	hematopoietic stem and progenitor cells
IFN	interferon
IL	interleukin
IRF	interferon regulatory factors
IV	intravenous
Keap1	Kelch-like ECH-associated protein 1
KI	knock-in
LCN2	Lipocalin-2
LM	*Listeria monocytogenes*
LPS	lipopolysaccharide
LRRK2	leucine-rich repeat kinase 2
LSK	Lin$^-$Sca-1$^+$c-Kit$^+$ cells (hematopoietic stem and multipotent progenitor cells)
LT-HSC	long-term hematopoietic stem cell
M-CSF	macrophage colony-stimulating factor
MAPK	mitogen-activated protein kinase
MAPKKK	mitogen-activate protein kinase kinase kinase

MEP megakaryocyte-erythroid progenitor
MFI median fluorescence intensity
MHC major histocompatibility complex
MKK mitogen activated protein kinase kinase
MOI multiplicity of infection
MP myeloid progenitor
MPO myeloperoxidase
MPP multipotent progenitor
Mtb *Mycobacterium tuberculosis*
MyD88 myeloid differentiation primary response 88
NAC *N*-Acetyl-L-cysteine
NADPH nicotinamide adenine dinucleotide phsophate
NAIP NLR family of apoptosis inhibitory proteins
NET neutrophil extracellular trap
NF-κB nucleur factor kappa-B
NK cells natural killer cells
NLR NOD-like receptors
NLRC4 NLR family CARD domain containing 4 protein
NO nitric oxide
NOD nucleotide-binding and oligomerization domain
NOX NADPH oxidase
Nrf2 nuclear factor-erythroid factor 2-related factor
OD optical density
PAMP pathogen-associated molecular pattern
PBS phosphate-buffered saline
PD Parkinson's disease
PRR pattern recognition receptor
R8 RPMI with 8% Fetal Bovine Serum
RIPK7 receptor-interacting protein kinase 7
RLR retinoic acid-inducible gene-I-like receptors
RONS reactive oxygen and nitrogen species
ROS reactive oxygen species
RPMI Roswell Park Memorial Institute Medium
RT-qPCR real-time quantitative polymerase chain reaction
SCV *Salmonella*-containing vacuole
SEM standard error of mean
SOD superoxide dismutase
SPI *Salmonella* pathogenicity island
ST *Salmonella enterica* serovar Typhimurium
ST-HSC short-term hematopoietic stem cell
ST-WT SL1344 strain *Salmonella enterica* serovar Typhimurium
ST-Δ*invA* *Salmonella enterica* serovar Typhimurium strain with a mutation in the *invA* gene
T3SS type III secretion system
TGF-β transforming growth factor-beta
TLR toll-like receptor
TMB 3,3',5,5'-tetramethylbenzidine

TNF-α	tumor necrosis factor-alpha
TRIF	TIR (Toll/interleukin-1 receptor) domain-containing adaptor protein inducing interferon beta
WT	C57BL/6 mice

LIST OF FIGURES AND TABLES

1. INTRODUCTION

1.1. The immune system

The immune system is a complex network of cells, tissues, organs, and soluble mediators that function to protect the host from infectious diseases. The immune system can be divided into two primary branches: (1) the non-specific innate immune system; and (2) the specific adaptive immune system. The innate immune system is the first line of defence against pathogens, and its response will occur to the same extent regardless of the number of times the infectious agent has been encountered.[1] Meanwhile, the adaptive immune system is able to select for the most appropriate immune receptor to target the invading pathogen, and the response typically improves with repeated exposure to a given infectious agent.[1,2] It is important to note that the two branches of the immune system do not act independently. Typically, immune responses involve the activity and interplay of both systems.[3]

1.1.1. Generation of hematopoietic cells

Hematopoiesis is the term used to describe the lifelong process of continuous formation and replacement of blood cells for everyday demands.[4] Immune cells originate from a common hematopoietic progenitor in the bone marrow (BM), the hematopoietic stem cell (HSC). Long-term HSCs (LT-HSCs) produce both new stem cells, through a process called self-renewal, and mature blood cells via differentiation.[4] LT-HSCs give rise to short-term HSCs (ST-HSCs), which are still capable of multilineage differentiation, but have decreased self-renewal potential.[5] The next precursor population, multipotent progenitors (MPPs), do not have self-renewal potential, but maintain the ability to differentiate into all mature cells.[5] MPPs subsequently give rise to progenitor cells committed to either the lymphoid lineage (common lymphoid progenitors; CLPs) or the myeloid lineage (common myeloid progenitors; CMPs).[6]

CLPs do not possess any myeloid potential, but have the ability to produce all cells of the lymphoid lineage, including B cells, T cells, and natural killer (NK) cells.[5] CLPs can also give rise to dendritic cells (DCs).[7] B cell development occurs in two phases: first, an antigen-independent phase in the BM, and, second, an antigen-dependent phase in peripheral lymphoid tissue (e.g., spleen or lymph nodes).[8] T cells migrate from the BM to the thymus, where they undergo differentiation, selection, and maturation prior to migrating to peripheral lymphoid tissues as effector cells.[8] NK cell development occurs in the BM.[8]

Lymphoid cells are uniquely able to continuously recirculate between the blood and lymphatic fluid.[9] Once they encounter their specific antigen on the surface of an antigen-presenting cell (APC) in a peripheral lymphoid organ, they become retained in those organs.[9]

Similar to how mature lymphoid cells develop from CLPs, all myeloid and erythroid cells arise from CMPs. CMPs are also able to develop into more specific progenitors, including granulocyte monocyte progenitors (GMPs) and megakaryocyte erythroid progenitors (MEPs).[10] As their name implies, MEPs produce erythrocytes and megakaryocytes. GMPs give rise to granulocytes and monocytes which migrate to tissues via the blood stream.[10] Figure 1 provides an overview of the generation of myeloid cells (myelopoiesis).

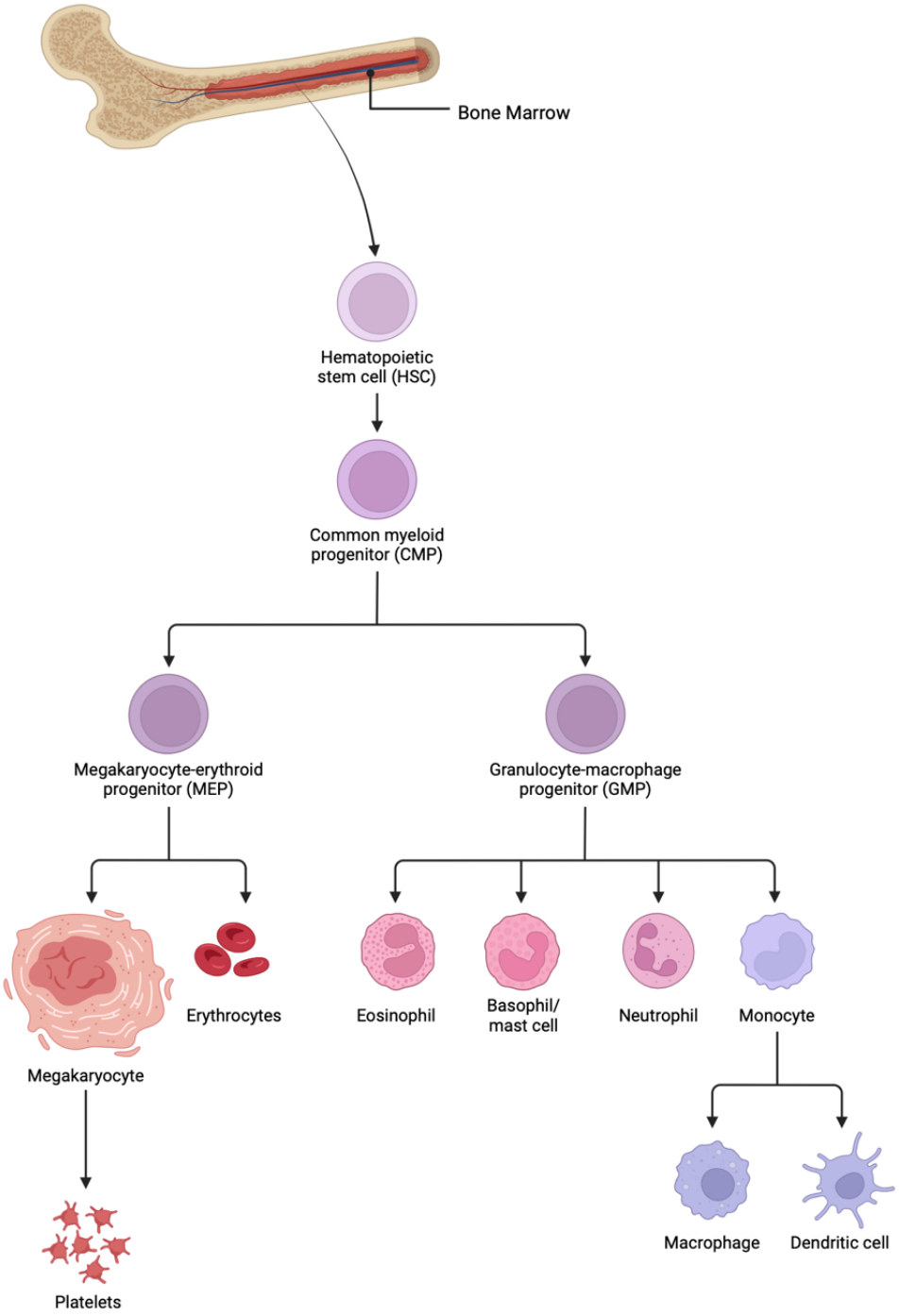
Bone Marrow
Hematopoietic stem cell (HSC)
Common myeloid progenitor (CMP)
Megakaryocyte-erythroid progenitor (MEP)
Granulocyte-macrophage progenitor (GMP)
Megakaryocyte
Erythrocytes
Eosinophil
Basophil/ mast cell
Neutrophil
Monocyte
Platelets
Macrophage
Dendritic cell

Figure 1. Diagram of key cells involved in myelopoiesis. Myelopoiesis involves a series a maturational steps leading to the formation of mature myeloid cells. Common myeloid progenitors (CMPs) give rise to granulocyte-monocyte progenitors (GMPs) and megakaryocyte-erythroid progenitors (MEPs). GMPs are responsible for producing granulocytes (eosinophils, basophils, neutrophils) and monocytes. As monocytes migrate into tissues, they can differentiate into macrophages or dendritic cells. MEPs produce megakaryocytes and erythrocytes. Created using Biorender.com.

1.1.2. Innate immune system

The innate immune system is an evolutionarily older defense system, compared to the adaptive immune system, that involves a rapid, but non-specific, response. It is composed of several types of defensive barriers, including physical and anatomical barriers, as well as effector cells, soluble mediators, and antimicrobial peptides.[3,11,12] Innate immune cells include monocytes, macrophages, DCs, granulocytes (mast cells, neutrophils, eosinophils, basophils), and NK cells. Innate immune cells are ubiquitously present in almost all tissues and will continually scan the tissue microenvironment for the presence of pathogens or infected cells. Upon pathogen recognition, tissue-resident innate immune cells will begin to produce cytokines, promoting inflammation.[12] The inflammatory response includes increased permeability of blood vessels, allowing for the recruitment and infiltration of immune cells to the infection site to aid in the elimination of pathogens.[13]

Unlike T cells and B cells in the adaptive immune system, which have high specificity, innate immune cells do not express specific antigen recognition receptors. Instead, the innate immune response relies on recognition of evolutionarily conserved structures on pathogens, called pathogen-associated molecular patterns (PAMPs).[14] PAMPs are recognized by germ-line host cell receptors, termed pattern recognition receptors (PRRs).[14] Microbial components, such as bacterial lipopolysaccharide (LPS), flagellin, and peptidoglycans are essential for survival and therefore invariant amongst various pathogens, making them excellent targets for pathogen recognition by PRRs.[15] Most PRRs in the innate immune system can be divided into five different families, based on protein domain homology: toll-like receptors (TLRs), nucleotide oligomerization domain (NOD)-like receptors (NLRs), retinoic acid-inducible gene-I-like receptors (RLRs), C-type lectin receptors (CLRs), and absent in melanoma-2 (AIM2)-like

receptors (ALRs).[15] PRRs are capable of recognizing and binding to their respective ligands, recruiting adaptor molecules, and ultimately triggering downstream signaling pathways to exert effects.[15,12] Intracellular signaling cascades activate transcription factors such as nuclear factor-κB (NF-κB) and mitogen-activated protein kinases (MAPK).[14] These transcription factors regulate the expression of genes involved in inflammation and antimicrobial host defenses, leading to the production of various molecules, including pro-inflammatory cytokines, chemokines, and immunoreceptors, orchestrating the early host response to infection.[14]

The production and release of cytokines from innate immune cells is critical for the host defence to inflammation and infection. Cytokines can act in either an autocrine manner (on the same cell) or a paracrine manner (on nearby cells), or in some instances, on distant cells (endocrine).[16] However, as cytokines have limited biological half-lives, they primarily act locally.[12] Cytokines can be functionally grouped into three main categories: growth factors, immunomodulatory cytokines, and chemokines. Colony-stimulating factors (CSF), such as granulocyte macrophage-CSF (GM-CSF) and macrophage-CSF (M-CSF), are growth factors that stimulate the proliferation of BM precursors and their differentiation into mature immune cells.[17] Chemokines, also referred to as chemotactic cytokines, are known for their ability to promote the migration of immune cells into tissues.[18] Finally, immunomodulatory cytokines can be divided as pro-inflammatory or anti-inflammatory. Pro-inflammatory cytokines, such as tumor necrosis factor-α (TNF-α), interleukin-6 (IL-6), and IL-1β, are involved in the upregulation of inflammatory reactions.[16] Meanwhile, anti-inflammatory cytokines, such as IL-10 and IL-4, act to control the activity of pro-inflammatory cytokines to regulate the immune response.[16]

In addition to production of cytokines, PRR engagement also promotes the direct elimination of pathogens through phagocytosis. One of the fastest acting mechanisms of the innate immune

system is the complement reaction. The complement system consists of a network of distinct plasma proteins that are able to react with one another to opsonize pathogens and induce an inflammatory response to help fight infection.[2] The complement system aids the immune response by improving uptake of pathogens by phagocytes, recruiting phagocytes to sites of infection, and improving the destruction of pathogens.[2,19] Phagocytosis is a form of endocytosis, in which a large particle (> 0.5 μm) is engulfed into a plasma membrane derived vesicle, known as the phagosome.[20] Opsonic receptors, such as Fc receptors and complement receptors, bind to host-derived opsonins, initiating signaling cascades that remodel the cell membrane to allow for ingestion.[20] After internalization, the phagosome undergoes maturation, and will eventually fuse with lysosomes to form the phagolysosome, a vesicle that can destroy the ingested particle.[20] Phagolysosomes are highly acidic and contain several hydrolytic enzymes and other microbicidal components, such as reactive oxygen species (ROS).[20]

During acute infectious and inflammatory conditions, a large number of myeloid cells, especially neutrophils, are consumed in peripheral organs, resulting in a high demand to continuously replenish them. Fortunately, pathogens can be sensed by PRRs expressed on hematopoietic stem and progenitor cells (HSPCs), resulting in the activation of downstream signaling cascades, and inducing a process known as emergency hematopoiesis (sometimes referred to as emergency granulopoiesis).[21] Through this process, dormant HSPCs proliferate and differentiate, replenishing the short-lived mature hematopoietic cells that were consumed during the immune response.[21,22] Unfortunately, emergency hematopoiesis can result in HSC exhaustion and eventual hematopoietic failure due to the stress placed on these cells during the process.[21]

1.1.3. Monocytes

Monocytes are circulating leukocytes that are capable of further differentiating into tissue macrophages and DCs. There are two main types of monocytes: (1) classical/inflammatory monocytes; and (2) non-classical/patrolling monocytes.[23,24] In mice, inflammatory monocytes have a high expression of Ly-6C (Ly-6C^{hi} monocytes), while patrolling monocytes have a relatively low expression of Ly-6C (Ly-6C^{low} monocytes).[24] Patrolling monocytes are less prevalent than inflammatory monocytes.[24]

Beyond replenishing macrophages and DCs, monocytes also employ their antimicrobial activity at sites of inflection.[24] The effector functions of inflammatory monocytes are dependent on the inflammatory context and the nature of the invading pathogen. Common functions of monocytes in response to inflammation or infection include chemokine and cytokine release (often TNF) and the production of nitric oxide (NO).[24,25] Some argue that monocytes are also capable of trafficking to draining lymph nodes, where they can present antigens to T cells and contribute to the activation of the adaptive immune system.[26]

1.1.4. Macrophages

As their name implies, macrophages are large in size and capable of engulfing their targets through phagocytosis. In addition to phagocytosing foreign pathogens, macrophages are also responsible for phagocytosing dying or dead cells and cellular debris.[27] Like dendritic cells, which are discussed in more detail in Section 1.1.5., macrophages act as a connection between innate and adaptive immune cells. After phagocytosis, the macrophage will degrade the pathogen by degradative enzymes and present pathogen-derived antigens to helper T cells, initiating the adaptive immune system.[28]

Macrophages can be of different origin (blood monocyte versus tissue) and exhibit different phenotypes. While macrophages were originally believed to derive solely from circulating monocytes, later studies demonstrated that most adult tissue-resident macrophages are seeded before birth, have self-renewal capacity, and are maintained independently of monocytes.[29–31] Tissue-resident macrophages are typically highly-specialized cells that perform specific functions for their tissue of residence.[32] Meanwhile, blood monocyte-derived macrophages will traffic into tissues in response to inflammatory and chemokine cues.[32] Tissue-resident macrophages are divided based on their anatomical location and functional phenotype, such as microglia in the central nervous system (CNS), alveolar macrophages in the lung, and osteoclasts in the bone.[33]

In addition to the separation between tissue resident and blood-derived macrophages, macrophages are also commonly divided based on their phenotype. Macrophages are highly plastic cells, meaning that they are capable of switching from one phenotype to another under different circumstances.[33] The M1-M2 dichotomy is the most common way to define macrophage phenotypes; however, it is important to note that this model simplifies the complexity of phenotypical diversity amongst macrophages.[34] A very basic view classifies M1 macrophages as proinflammatory and M2 macrophages as anti-inflammatory. M1 macrophages are believed to participate in the first line of defence against intracellular pathogens and promote the polarization of Type 1 helper T cells.[35] M1 macrophages are thought to develop in an inflammatory environment, often in response to TLR and interferon (IFN) signaling.[35] M1 macrophages play a key role in the acute inflammatory response by demonstrating high levels of phagocytosis and producing several pro-inflammatory cytokines and chemokines (e.g., IL-6, IL-12, IL-1β, TNF-α, etc.), as well as reactive oxygen and nitrogen species (RONS) to protect

against bacteria and viruses.[35] Meanwhile, M2-like macrophages are primarily involved in the anti-inflammatory response and repair of damaged tissues.[36] Most tissue resident macrophages are described as being similar to M2 macrophages.[29] M2 macrophages negatively regulate pro-inflammatory cytokines and induce production of anti-inflammatory mediators, such as IL-4, IL-10, and transforming growth factor-beta (TGF-β).[35] They are also highly endocytic, and partially phagocytic, and are involved in many important functions, such as tissue repair, apoptotic cell clearing, and angiogenesis.[35]

1.1.5. Dendritic cells (DCs)

DCs are APCs that are responsible for capturing, processing, and presenting antigens to lymphocytes, an important mechanism for initiating and regulating the adaptive immune system.[37] Immature DCs can take up antigens via phagocytosis, receptor-mediated endocytosis, or macropinocytosis.[38] Recognition of a danger signal triggers the differentiation and activation of immature DCs to mature DCs.[39] DC activation and maturation initially results in a transient increase in their ability to take up antigens as well as changes in expression of homing and chemokine receptors that are important for directing migration of DCs to lymphoid tissue.[39] After internalization, antigens are digested into peptides, which associate with major histocompatibility complex class II (MHC II) molecules.[38] Peptide-loaded MHC II molecules are then delivered to the cell surface to allow for antigen presentation.[38] Mature DCs will also begin to express T cell co-stimulatory molecules, such as cluster of differentiation 40 (CD40) and B7.[40] As DCs enter secondary lymphoid organs, pathogen-derived antigens are presented to T cells, promoting the differentiation of naïve T cells into mature T cell types.[39,40] The internalization of antigens will eventually be downregulated in mature DCs, allowing for specific T cell stimulation to the antigens encountered in the periphery (where the DCs were immature).[38] Additionally, activated

DCs have been shown to secrete various chemokines and inflammatory cytokines, further aiding in their response to infection and/or inflammation.[39]

1.1.6. Neutrophils

Neutrophils are the most abundant leukocyte in human blood, and are produced in large numbers in the BM.[41] Once produced, neutrophils have a short lifespan (12-24 hours), and will quickly enter circulation and migrate to tissues.[41,42] Eventually, they are eliminated by macrophages.[41,42] During the development of inflammatory reactions, neutrophils become activated, and their lifespan is extended.[43] Neutrophils are constantly patrolling for signs of microbial infections and are endowed with many effector functions to aid in the innate immune response. These effector functions include phagocytosis, the release of ROS, degranulation, and the formation of neutrophil extracellular traps (NETs), which will be discussed in more detail below.

A unique feature of neutrophils is that their phagocytic receptor signalling also rapidly employs both oxidative and non-oxidative host defense mechanisms via simultaneous assembly and activation of the Nox2-containing nicotinamide adenine dinucleotide phosphate (NADPH) oxidase complex and mobilization of granules.[44] The speed and efficiency of this process creates a highly lethal environment in the phagosome, allowing neutrophils to kill the majority of ingested pathogens within 30 minutes.[45]

Granules are intracellular vesicles formed during neutrophil differentiation that contain an assortment of antimicrobial proteases, and can be divided into four main types: secretory, specific, gelatinase, and azurophil.[45,46] Each granule type is grouped based on the specific proteins that they contain. Secretory granules are released readily throughout the life span of the neutrophil, as they contain plasma proteins and several cell surface receptors that integrate into

the plasma membrane of neutrophils as exocytosis takes place.[45,46] Specific granules contain the antibacterial proteins lactoferrin, neutrophil gelatinase-associated lipocalin, cathelicidin, collagenase, and lysozyme.[46] Meanwhile, gelatinase granules primarily contain matrix metalloproteinase 9 (MMP9), lysozyme, and leukolysin.[46] Azurophil granules contain the most pro-inflammatory and antimicrobial proteins and their degranulation occurs during the late stage of neutrophil activation.[45,46] Azurophil granules contain proteins such as myeloperoxidase (MPO), defensins, cathepsins, neutrophil elastase, and azurocidin.[45] Although the antimicrobial peptides contained within granules are critical for killing bacteria, this process must be tightly regulated, as excessive degranulation can damage the host tissue.[45]

In addition to degranulation, NADPH oxidase also plays a critical role in microbial killing. In fact, dysfunction of NADPH oxidase is known to cause a condition called chronic granulomatous disease (CGD), characterized by recurrent life-threatening infections, due to an inability of phagocytes to appropriately destroy microbes.[47] NADPH oxidase consists of a core component, referred to as flavocytochrome b_{558}, which is a heterodimer composed of one molecule of $p22^{phox}$ (*Cyba*), and one molecule of $gp91^{phox}$ (*Cybb*).[48] In order for electron transport to occur through the flavocytochrome, it must be activated by a number of cytosolic proteins, which change the conformation of the flavocytochrome. One of the cytosolic subunits, $p67^{phox}$, attaches directly to the flavocytochrome.[48] At high concentrations and in combination with a Rac, $p67^{phox}$ is sufficient to induce electron transport.[48] The protein $p40^{phox}$ binds to $p67^{phox}$, and is thought to act as a shuttle, aiding in the translocation of $p67^{phox}$ to the core component of NADPH oxidase.[48] Meanwhile, $p47^{phox}$ is heavily phosphorylated during neutrophil activation and is thought to stabilize the interaction between the core component and $p67^{phox}$.[48] After neutrophil activation, such as in response to microbial infections, $p67^{phox}$, $p40^{phox}$, and $p47^{phox}$ all work together to

facilitate the activation of NADPH oxidase. Figure 2 provides an overview of the NADPH oxidase structure in a resting and activated state.[49]

The activity of NADPH oxidase is essential for effective microbial killing through its production of oxygen radicals and their reactive products, collectively referred to as ROS.[48] The direct product of NADPH oxidase activity is superoxide anion (O_2^-), which is produced in large amounts in neutrophils, and directly pumped into the phagocytic vacuole.[48] O_2^- will then undergo spontaneous or enzymatic dismutation to hydrogen peroxide (H_2O_2).[50] Through the Fenton reaction, H_2O_2 can oxidize ferrous iron to generate the highly reactive hydroxyl radical OH·.[50] Furthermore, during oxidative burst in neutrophils, the granule-associated enzyme MPO will convert H_2O_2 to the highly bactericidal hypochlorous acid (HOCl).[50] These oxygen derivates can restrict bacterial growth by damaging their DNA, protein, and lipid molecules.[50]

Finally, in response to pathogens, neutrophils will also release NETs, through a process known as NETosis. NETs are extracellular web-like structures composed of DNA-histone complexes and a number of different neutrophil granule proteins, such as elastase, MPO, and cathepsins.[51] NETs function to trap microbes, preventing them from spreading, while also ensuring a high concentration of antimicrobial peptides within the NET to kill the microbes.[51]

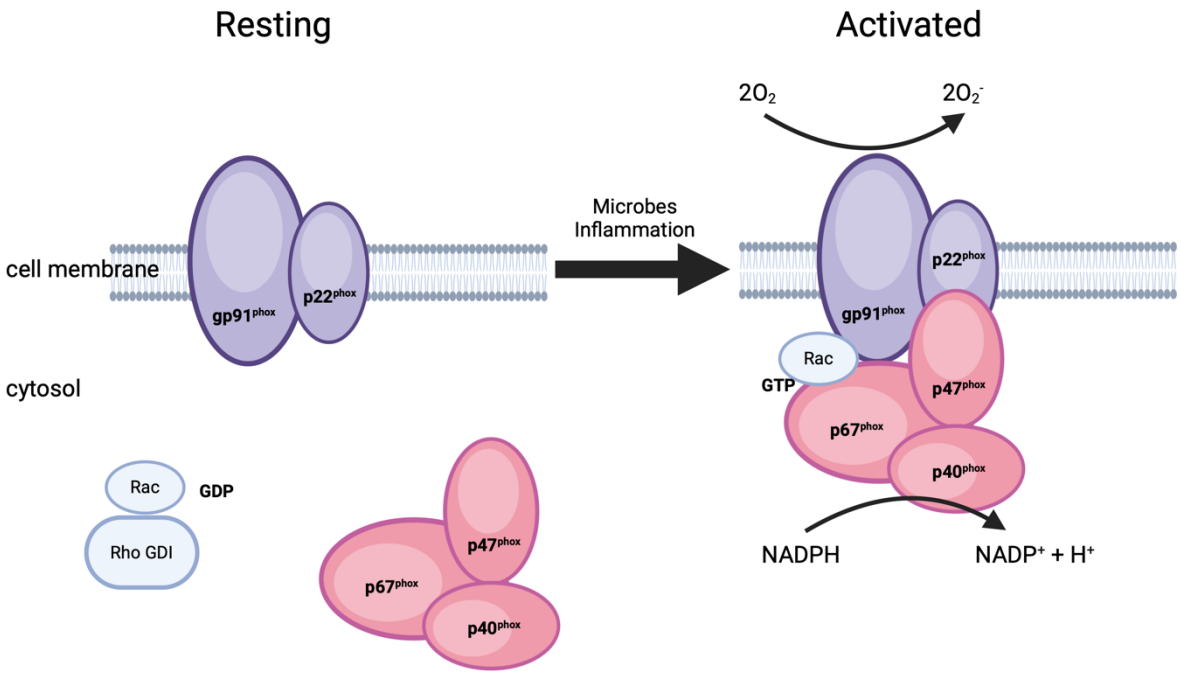
Resting
Activated
$2O_2$
$2O_2^-$
Microbes
Inflammation
cell membrane
cytosol
gp91phox
p22phox
Rac
GDP
Rho GDI
p47phox
p67phox
p40phox
GTP
NADPH
NADP+ + H+

Figure 2. Schematic representation of NADPH oxidase in a resting and activated state. The catalytic subunit, gp91^{phox}, along with p22^{phox}, form the core component (flavocytochrome b_{558}). The three components, p47^{phox}, p67^{phox}, and p40^{phox} form a cytosolic complex in a resting cell, but upon activation, will translocate to the core component in the membrane. The G-protein Rac, when bound to GDP, is found in the cytosol in the resting state, and will also translocate to the membrane component upon activation. Upon assembly, the NADPH oxidase enzyme generates superoxide anion (O_2^-) by transferring electrons from cytoplasmic NADPH and donating them to molecular oxygen (O_2). Created using Biorender.com

1.2. *Salmonella* typhimurium (ST)

Salmonella enterica (*S. enterica*) is a Gram-negative, facultative intracellular anaerobe, capable of infecting both humans and animals. *S. enterica* causes different types of disease in different species, including typhoid fever. *S. enterica* can be divided into six different subspecies, which are then further divided into over 2,500 serovars, differentiated based on their flagellar, carbohydrate, and LPS structures.[52] Non-typhoidal serovars (which do not cause typhoid fever), such as *Salmonella enterica* serovar Enteritidis and *Salmonella enterica* serovar Typhimurium (ST), are capable of infecting a broad range of hosts including humans, cattle, poultry, and swine.[52] Interestingly, ST causes an acute self-limiting gastroenteritis in humans, but a systemic disease resembling typhoid fever in mice.[53] Meanwhile, *Salmonella* serovars Typhi and Paratyphi are only capable of infecting humans, and cause systemic typhoid or enteric fever.[52]

As infection with ST in mice leads to typhoid-like fever, this model is frequently used to study human typhoidal infection. However, it is important to note that there are limitations with this model. First, as ST causes enteritis, rather than typhoid fever, in humans, the host responses to ST are likely quite different.[54] Second, genes associated with serotype Typhi that are required for causing typhoid fever in humans are not present or are altered in ST, making it difficult to study their role and impact during infection.[54] Nevertheless, several strengths of this mouse model outweigh its limitations. ST-infected mice have been critical for identifying and establishing the role of different virulence mechanisms of serotype Typhimurium, such as *Salmonella* pathogenicity islands (SPI) 1 and 2.[54] This mouse model has also been successfully used to identify and test various typhoid fever vaccine candidates, further highlighting the usefulness of ST infection in mice to better understand the pathogenesis of typhoid fever.[54]

1.2.1. ST mechanism of infection

Salmonella infections are typically acquired through contaminated food. They are one of the most common causes of food-borne illness in both developed and developing countries.[55] Since *Salmonella* is often ingested, the first obstacle ST must overcome is the acidic pH in the stomach of the host. Fortunately for ST, it is able to protect itself against acid shock via the acid tolerance response, which allows ST to maintain the intracellular pH at values higher than those in the extracellular environment.[56] Once past the stomach and in the small intestine, ST must traverse the intestinal mucosal layer prior to adhering to intestinal epithelial cells.[55] In mice, ST appears to preferentially adhere to M cells of the Peyer's patches in the intestinal epithelium, resulting in the formation of membrane ruffles that further engulf adherent bacteria in large vesicles called *Salmonella*-containing vacuoles (SCVs).[55] SCVs are unique membrane-bound compartments, distinct from a phagosome or lysosome. They are the only intracellular compartment in which *Salmonella* can survive and replicate.[57] Meanwhile, the secretion of small chemo-attractant proteins, such as IL-8, in the intestinal epithelium is induced.[58] The release of chemo-attractant proteins initiates the recruitment and migration of phagocytes into the lumen.[58] Once across the epithelium, *Salmonella* is engulfed by resident macrophages.[59] Macrophage death, and the escape of bacteria from the intracellular environment, can result in further systemic infection (as the bacteria can enter the bloodstream).[59] Once in circulation, the bacteria are opsonized by complement factors, allowing for quick cellular uptake, typically in the liver, spleen, or BM.[59]

ST pathogenesis relies on the ability of the bacteria to invade and replicate within host cells. As previously mentioned, following invasion into cells, ST resides within the SCV. In order to create and maintain the SCV, ST uses specialized secretion systems that are capable of modifying host cell function by injecting a number of effector proteins into the cytoplasm of the host cell.[60]

These effector proteins can alter basic host cell functions, such as membrane trafficking, signal transduction, and cytokine gene expression.[58] ST employs two different type III secretion systems (T3SSs), which are encoded by *Salmonella* pathogenicity islands 1 (T3SS1) and 2 (T3SS2). The two secretion systems have different functions – T3SS1 is required for the invasion of non-phagocytic cells, while T3SS2 is involved in intracellular survival and biogenesis of the SCV.[61]

1.2.2. Host response to ST

Salmonella, though residing within the SCV, is not entirely shielded from the surveillance of the host immune system. Internalized ST introduces various PAMPs, such as LPS, flagella, and bacterial DNA, which can be detected by PRRs expressed by immune cells.[53] TLRs are the first PRRs to recognize infection with ST, with various isoforms distributed on the outer membrane of the cell or within intracellular vesicles.[53] Upon encountering PAMPs, TLRs engage signaling adaptors, including MyD88 (myeloid differentiation primary response 88) and TRIF [TIR (Toll/interleukin-1 receptor) domain-containing adaptor protein inducing interferon beta], initiating a cascade of events that activate transcription factors, such as NF-κB and interferon regulatory factor 3 (IRF3).[53] This activation ultimately leads to the production of pro-IL-1β (among other inflammatory cytokines) and a type I IFN response that is crucial for orchestrating the host defense against *Salmonella* infection.[53]

Additionally, once *Salmonella* is contained in the SCV, NLRs can sense PAMPs within the cytosol. A subfamily of cytosolic PRRs, known as NAIPs (the NLR family apoptosis inhibitory proteins), recognize components of the SPI-1 T3SS and flagellin, which recruit NLRC4 (nucleotide-binding domain, leucine rich repeat-containing family, and CARD (caspase recruitment domain)-containing protein 4) to form multimeric signaling complexes called

inflammasomes.[62] This complex formation typically requires an adaptor protein, ASC (an apoptosis-associated speck-like protein with a CARD), which recruits pro-Caspase-1, a protease crucial for cytokine maturation.[53] Activated Caspase-1 cleaves pro-IL-1β and pro-IL-18 into their mature forms, as well as the pore-forming protein gasdermin-D (GSDMD).[53,62] Cleaved GSDMD creates pores in the plasma membrane of host cells, releasing pro-inflammatory cytokines and inducing an inflammatory form of cell death known as pyroptosis, effectively eliminating the infected cell.[62]

1.3. Leucine rich repeat kinase 2 (LRRK2)

The *Lrrk2* gene is found in the *Park8* locus on chromosome 12q12 in humans and on chromosome 15 in mice.[63,64] The murine homolog of *Lrrk2* is up to 88% identical to human *Lrrk2*, showing conservation of disease-causing residues.[65] It is therefore appropriate to examine murine models of *Lrrk2* mutations. *Lrrk2* encodes a large, 286-kDa protein, called LRRK2 or receptor-interacting protein kinase 7 (RIPK7), that contains several functional domains.[66] The central core includes a Roc (Ras of Complex proteins) domain which encodes a GTPase, a COR (C-terminal of Roc domain), and a serine/threonine kinase domain, all surrounded by multiple protein-protein interaction domains.[64,67–69] The N-terminus harbours the armadillo, ankyrin, and leucine-rich repeat region, while the C-terminus contains the WD40 domain, which is crucial for protein folding.[69,70] Structural studies and cell-based assays indicate that the biochemical activity of LRRK2 is orchestrated through a complex interplay between the scaffolding and enzymatic domains of the protein.[66] With the diverse enzymatic and protein-interacting domains of LRRK2, it is likely that LRRK2 is involved in many different cellular pathways and interacts with several different binding partners.[71]

1.3.1. LRRK2 tissue distribution

LRRK2 is expressed at low levels throughout the body, with highest levels in the kidney, lung, and BM.[63,72] Several studies also point to the high expression of LRRK2 in immune cells, such as neutrophils, monocytes, macrophages, microglia, and B lymphocytes.[72–74] LRRK2 protein expression has also been confirmed in BMDMs.[73] Hakimi et al. further observed a significant upregulation in *Lrrk2* mRNA in BMDMs following exposure to microbial structures, such as bacterial LPS and lentiviral particles.[73]

1.3.2. LRRK2 and inflammatory conditions

The *Lrrk2* gene has been linked to disease susceptibility in several inflammatory disorders. Familial and genome wide association studies (GWAS) implicated LRRK2 in the susceptibility to Parkinson's disease (PD), Crohn's disease (CD), and leprosy.[75–77]

PD is a progressive, late-onset disorder of the nervous system, and aberrant functioning of the immune system has been proposed as a component of susceptibility to and progression of PD.[78] Mutations in *Lrrk2* are the most common known cause of autosomal-dominant PD.[79] Many variants of the *Lrrk2* gene have been described; however, only six are considered pathogenic: *p.N1437H, p.R1441C, p.R1441G, p.Y1699C, p.G2019S,* and *p.I2020T.*[67,79,80] Of these mutations, the *p.G2019S* mutation is the most common PD-associated *Lrrk2* mutation, accounting for approximately 1% of all sporadic cases and 4-5% of familial PD cases.[81] The $Lrrk2^{G2019S}$ mutation affects the kinase domain of LRRK2, and has been demonstrated to result in a hyperactive kinase, increasing autophosphorylation and phosphorylation of other substrates.[80]

CD is a chronic inflammatory bowel disease, characterized by inflammation of the gastrointestinal tract, and is thought to result from a dysregulated immune response to

commensal intestinal microbiota.[82] The involvement of the *Lrrk2* locus in CD was first suggested by a meta-GWAS in 2008, and later confirmed by other meta-GWAS.[77,83]

Leprosy is a chronic dermato-neurological infectious disease caused by *Mycobacterium leprae.*[76] In 2009, Zhang et al. identified a trend toward the presence of leprosy and a single-nucleotide polymorphism (SNP) in *Lrrk2.*[84] Later studies revealed a significant association of *Lrrk2* with Type-1 reactions, which are the main contributors to nerve damage in leprosy.[76,85]

The association of *Lrrk2* with various immune and inflammatory conditions suggest its involvement in the immune system. However, the precise mechanisms by which distinct *Lrrk2* mutations mediate their pathogenicity remain unclear and require further investigation.

1.3.3. LRRK2 and bacterial infections

The role of LRRK2 in bacterial infections is not clear, with some studies showing a protective role, while others suggesting a potential detrimental effect of LRRK2. With respect to *Salmonella* infection, Gardet et al. successfully showed that LRRK2 contributes to the restriction of *Salmonella* in macrophages *in vitro*, with LRRK2 knock-down cells showing greater bacterial burden following infection with ST.[74] Other studies have also shown that *Lrrk2*$^{-/-}$ mice exhibited impaired clearance of ST, while mice harbouring the hyperactive *Lrrk2*^{G2019S} mutation showed enhanced resistance to ST following *in vivo* infection.[72,86] Similarly, *Lrrk2*$^{-/-}$ mice showed increased susceptibility to oral infection with *Listeria monocytogenes* (LM), a facultative, Gram-positive and intracellular bacterium.[87]

In contrast to ST and LM infection, inhibition of LRRK2 kinase activity has been shown to enhance restriction of *Mycobacterium tuberculosis* (Mtb), an intracellular pathogen, by human and mouse macrophages.[88] Furthermore, *Lrrk2*$^{-/-}$ mice showed an early protective effect against aerosol Mtb infection, while *Lrrk2*^{G2019S} mice showed significantly higher bacterial burdens.[88,89]

Together, these findings point to the importance of LRRK2 in exerting pleiotropic effects on bacterial control and inflammation through mechanisms that appear to depend on the type of bacterial infection and host susceptibility.

1.4. Rationale

Various *Lrrk2* mutations are associated with different inflammatory diseases such as PD, CD and leprosy.[75–77] Previous studies have shown that LRRK2 is highly expressed in immune-related tissues, such as the BM, and various myeloid cells, including neutrophils, monocytes, and macrophages.[72,73] Increased LRRK2 expression has also been observed in response to bacterial components in murine BMDMs.[73] Therefore, LRRK2 likely has a function in the innate immune system.

Previous work from Shutinoski et al. has demonstrated that *Lrrk2* deficiency in female mice led to relatively higher ST bacterial burden and reduced survival.[72] Conversely, female mice harbouring the *Lrrk2*^{G2019S} mutation controlled infection with ST better, and displayed enhanced survival, suggesting that the agonistic *Lrrk2*^{G2019S} mutation results in an enhanced inflammatory response to infection with ST.[72] It was further shown that the *p.G2019S* mutation and loss of function effect conferred by *Lrrk2* KO was mediated by myeloid cells, which are critical players in the innate immune system.[72]

1.5. Hypothesis

Lrrk2^{G2019S} mutation modulates the expansion and function of myeloid cells which confers better control of ST infection in mice.

1.6. Objectives

Aim 1. Evaluate the impact of *Lrrk2*^{G2019S} mutation on the BM compartment following infection with ST.

Aim 2. Determine whether the *Lrrk2*^{G2019S}-mediated protection from ST infection is due to an enhanced inflammatory response and/or an improved intrinsic ability of myeloid cells to fight infection.

Aim 3. Investigate the molecular mechanisms contributing to the reduced bacterial burden in *Lrrk2*^{G2019S} myeloid cells.

2. MATERIALS AND METHODS

2.1. Animal strains

All mice used were housed at the University of Ottawa's animal facility under specific pathogen-free conditions and maintained in accordance with the Canadian Council on Animal Care (CCAC) guidelines. Protocols and procedures were monitored by the University of Ottawa Animal Care Committee and Ethics Board. All mice used were females and were age-matched for experiments.

C57BL/6 mice were obtained from Jackson Laboratories and were bred and maintained in our facility. *Lrrk2*^{G2019S} knock-in mice were originally generated by Novartis Pharmaceuticals and were obtained from Dr. Schlossmacher. *Lrrk2*^{G2019S} mice were maintained in our facility and bred as homozygous mouse lines. *Lrrk2*^{D1994S} mice were a kind gift from Dr. Schlossmacher and were bred and maintained by the Schlossmacher lab.

2.2. Bacterial strains

Three bacterial strains were used for experiments:

1. SL1344 strain *Salmonella enterica* serovar Typhimuirum (ST-WT)
2. ST strain with a mutation in the *invA* gene (ST-Δ*invA*), which codes for an inner membrane component of the SPI-1 T3SS. Therefore, no myeloid cell death will occur with ST-Δ*invA,* but as the SPI-2 T3SS remains intact, intracellular replication is not affected.
3. 021915 strain of *Listeria monocytogenes* (LM)

2.3. *In vivo* infection model

Animals were infected by intravenous (IV) tail vein injections. ST-WT bacteria were re-suspended at 2 x 10^3 CFU/mL in cold phosphate-buffered saline (PBS) and 100 µL were injected

into each mouse. Mice were sacrificed five days after infection. The bacterial burden in the BM and spleens was assessed upon euthanasia. To collect BM cells, hind limbs were excised and placed in R8 medium [RPMI-1640 (Gibco, #31800-089) supplemented with 8% fetal bovine serum (FBS; Gibco, #12483-020) and 55 µM 2-mercaptoethanol (Gibco, #21985-023)]. Bones were then flushed using a 26-gauge needle (BD, #309625) through a 100 µm cell strainer. The resulting single cell suspension was centrifuged at 1500 rpm for 7 minutes and resuspended in R8 medium for a final concentration of 10^7 cells/mL. Cells were counted manually on a haemocytometer using 3% Acetic Acid with methylene blue (StemCell Technologies, #07060). Methylene blue selectively stains nucleated cells, and thus will not count red blood cells. Whole spleens were homogenized using frosted glass slides (Fisherbrand, #22-034-486) and filtered through a 70 µm cell strainer. The resulting single-cell suspension was centrifuged at 500 x *g* for 5 minutes and resuspended in 10 mL R8 medium. Ten-fold serial dilutions of the BM and spleen cell suspensions were made, and 100 µL aliquots were plated onto LB-agar plates (LB Broth: Fisher BioReagents, #BP1426; Difco Agar: BD, #214010) containing 50 µg/mL streptomycin (Sigma-Aldrich, #S6501). Plates were incubated at 37˚C overnight and colony-forming units (CFU) were then counted.

2.4. Flow cytometry

Uninfected and infected mouse BM immune cells were analyzed by flow cytometry. BM cells were prepared as described above. Up to 6 x 10^6 cells were transferred to 5 mL tubes (Falcon, #352052) and washed with PBS. To assess cell death, Zombie Yellow™ (BioLegend, #423104) was used (an amine-reactive fluorescent dye that can pass through cells with damaged membranes). Zombie Yellow dye was diluted (1:100 in PBS) and 100 µL was added to each tube. The tubes were incubated for 15 minutes at room temperature, protected from light, prior to

proceeding to surface staining. To prevent non-specific binding of antibodies, FcBlock (anti-CD16/32) (BD BioSciences, #553142) was added to the cells in PBS followed by a 5-minute incubation period at 4°C. Then, fluorophore-conjugated antibodies against various cell surface receptors were added. Cells were protected from light and incubated for 30 minutes at 4°C. A list of antibodies used can be found in Table 1.

Table 1. Flow cytometry staining antibodies

Antibody	Conjugated Fluorophore	Source	Catalog Number
Lin*	FITC	eBioscience	22-7770-72
c-Kit	Pe-Cy7	eBioscience	25-1171-82
Sca-1	APC	BioLegend	122511
	PerCp-Cy5.5	eBioscience	45-5981-80
CD16/32	PE	eBioscience	12-0161-82
	PerCP-Cy5.5	BioLegend	156623
CD34	eFluor450	eBioscience	48-0341-80
CD11b	APC	BioLegend	101212
	Pe-Cy7	BioLegend	101215
CD11c	FITC	BioLegend	117305
MHC-II	APC	eBioscience	17-5321-81
Ly-6C	PE	BioLegend	128008
	PerCp-Cy5.5	eBioscience	45-5932-82
Ly-6G	FITC	Proteintech	FITC-65078
	eF450	eBioscience	48-9668-82
	PE	BioLegend	127067
LRRK2	AlexaFluor594	Novus Biologicals	NB300-268AF594

*Lin cocktail contains antibodies against the following markers: CD3, CD45R, CD11b, Ter-119, Ly-6G

Cells were washed with PBS to remove excess unbound antibodies and resuspended in PBS. Cells were acquired the same day as staining on the flow cytometer (BD LSRFortessa or BD Celesta). Data was analyzed using FlowJo software.

For LRRK2 staining, cells were first stained with cell surface markers (as described above). To allow for intracellular staining of LRRK2, cells were fixed and permeabilized using an Intracellular Fixation & Permeabilization Buffer Set (eBioscience, #88-8824-00), according to

the manufacturer's protocol. For the protocol, cells were stained with the LRRK2 antibody for 30 minutes at room temperature, protected from light.

2.5. Generation of bone marrow-derived macrophages (BMDMs)

BM progenitors harvested from the hip, tibia, and femur of representative mouse strains were extracted and flushed as described above. 100 mm plastic petri dishes were coated with 50 ng of M-CSF (BioLegend, #576404). Thirteen to fifteen million BM cells were resuspended in 10 mL R8 medium (containing 50 μg/mL gentamicin (Gibco, #15750-060) and added to each petri dish. Cells were incubated at 37˚C for 6-8 days to allow macrophage differentiation to occur.

For seeding, cells were rinsed with PBS, and then incubated in PBS for five minutes at 37˚C. Cells were gently scraped with a cell scraper and collected. Cells were resuspended in R8 medium and seeded at 10^5 cells/well in 96 well plates or 3 x10^5 cells/well in 24 well plates.

2.6.Purification of monocytes

BM cells were harvested in a similar manner as described previously. EasySep Mouse Monocyte Isolation Kit (StemCell Technologies, #19861A) was used to purify and isolate monocytes. The purity of monocytes was confirmed by flow cytometry ($CD11b^+Ly\text{-}6C^+Ly\text{-}6G^-$) (Figure 3A). Monocytes were seeded at 10^5 cells/well in 96 well plates, and 4 x 10^5 cells/well in 24 well plates.

2.7. Purification of neutrophils

BM cells were harvested in a similar manner as described previously. EasySep Mouse Neutrophil Enrichment Kit (StemCell Technologies, #19762A) was used to enrich the neutrophil population. To obtain higher purity, cells were sorted with the Sony SH800 Cell Sorter using a 100 μM sorting chip. Cells were sorted as $Ly\text{-}6G^+$ and stained as described previously. WT and *Lrrk2*^{G2019S} cells were sorted at the same time, after being stained individually with Ly-6G

antibodies conjugated to different fluorophores. After sorting, cells were immediately resuspended in R8 medium to maintain cell viability. Neutrophils were plated at 10^5 cells/well in 96 well plates, and 4 x 10^5 cells/well in 24 well plates. Purity of isolated neutrophils was assessed via flow cytometry (Figure 3B).

2.8. Generation of bone marrow-derived dendritic cells (BMDCs)

BM progenitors were extracted and flushed as described above. BM progenitors were cultured at a concentration of 1 million cells/mL in 10 mL R8 medium in the presence of 10 ng/mL GM-CSF (StemCell Technologies, #78017) in T25 flasks at 37˚C. The media was replaced on day 2, 4, and 6 to remove any floating cells. By day 8, GM-CSF DCs differentiate from adherent cells and become floating cells that can be collected from the supernatant. BMDCs generated *in vitro* using GM-CSF mimic monocyte DCs, and purity was assessed via flow cytometry (Figure 3C).

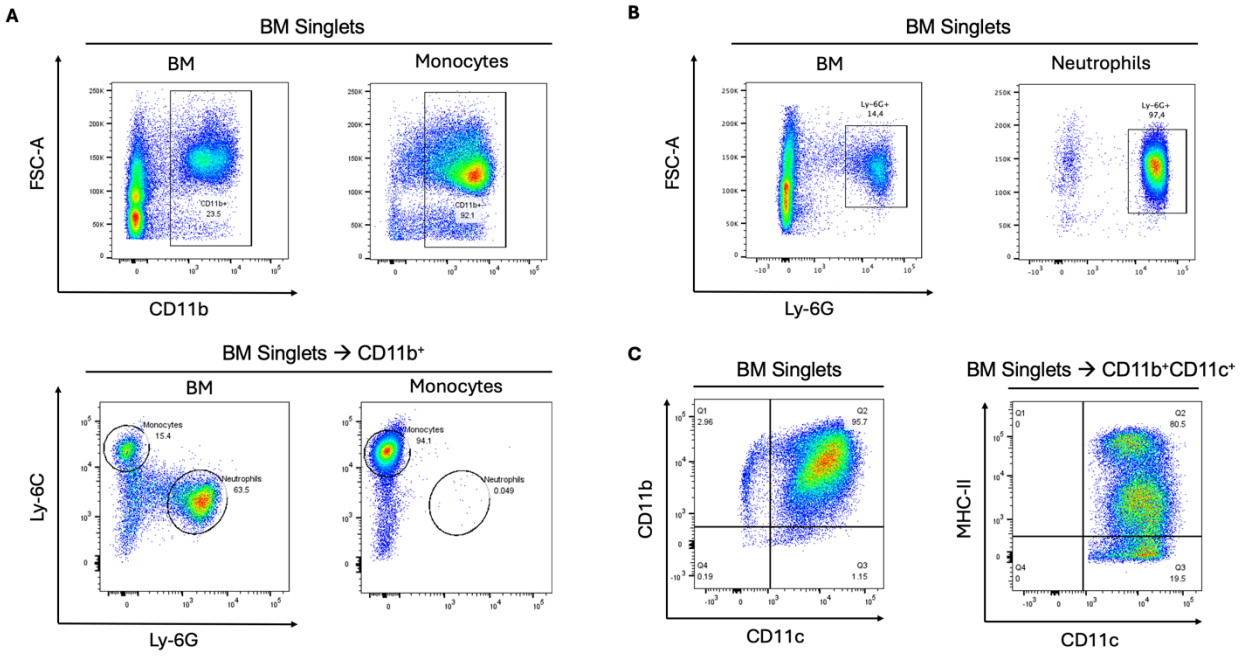
A
BM Singlets
BM
Monocytes
FSC-A
CD11b
CD11b+
23.5
CD11b+
92.1
BM Singlets → CD11b+
BM
Monocytes
Ly-6C
Ly-6G
Monocytes
15.4
Neutrophils
63.5
Monocytes
94.1
Neutrophils
0.049
B
BM Singlets
BM
Neutrophils
FSC-A
Ly-6G
Ly-6G+
14,4
Ly-6G+
97,4
C
BM Singlets
BM Singlets → CD11b+CD11c+
CD11b
CD11c
MHC-II
CD11c
Q1
2.96
Q2
95.7
Q4
0.19
Q3
1.15
Q1
0
Q2
80.5
Q4
0
Q3
19.5

Figure 3. Purity of isolated myeloid cells. (**A)** Representative FACS plot of monocyte purity in the start (BM) and final (Monocytes) isolated fractions. Monocytes were isolated using the EasySep Mouse Monocyte Isolation Kit. (**B)** Representative FACS plot of neutrophil purity in the start (BM) and final (Neutrophils) sorted fractions. Neutrophils were enriched in BM samples using the EasySep Mouse Neutrophil Enrichment Kit and sorted as Ly-6G^{+} on a Sony SH800 Cell Sorter. (**C)** Representative FACS plot of BMDC purity. BMDCs were differentiated from BM cell samples cultured in the presence of GM-CSF for 8 days. Data was analyzed using FlowJo software.

2.9. *In vitro* TLR agonist treatment

BMDMs were seeded after differentiation in M-CSF-coated dishes. Cells were incubated overnight at 37°C to prevent cellular stress. The following day, cells were treated with the TLR agonists outlined in Table 2. Cells were treated for 6 and 24 hours prior to supernatant collection to measure the production of cytokines.

Table 2. TLR agonists used for experiments

Agonist	Source	Catalogue Number	Concentration
LPS from *E. coli* O55:B5 (TLR4)	Sigma-Aldrich	L4524	100 ng/mL
R848 (TLR7/8)	InvivoGen	tlrl-R848	100 ng/mL
Pam3CSK4 (TLR1/2)	InvivoGen	tlrl-pms	100 ng/mL
CpG ODN 1826 (TLR9)	InvivoGen	tlrl-1826	100 ng/mL
Poly I:C	Sigma-Aldrich	P1530	100 ng/mL

2.10. *In vitro* infection with ST and CFU assay

To measure the production of cytokines, cells were infected with 5 MOI (multiplicity of infection) ST-WT. Cells were seeded in 96-well plates in R8 medium without gentamicin. To prevent the effects of plating-derived cellular stress, BMDMs were incubated overnight at 37°C prior to infection, and BMDCs, monocytes, and neutrophils were allowed to settle for at least 1 hour at 37°C prior to infection. Briefly, frozen stocks of ST-WT were quickly thawed, washed with PBS, and resuspended in R8 medium. Bacteria were added to cells, and plates were centrifuged at 2500 rpm for 6 minutes, followed by a 15-minute incubation period to allow bacteria to penetrate the cells. Since ST is an intracellular bacterium, cells were rinsed with PBS, then incubated with R8 medium containing gentamicin [50 μg/mL]. After 1.5 hours, cells were rinsed with PBS, and R8 medium containing a lower concentration of gentamicin [10 μg/mL]

was added. Cells were incubated for 6 or 24 hours prior to supernatant collection for use in enzyme-linked immunosorbent assays (ELISAs).

To measure cell death in BMDMs and BMDCs and IL-1β secretion in myeloid cells, approximately 1 hour after seeding cells in 96-well plates, cells were stimulated with LPS [10 ng/mL] (Sigma-Aldrich, L4524) and incubated at 37˚C overnight. LB broth containing streptomycin [50 μg/mL] was inoculated with crystals from a frozen stock of ST-WT and incubated overnight at 37˚C and shaking at 250 rpm. The next day, the overnight culture of ST-WT was sub-cultured (1:80) in LB containing streptomycin [50 μg/mL] at 37˚C and shaking at 250 rpm. The culture was grown until it reached an OD (optical density) at 600 nm of 0.83, where the CFU was estimated to be 5.6 x 10^8 CFU/mL. Sub-cultured ST-WT was resuspended in R8 medium and added to the LPS-primed cells at various MOIs. Upon addition of bacteria, cells were centrifuged at 2500 rpm for 6 minutes and incubated for 3 hours or 6 hours prior to measuring cell viability via Neutral Red Assay and collecting cell supernatants for ELISAs.

To assess intracellular bacterial burden, ST-Δ*invA* was used to allow for quantification of intracellular ST replication without cell death acting as a confounding variable. Cells were seeded at the appropriate density in 24-well plates. To prevent the effects of plating-derived cellular stress, BMDMs were incubated overnight at 37˚C prior to infection, and BMDCs, monocytes, and neutrophils were allowed to settle for at least 1 hour at 37˚C prior to infection. ST-Δ*invA* was cultured overnight in LB containing 100 μg/mL streptomycin at 37˚C and shaking at 250 rpm. The next day, when the overnight culture reached an OD at 600 nm of 2.3 [9.2 x 10^9 CFU/mL], the bacteria was resuspended in normal mouse serum (diluted 1:4 in PBS) (Jackson ImmunoResearch Laboratories, #015-000-120) and incubated at 37˚C, shaking at 250 rpm for 25 minutes. The normal mouse serum acts to opsonize the bacteria, improving uptake by cells.

Opsonized ST-Δ*invA* was washed two times with PBS and resuspended in R8 medium. Bacteria were added to cells at 10 MOI, centrifuged at 800 x *g* for 5 minutes, and incubated at 37˚C for 25 minutes. Cells were then rinsed two times with PBS containing gentamicin [50 μg/mL] and incubated with R8 medium containing gentamicin [50 μg/mL]. After 1.5 hours, cells were rinsed two times with PBS containing gentamicin [50 μg/mL], and media was changed to R8 medium containing a lower concentration of gentamicin [10 μg/mL]. For the 30-minute time point, after the addition of bacteria, cells were centrifuged and incubated at 37˚C for 15 minutes. Cells were then rinsed two times with PBS containing gentamicin [50 μg/mL] and incubated for a further 15 minutes with R8 medium containing gentamicin [50 μg/mL]. At specified time points, cells were lysed using Triton-X (1% in PBS). Ten-fold serial dilutions of the cell suspensions were made, and 100 μL aliquots were plated onto LB-agar plates containing streptomycin [100 μg/mL]. Plates were incubated at 37˚C overnight and CFU were then counted.

The same process was followed to measure the CFU using LM. Similarly, LM was cultured overnight in LB containing streptomycin [100 μg/mL] at 37˚C and shaking at 250 rpm until it reached an OD of 0.5 [9.65 x 10^8 CFU/mL]. All further steps proceeded as described above.

In some CFU experiments, cells were also treated with various inhibitors. Here, the inhibitors were supplied for at least 1 hour prior to infection, and continuously supplied throughout the duration of infection with ST-Δ*invA*. A list of inhibitors used can be found in Table 3.

Table 3. Inhibitors used in CFU experiments

Inhibitor	Source	Catalogue Number	Concentration
***N*-acetyl-L-cysteine**	Sigma-Aldrich	A9165	5 mM or 10 mM
MitoTEMPO	Sigma-Aldrich	SML0737	10 μM
Sivelestat	MedChemExpress	HY-17443	1 or 10 μM
Apocynin	Sigma-Aldrich	178385	100 500 μM

2.11. Cytokine analysis

ELISAs were used to measure the concentrations of cytokines in the supernatants of ST-infected myeloid cells, as well as macrophages treated with various TLR agonists *in vitro*. Murine TNF-α, IL-12, IL-6, IL-10, and IL-1β were measured using kits purchased from BD Biosciences (TNF-α: #555268; IL-6: #555240; IL-12: # 555256; IL-10: #555252) and R&D Systems (IL-1β: #DY401). Extra-high binding 96-well plates (Fisher Scientific, #12565135) were used and TMB (3,3',5,5'-tetramethylbenzidine) was used as a chromogenic substrate (Thermo Fisher, #002023). The reaction was stopped with sulfuric acid. The absorbance was detected at 450-570 nm on a FilterMax F5 multimode microplate reader (Molecular Devices). Data were analyzed using SoftMax Pro software.

2.12. Phagocytosis assays

Neutrophils were isolated as described previously, and 3 x 10^5 purified neutrophils were added to 5 mL tubes (Falcon, #352052) and washed with PBS. Meanwhile, pHrodo Deep Red *E. coli* BioParticles were resuspended in PBS at 1 mg/mL (containing approximately 3 x 10^8 *E. coli* particles per 1 mg) and vortexed well. Particles were opsonized using normal mouse serum (diluted 1:4 in PBS) for 25 minutes at 37˚C and shaking at 250 rpm. Bioparticles were added to neutrophils at 10 MOI (to replicate MOI used for CFU experiments) and were incubated at 37˚C for 15 minutes. Samples were immediately acquired on BD-LSRFortessa.

As another indicator of phagocytic ability, neutrophils were infected with ST-Δ*invA*, as described previously. However, after addition of bacteria to the cells, cells were centrifuged at 800 x *g* for 5 minutes and incubated for 15 minutes at 37˚C. Cells were then rinsed 2 times with PBS containing gentamicin [50 μg/mL] and lysed using Triton-X (1% in PBS). Ten-fold serial dilutions of the cell suspensions were made, and 100 μL aliquots were plated onto LB-agar plates

containing streptomycin [100 μg/mL]. Plates were incubated at 37˚C overnight and CFU were then counted.

2.13. Quantitative PCR

Neutrophils were purified and infected with 10 MOI opsonized ST-Δ*invA,* as described above. Cells were rinsed with sterile PBS. RNA was prepared using RNeasy Mini Kit (Qiagen, #74104) according to the manufacturer's instructions. RNA concentration was determined using a Nanodrop spectrophotometer (Thermo Fisher). Complementary DNA (cDNA) was prepared using iScript cDNA Synthesis Kit (BioRad, #1708891) according to manufacturer's instructions. Real-time quantitative polymerase chain reactions (RT-qPCR) were conducted using SYBR Green PCR Master Mix (Thermo Fisher, cat. # 4309155) and the reactions were run on a CFX96 Real-Time PCR System (Bio-Rad). Primer sequences are outlined in Table 4.

Table 4. RT-qPCR primers

Gene	Forward Primer Sequence (5'-3')	Reverse Primer Sequence (5'-3')
GAPDH	CCCACTCTTCCACCTTCG	TCCTTGGAGGCCATGTAGGCCAT
Cyba	TGCCAGTGTGATCTATCTGCT	TCGGCTTCTTTCGGACCTCT
Cybb	AGTGCGTGTTGCTCGACAA	GCGGTGTGCAGTGCTATCAT
Ncf1	ACACCTTCATTCGCCATATTGC	CCTGCCACTTAACCAGGAACA
Ncf2	GGAGAAGTACGACCTTGCTATCA	ACAGGCAAACAGCTTGAACTG
Ncf4	CAGGGTCCTTCGTGAAGATCC	CATAGAAGTAGCATCGTAGCCAG
Nox1	CCTGATTCCTGTGTGTCGAAA	TTGGCTTCTTCTGTAGCGTTC
Nox3	TGGCAGTAAACGCCTATCTGT	CGGAACCCAGAATAACTCGTGTA
Duox2	TGACGGTGTTTATCAGGCTCT	TTTGCCCTTAGCGACAGCATC
Mpo	AGTTGTGCTGAGCTGTATGGA	CGGCTGCTTGAAGTAAAACAGG
Elane	CAGGAACTTCGTCATGTCAGC	AGCAGTTGTGATGGGTCAAAG
Lcn2	TTTCACCCGCTTTGCCAAGT	GTCTCTGCGCATCCCAGTCA
Catalase	GTGCCCCCAACTATTACCCC	AGAATGTCCGCACCTGAGTG
SOD1	GGAACCATCCACTTCGAGCA	CTGCACTGGTACAGCCTTGT
SOD2	GTGTCTGTGGGAGTCCAAGG	AGCGGAATAAGGCCTGTTGT
Nfe2l2	TAGATGACCATGAGTCGCTTGC	GCCAAACTTGCTCCATGTCC
Keap1	TCGAAGGCATCCACCCTAAG	CTCGAACCACGCTGTCAATCT
Gclm	TCCTGCTGTGTGATGCCACCAG	GCTTCCTGGAAACTTGCCTCAG
Gsr	CACGGCTATGCAACATTCGC	GTGTGGAGCGGTAAACTTTTTC
Gpx2	ATGGCTTACATTGCCAAGTCG	TGCCTCTGAACGTATTGAAGTC
Gclc	CTACCACGCAGTCAAGGACC	CCTCCATTCAGTAACAACTGGAC
Gstp1	TCTACGCAGCACTGAATCCG	GGAGCTGCCCATACAGACAA

Gstm1	CACACAAGATCACCCAGAGCA	TGGAACAGCCACAAAGTCAGG
Gstm2	ACACCCGCATACAGTTGGC	TGCTTGCCCAGAAACTCAGAG
Gstm3	CTCACAGCCCTTTTCTGCAATC	GGCAGCTCCTTAAACAGGAACA
Gsta3	ATCTCGTTGGCAACAGGCTGAG	GAGGTTGCTGACTCTGCTTCTC
Nqo1	GCCGAACACAAGAAGCTGGAAG	GGCAAATCCTGCTACGAGCACT

2.14. Neutral Red Assay

To determine cell death after infection with ST-WT, a Neutral Red assay was performed 6 hours after LPS-primed cells were infected with ST-WT. A 5% Neutral Red solution (Sigma-Aldrich #N2889) was prepared in R8 medium. Cells were incubated with the Neutral Red solution for 15 minutes. The stain was then removed by aspiration and the cells were rinsed with PBS. Next, the dye was solubilized with a solution of ethanol and acetic acid in sterile water. The absorbance of the dye was immediately measured at 570 nm using a FilterMax F5 plate reader (Molecular Devices). Cell viability was calculated relative to the uninfected control of each genotype.

2.15. ROS Measurements

Various methods were used to evaluate the production of ROS in myeloid cells. To determine the production of ROS following *in vivo* infection with ST, BM cells were isolated from mice at day 5 post-infection with ST, as previously described. Up to 6 x 10^6 cells were transferred to 5 mL tubes and washed with phenol red-free RPMI (Gibco, #11835-030). Cells were then incubated with 2',7'-dichlorodihydrofluorescein diacetate (H_2DCFHDA) [10 μM] (Invitrogen, #D399) for 30 minutes at 37˚C. Samples were washed with phenol red-free RPMI medium and then stained with cell surface antibodies, as previously described.

To evaluate superoxide production *in vitro*, neutrophils were purified, plated, and infected with opsonized ST-Δ*invA,* as previously described. After a 30-minute incubation period with opsonized ST-Δ*invA,* cells were rinsed twice with PBS containing gentamicin (50 μg/mL).

Phenol red-free R8 medium (phenol red-free RPMI with 8% FBS and 50 μg/mL gentamicin) containing L-012 sodium salt [50 μM] (MedChemExpress, #HY-108537) was added to cells and the luminescence was immediately measured on a FilterMax F5 plate reader at 37˚C. The luminescence in the plate was read every 3 minutes, for a total of 30 minutes.

To measure H_2O_2 production *in vitro*, neutrophils were purified, plated, and infected with opsonized ST-Δ*invA* as previously described. Phenol red-free R8 medium was used during the infection. After 30 minutes of infection, cell supernatants were collected and used in the Amplex Red Hydrogen Peroxide Assay (Invitrogen, #A22188), according to the manufacturer's instructions to assess H_2O_2 secreted by neutrophils. The fluorescence was detected at 535 nm excitation and 595 nm emission on a FilterMax F5 multimode microplate reader (Molecular Devices). Data were analyzed using SoftMax Pro software.

2.16. Statistical analysis

Data is plotted as mean, with error bars representing standard error of mean (SEM). Unpaired two-tailed student's t-test and two-way ANOVAs were used to determine statistical significance. All statistical analyses were performed using GraphPad Prism version 10 software.

3. RESULTS

3.1. Impact of *Lrrk2*^{G2019S} mutation on the BM compartment

3.1.1. *Lrrk2*^{G2019S} mutation promotes enhanced resistance against infection with ST in the BM

As we hypothesize that *Lrrk2*^{G2019S} mutation confers enhanced resistance to infection with ST through its role in the BM compartment, we first aimed to confirm that the genesis of this phenotype was in the BM. To do so, both C57BL/6 wildtype (WT) mice and *Lrrk2*^{G2019S} KI mice (GS), were intravenously injected with 200 CFU of ST-WT. At day 5 post-infection with ST (5 dpi), spleen and BM (isolated from the tibia, femur, and hip bones) cells were plated on LB-agar-streptomycin plates to perform CFU counts to compare the bacterial burden between WT and GS mice. Our results indicated a significant reduction of CFU in both the spleen and BM cells of GS mice, compared to WT mice (Figure 4). These findings confirm previous data that the *Lrrk2*^{G2019S} mutation promotes enhanced control of ST in the spleen[72], and further suggests that the *Lrrk2*^{G2019S} mutation has a functional role in BM cells to promote better control of infection with ST.

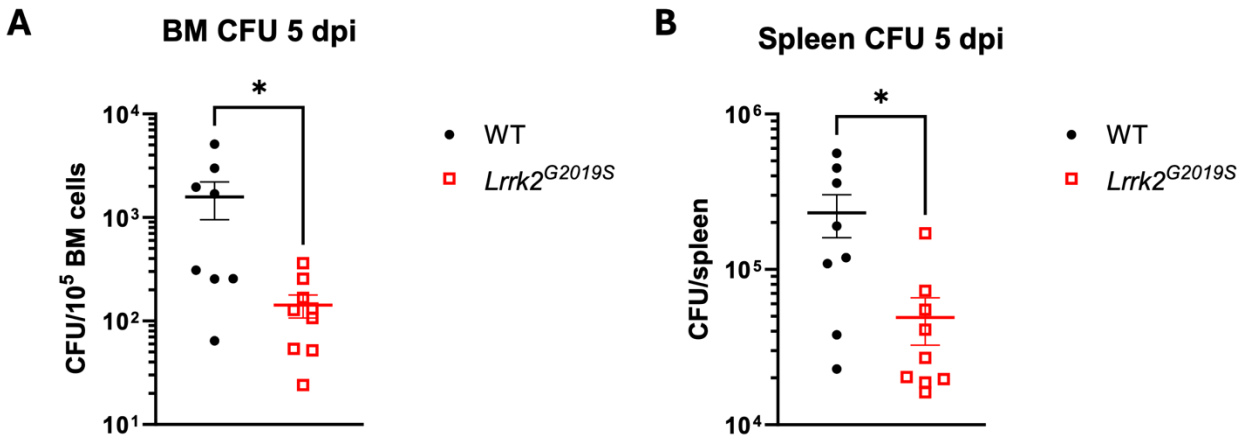
A
BM CFU 5 dpi
CFU/10^5 BM cells
10^4
10^3
10^2
10^1
*
WT
Lrrk2G2019S
B
Spleen CFU 5 dpi
CFU/spleen
10^6
10^5
10^4
*
WT
Lrrk2G2019S

Figure 4. *Lrrk2*^{G2019S} mutation reduces bacterial burden of ST in the BM and spleen of mice. Colony-forming units (CFU) were counted from BM cells (**A**) and spleens (**B**) of mice 5 days post-infection with ST (5 dpi). BM cells and spleens were collected from C57BL/6 wildtype (WT) and *p.G2019S* mutant *Lrrk2* knock-in animals (*Lrrk2*^{G2019S}). Graph depicts mean ± SEM (unpaired two-tailed t-test; n = 8; *$p < 0.05$).

3.1.2. LRRK2 expression in hematopoietic progenitor and mature myeloid cells

To determine which cell types in the BM most highly express LRRK2, we used a flow cytometric approach, allowing us to identify progenitors, such as hematopoietic stem and multipotent progenitor cells (HSPCs/LSKs), myeloid progenitors (MPs), CMPs, GMPs, MEPs, as well as mature cells, including monocytes, and neutrophils. Figure 5 demonstrates the gating strategies used to identify each cell population.

BM cells from both naïve and ST-infected (5 dpi) WT mice were stained with antibodies against LRRK2 and specific cell surface markers. Cells were fixed and permeabilized to allow for intracellular staining of LRRK2. Our results indicated that among the cell types investigated, LRRK2 is more highly expressed in mature immune cells (Lin^+), compared to the overall immature population (Lin^-), in both naïve and infected cells (Figure 6A). However, it is important to note that the specific immature cells of our interest (LSKs, MPs, GMPs, CMPs, and MEPs) demonstrated similar median fluorescence intensities (MFI) to that of the mature immune cells (Figure 6B & 6C). This could indicate that there is lower expression of LRRK2 in the lymphoid progenitors present in the Lin^- population (thus reducing the MFI of Lin^- cells) but requires further investigation. Similarly, myeloid cells ($CD11b^+$), showed higher LRRK2 expression than non-myeloid BM cells ($CD11b^-$) in both a naïve and infected state (Figure 6D). We did not observe a difference in LRRK2 expression between monocytes and neutrophils (Figure 6E).

A

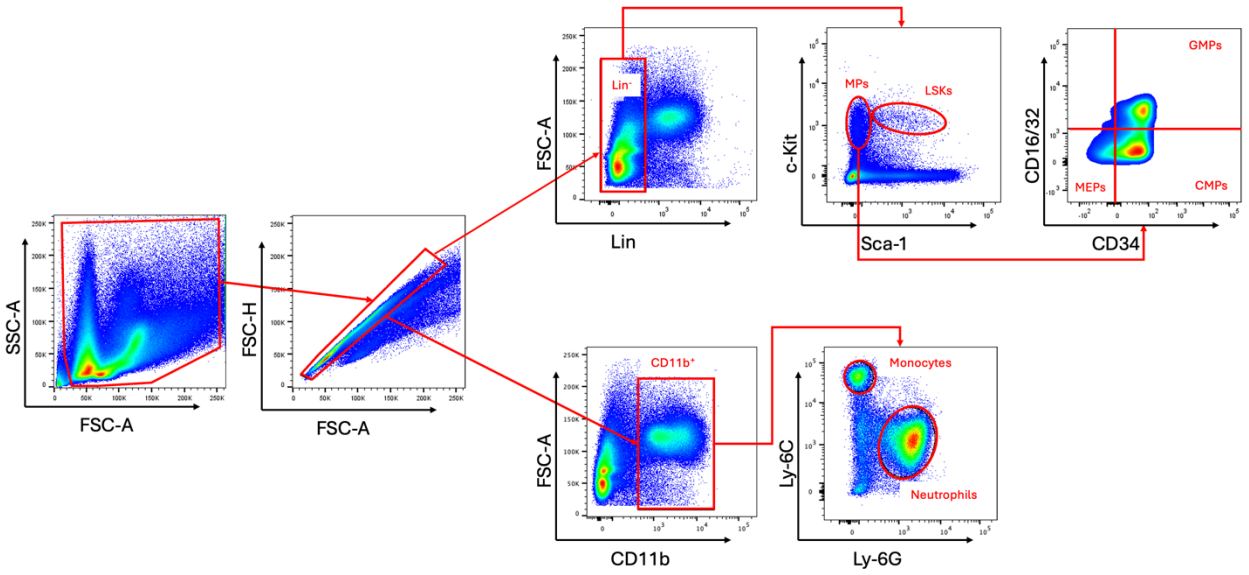

B

Cell Type	Markers
LSKs	$Lin^-c\text{-}Kit^+Sca\text{-}1^+$
MPs	$Lin^-c\text{-}Kit^+Sca\text{-}1^-$
GMPs	$Lin^-c\text{-}Kit^+Sca\text{-}1^-CD16/32^+CD34^+$
CMPs	$Lin^-c\text{-}Kit^+Sca\text{-}1^-CD16/32^+CD34^-$
MEPs	$Lin^-c\text{-}Kit^+Sca\text{-}1^-CD16/32^-CD34^-$
Monocytes	$CD11b^+Ly\text{-}6C^+Ly\text{-}6G^-$
Neutrophils	$CD11b^+Ly\text{-}6C^{-/int}Ly\text{-}6G^+$

Figure 5. Gating strategy for hematopoietic progenitor and myeloid cell populations. BM cells were obtained from hindlimbs of naïve WT and *Lrrk2*^{G2019S} mice. Cells were stained with fluorophore-conjugated antibodies against cell surface markers. Samples were acquired on a flow cytometer (BD LSRFortessa). (**A**) Representative gating strategy employed for HSPCs and myeloid cells. Data were analyzed using FlowJo software. (**B**) Markers used to identify specified cell populations. Lin cocktail contains antibodies against the following markers: CD3, CD45R, CD11b, Ter-119, Ly-6G.

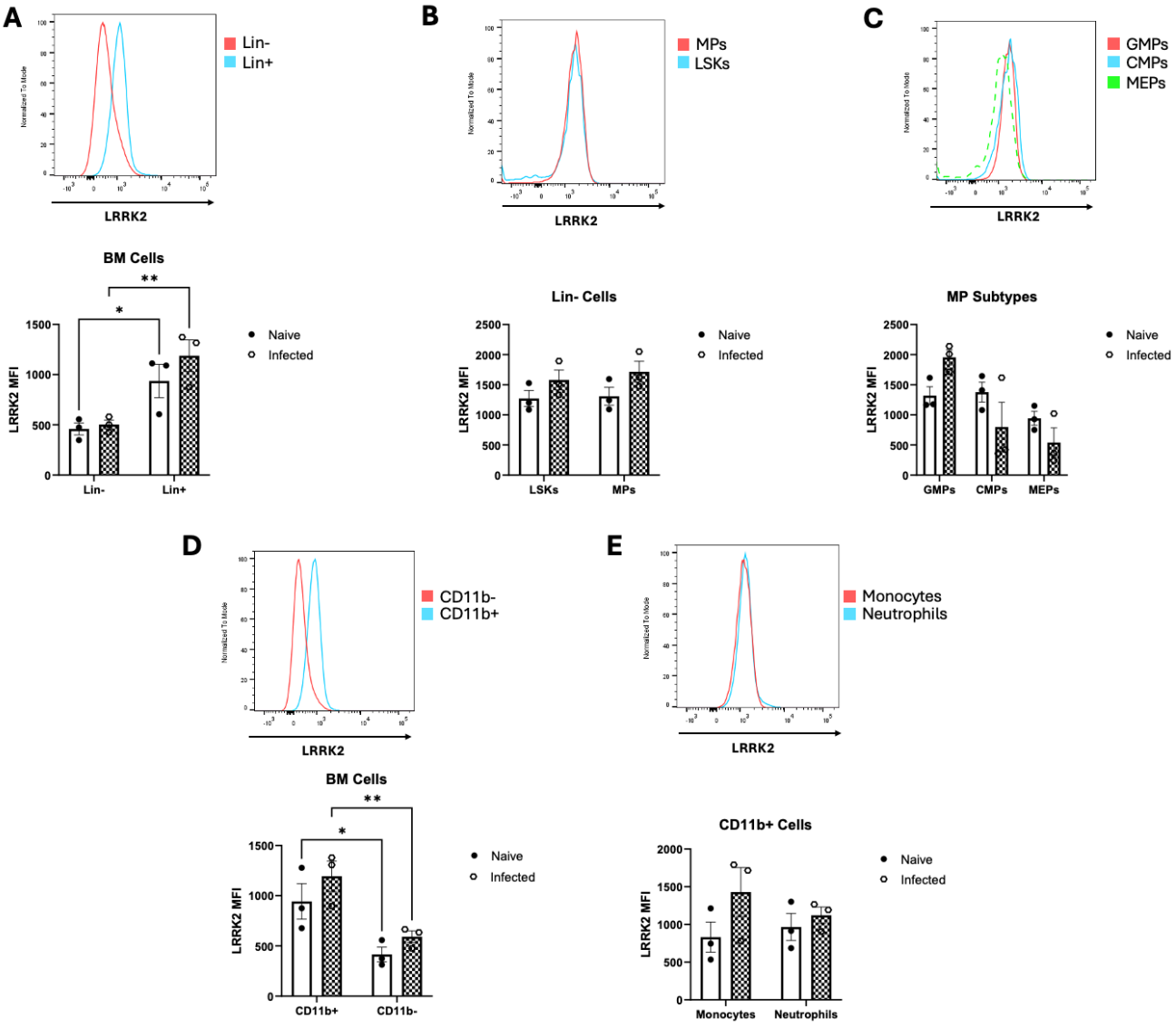
A
Lin-
Lin+
LRRK2
BM Cells
LRRK2 MFI
Lin-
Lin+
Naive
Infected
B
MPs
LSKs
LRRK2
Lin- Cells
LSKs
MPs
C
GMPs
CMPs
MEPs
MP Subtypes
GMPs
CMPs
MEPs
D
CD11b-
CD11b+
BM Cells
CD11b+
CD11b-
E
Monocytes
Neutrophils
CD11b+ Cells
Monocytes
Neutrophils

Figure 6. LRRK2 expression in hematopoietic progenitor and myeloid cell populations in the BM. BM cells isolated from WT naïve mice and WT mice infected with ST (5 dpi) were stained with cell surface markers. Cells were then fixed and permeabilized to allow for intracellular LRRK2 staining. Samples were acquired on a flow cytometer and data were analyzed using FlowJo software. Representative histograms of LRRK2 MFI in naïve mice, and LRRK2 expression in naïve versus infected cells are shown for various cell populations: mature (Lin+) and immature (Lin-) BM cells **(A),** MPs and LSKs **(B),** GMPs, CMPs, and MEPs **(C),** myeloid (CD11b+) and non-myeloid cells (CD11b-) **(D),** and monocytes and neutrophils **(E).** Graphs depict mean ± SEM (two-way ANOVA; n = 3; *$p < 0.05$, **$p < 0.01$).

3.1.3. Steady-state hematopoietic progenitor and mature cell numbers are similar between WT and *Lrrk2*^{G2019S} mice

As hematopoiesis is an important process necessary for the maintenance and production of immune cells, our next aim was to determine the impact of the agonistic *Lrrk2*^{G2019S} mutation on the numbers of various immune cell types in mice before and upon infection with ST. First, total BM cell numbers were compared between WT and GS mice. To count cells, 3% acetic acid with methylene blue was used. Methylene blue only stains nucleated cells; thus, our total cell numbers do not include red blood cells. As indicated in Figure 7A, there were no differences in total bone marrow cell counts between WT and GS mice.

To further investigate the impact of the *Lrrk2*^{G2019S} mutation on specific immune cell subsets, flow cytometry was used to analyze HSPC and myeloid cell populations, using the gating strategy previously described. There were no significant differences in the LSK, MP, CMP, GMP, and MEP cell numbers between WT and GS mice (Figure 7B & 7C).

Myeloid cell numbers in the BM of WT and GS mice were also analyzed using flow cytometry. The cell populations were identified using the gating strategy previously described. Similar numbers of overall myeloid cells (CD11b+) as well as monocytes and neutrophils were observed in WT and GS mice (Figure 8).

Taken together, these results indicate that the *Lrrk2*^{G2019S} mutation does not appear to impact hematopoietic progenitor and myeloid cell numbers at a steady state.

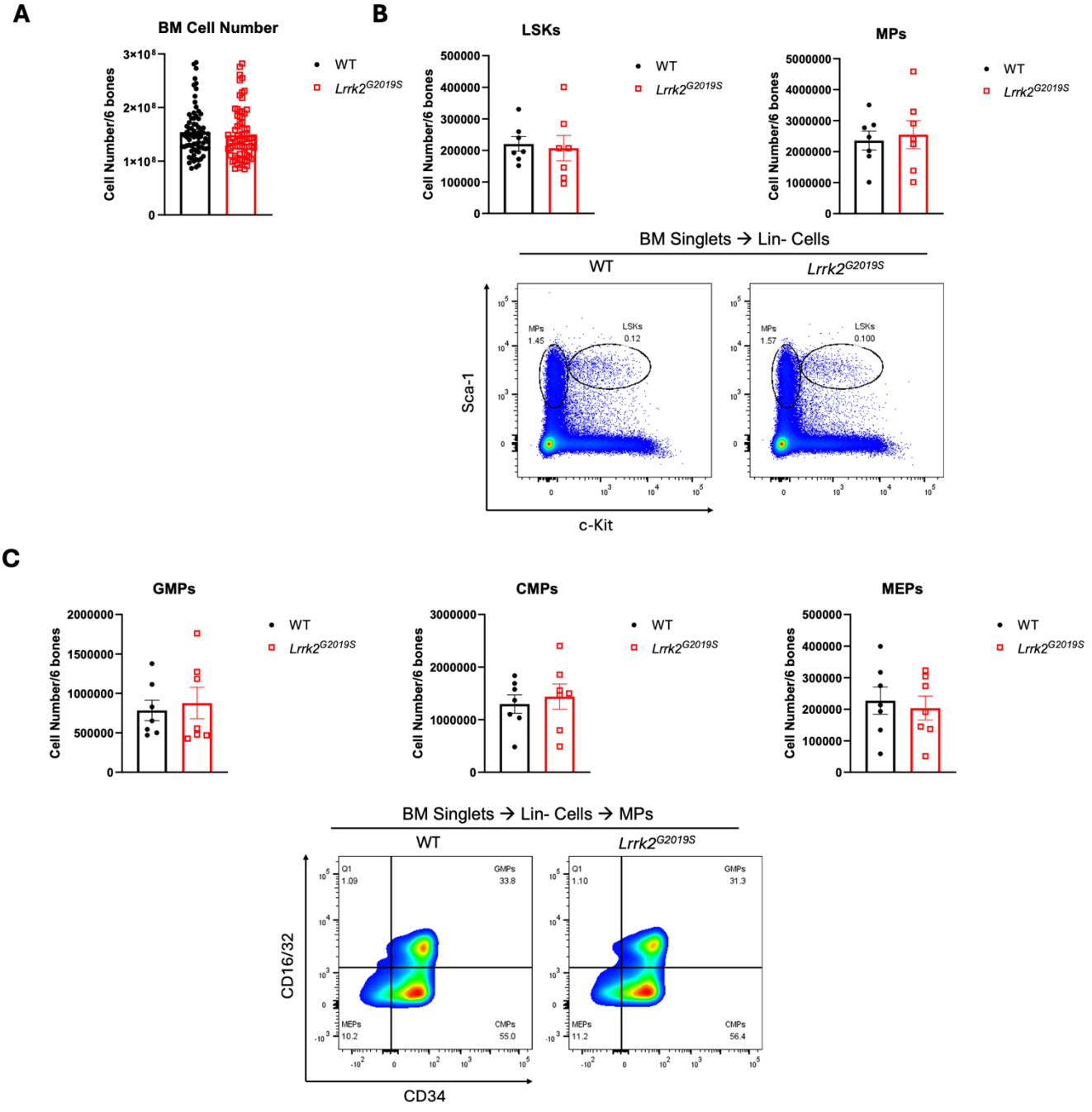
A
BM Cell Number
Cell Number/6 bones
WT
Lrrk2G2019S
B
LSKs
MPs
BM Singlets → Lin- Cells
WT
Lrrk2G2019S
MPs
1.45
LSKs
0.12
1.57
0.100
Sca-1
c-Kit
C
GMPs
CMPs
MEPs
BM Singlets → Lin- Cells → MPs
Q1
1.09
1.10
GMPs
33.8
31.3
MEPs
10.2
11.2
CMPs
55.0
56.4
CD16/32
CD34

Figure 7. Hematopoietic stem and progenitor cell numbers are similar in naïve WT and *Lrrk2*^{G2019S} mice. (A) BM cell number extracted from tibias, femurs, and hips of naïve WT and *Lrrk2*^{G2019S} KI mice (n = 77). Cells were manually counted using a hemocytometer and methylene blue stain. Cells were stained with appropriate cell surface antibodies, acquired on a flow cytometer, and analyzed using FlowJo software. Representative FACS plots and cell numbers of LSKs, MPs **(B)** and GMPs, CMPs, MEPs **(C)** from naïve WT and *Lrrk2*^{G2019S} mice. All graphs depict mean ± SEM (n = 7; no significance was detected with unpaired two-tailed t-tests).

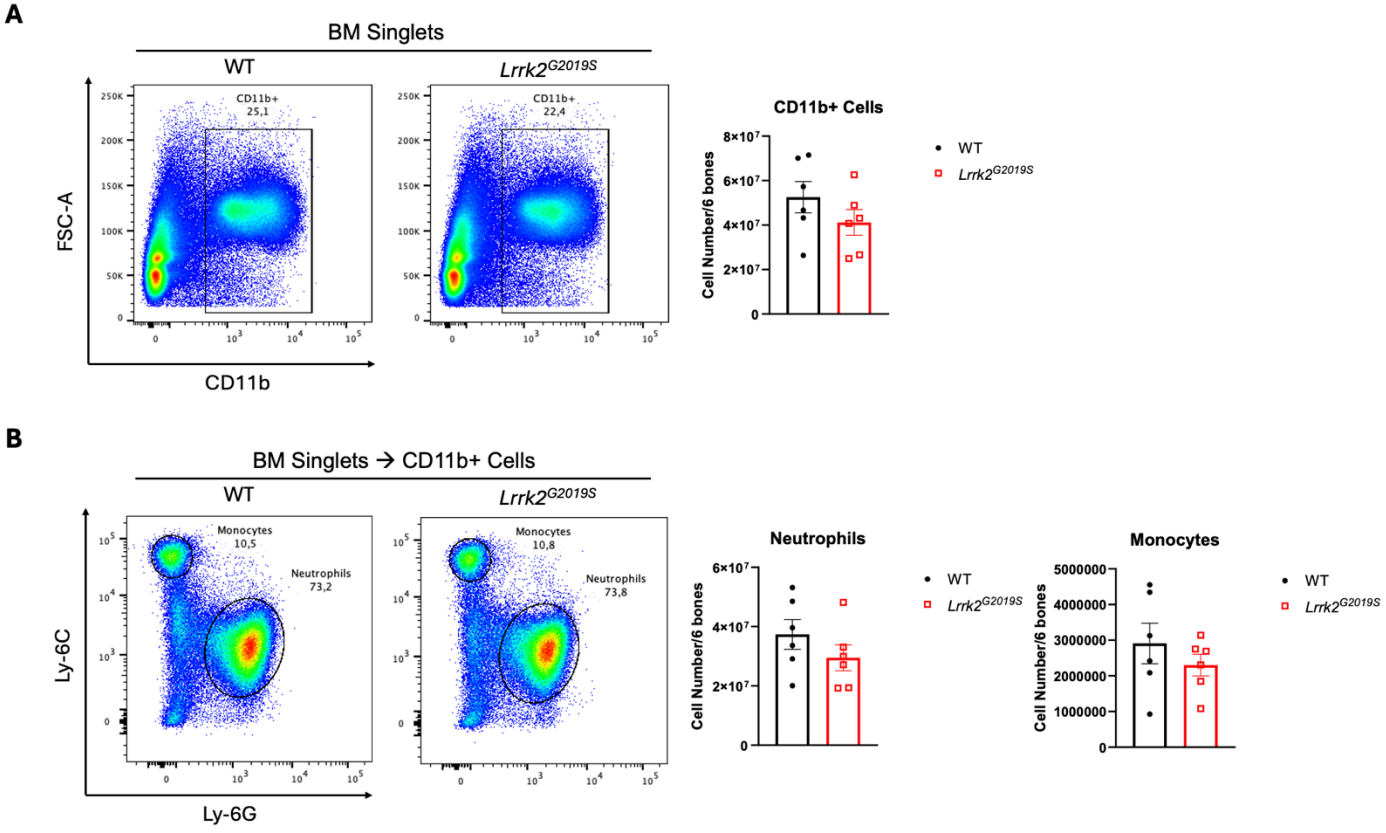
A
BM Singlets
WT
Lrrk2G2019S
CD11b+
25,1
CD11b+
22,4
FSC-A
CD11b
CD11b+ Cells
Cell Number/6 bones
WT
Lrrk2G2019S
B
BM Singlets → CD11b+ Cells
WT
Lrrk2G2019S
Monocytes
10,5
Neutrophils
73,2
Monocytes
10,8
Neutrophils
73,8
Ly-6C
Ly-6G
Neutrophils
Monocytes
Cell Number/6 bones
WT
Lrrk2G2019S

Figure 8. Myeloid cell numbers are similar in naïve WT and *Lrrk2*^{G2019S} mice. BM cells from naive WT and *Lrrk2*^{G2019S} mice were manually counted using a hemocytometer and methylene blue stain. Cells were stained with appropriate cell surface antibodies, acquired on a flow cytometer, and analyzed using FlowJo software. Representative FACS plots and cell numbers of myeloid cells ($CD11b^+$) **(A)** and monocytes and neutrophils **(B)** are shown. All graphs depict mean ± SEM (n = 6; no significance was detected with unpaired two-tailed t-tests).

3.1.4. *Lrrk2*^{G2019S} mutation promotes BM cell expansion following infection with ST

After observing similar cell numbers between WT and GS mice at a steady state, the next aim was to determine the impact of the agonistic *Lrrk2*^{G2019S} mutation on immune cell numbers during infection with ST, especially as GS mice showed enhanced resistance to ST in the BM compartment. Therefore, WT and GS mice were IV infected with 200 CFU of ST-WT. At day 5 post-infection with ST, total BM cell counts were determined using methylene blue stain. Although BM cell numbers decreased in both groups, relative to naïve mice, GS mice showed significantly higher total BM cell counts, compared to WT mice (Figure 9A).

We further investigated the impact of *Lrrk2*^{G2019S} mutation on specific immune cell populations in the BM of mice infected with ST. Cell numbers for immune cell populations are shown as fold change, relative to the cell numbers of the naïve mice for each genotype. LSKs showed a fold increase for both genotypes, with GS mice showing a significantly greater increase, compared to WT mice (Figure 9B). This finding suggests that the *Lrrk2*^{G2019S} mutation may act to promote HSPC expansion during infection. Infection with ST resulted in a fold decrease of MP, CMP, and MEP numbers, but an increase in GMPs, compared to naïve cell numbers, to a similar extent in both genotypes (Figure 9B & 9C).

Subsequently, mature myeloid cell populations in the BM were analyzed. Although overall myeloid cell numbers were lower in both genotypes, compared to naïve mice, GS mice showed significantly less reduction, compared to WT mice (Figure 10A). Similarly, neutrophil counts were lower relative to naïve mice, but GS mice showed significantly less reduction of neutrophils following infection (Figure 10B). Interestingly, monocyte cell numbers were relatively similar between naïve and infected WT mice, while GS mice appeared to show a slight

increase compared to naïve numbers, although the difference between genotypes is not significant (Figure 10B).

Together, these results indicate that the *Lrrk2*^{G2019S} mutation promotes HSC cell expansion and resistance to myeloid cell loss during infection with ST.

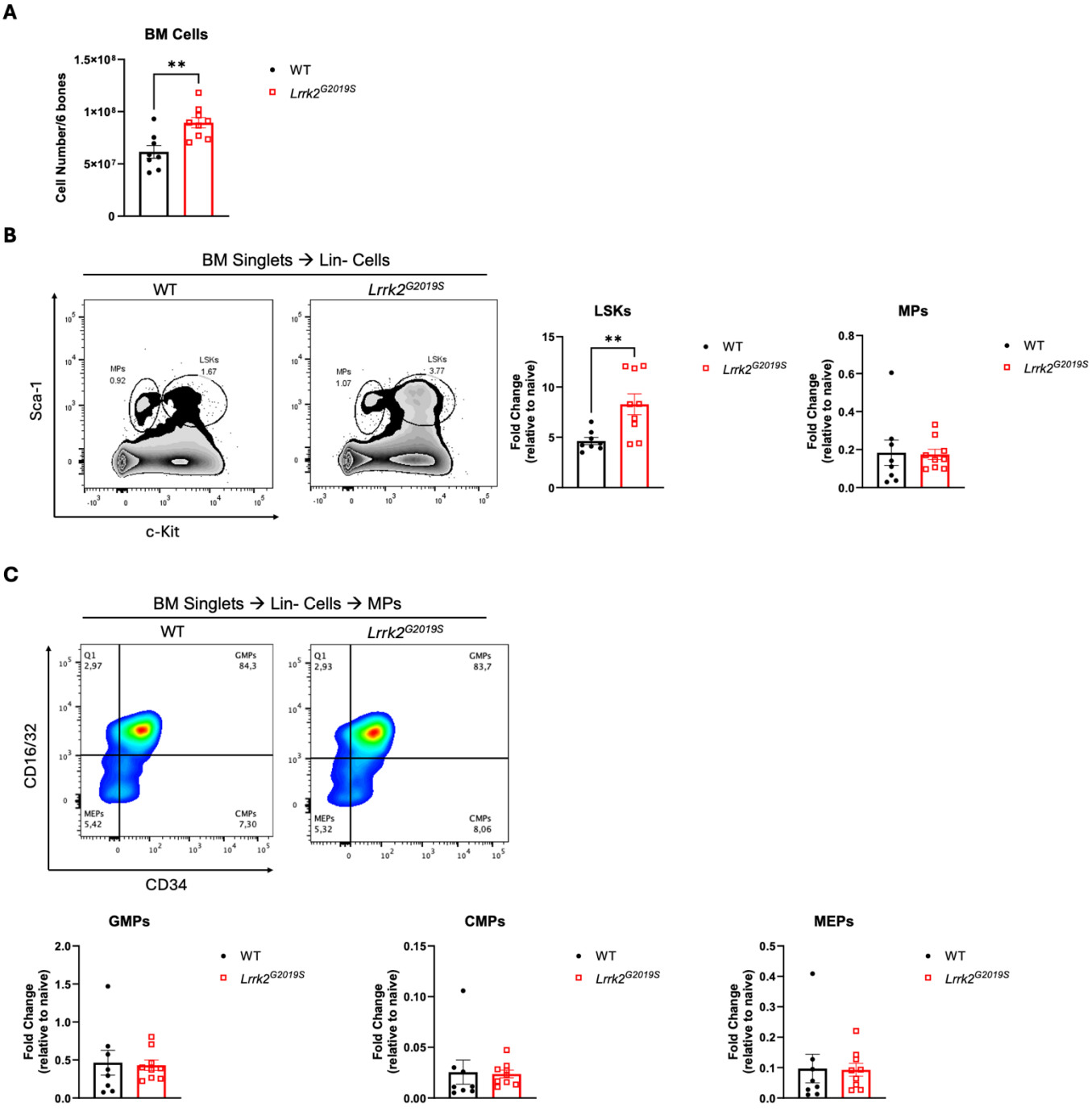
A
BM Cells
Cell Number/6 bones
1.5×10⁸
1×10⁸
5×10⁷
0
**
WT
Lrrk2G2019S
B
BM Singlets → Lin- Cells
WT
Lrrk2G2019S
Sca-1
c-Kit
MPs
0.92
LSKs
1.67
MPs
1.07
LSKs
3.77
LSKs
Fold Change (relative to naive)
15
10
5
0
**
WT
Lrrk2G2019S
MPs
Fold Change (relative to naive)
0.8
0.6
0.4
0.2
0.0
WT
Lrrk2G2019S
C
BM Singlets → Lin- Cells → MPs
WT
Lrrk2G2019S
CD16/32
CD34
Q1
2,97
GMPs
84,3
MEPs
5,42
CMPs
7,30
Q1
2,93
GMPs
83,7
MEPs
5,32
CMPs
8,06
GMPs
Fold Change (relative to naive)
2.0
1.5
1.0
0.5
0.0
WT
Lrrk2G2019S
CMPs
Fold Change (relative to naive)
0.15
0.10
0.05
0.00
WT
Lrrk2G2019S
MEPs
Fold Change (relative to naive)
0.5
0.4
0.3
0.2
0.1
0.0
WT
Lrrk2G2019S

Figure 9. *Lrrk2*^{G2019S} mutation promotes BM cell expansion following infection with ST in mice. (A) BM cell number extracted from tibias, femurs, and hips of WT and *Lrrk2*^{G2019S} KI mice 5 dpi with ST. Cells were manually counted using a hemocytometer and methylene blue stain. Cells were stained with appropriate cell surface antibodies, acquired on a flow cytometer, and analyzed using FlowJo software. Representative FACS plots and fold change of LSKs, MPs **(B),** GMPs, CMPs, and MEPs **(C)** in WT and *Lrrk2*^{G2019S} mice 5 dpi with ST. Fold change values are relative to each genotype's naïve controls. All graphs depict mean ± SEM (unpaired two-tailed t-test; n = 8; **$p < 0.01$).

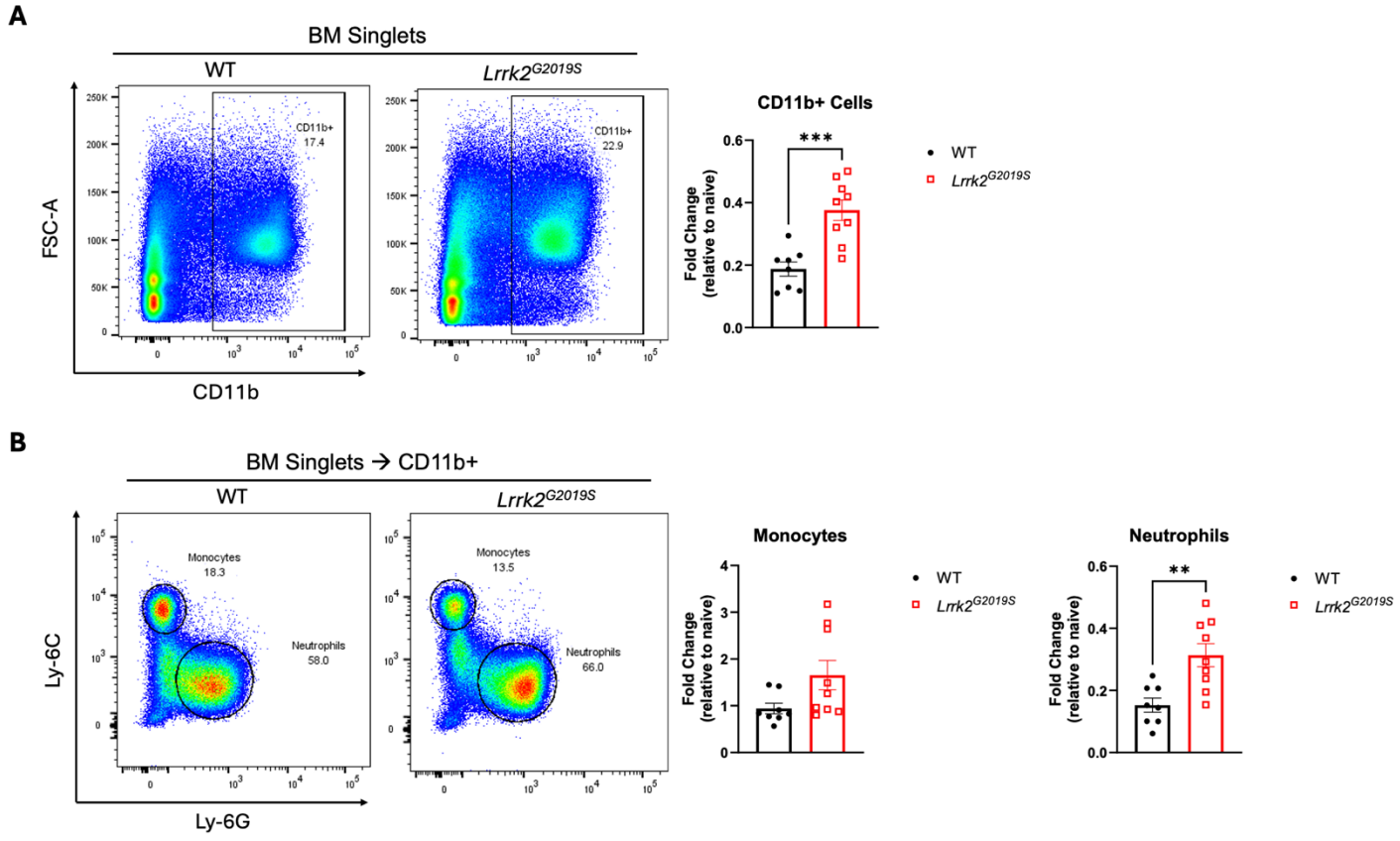
A
BM Singlets
WT
Lrrk2G2019S
FSC-A
CD11b
CD11b+
17.4
CD11b+
22.9
CD11b+ Cells
***
Fold Change
(relative to naive)
WT
Lrrk2G2019S
B
BM Singlets → CD11b+
WT
Lrrk2G2019S
Ly-6C
Ly-6G
Monocytes
18.3
Neutrophils
58.0
Monocytes
13.5
Neutrophils
66.0
Monocytes
Neutrophils
**
Fold Change
(relative to naive)
WT
Lrrk2G2019S

Figure 10. *Lrrk2*^{G2019S} mutation promotes maintenance of myeloid cells during infection with ST in mice. BM cells isolated from WT and *Lrrk2*^{G2019S} mice 5 dpi with ST were manually counted using a hemocytometer and methylene blue stain. Cells were stained with appropriate cell surface antibodies, acquired on a flow cytometer, and analyzed using FlowJo software. Representative FACS plots and fold change of myeloid cells (CD11b^{+}) **(A)** and monocytes and neutrophils **(B)** are shown. Fold change values are relative to the naïve control of each genotype. All graphs depict mean ± SEM (unpaired two-tailed t-test; n = 8; **p < 0.01, ***p < 0.001).

3.2. *Lrrk2*^{G2019S} mutation does not impact the production of cytokines or cell death in myeloid cells

3.2.1. WT and *Lrrk2*^{G2019S} myeloid cells show similar levels of cytokines upon infection with ST

Our next aim was to determine whether the agonistic *Lrrk2*^{G2019S} mutation may act to enhance the inflammatory response in myeloid cells. As cytokines are important mediators of the innate immune response, we wondered if the enhanced resistance to ST observed in the BM of GS mice is due to an altered inflammatory cytokine profile. We isolated monocytes and neutrophils from the BM of WT and GS mice. As well, we stimulated BM cells with M-CSF or GM-CSF to promote differentiation into BMDMs and BMDCs, respectively. Each isolated cell type was infected with ST-WT at 5 MOI. Cell supernatants were collected at 6- and 24-hours post-infection and secreted cytokine concentrations were determined by ELISA. Pro-inflammatory cytokines (IL-6, IL-12, and TNF-α) and the anti-inflammatory cytokine IL-10 were assessed. Upon infection with ST, all cytokine concentrations were increased in both WT and GS myeloid cell supernatants relative to uninfected controls. Overall, the production of cytokines was similar between WT and GS myeloid cells in response to infection with ST (Figure 11).

As TLRs are the first PRRs stimulated during infection with ST[53], we also investigated the impact of *Lrrk2*^{G2019S} mutation on the production of cytokines during TLR signalling. WT and GS macrophages were stimulated with various molecules that are known activators of different TLRs: Pam3CSK4 (TLR1/2), Poly I:C (TLR3), LPS (TLR4), R848 (TLR7/8), and CpG (TLR9). Supernatants were collected from BMDMs 6- and 24-hours after stimulation and secreted cytokine concentrations were determined by ELISA. Similarly, no difference was observed

between WT and GS macrophage cytokine secretion profiles in response to treatment with TLR agonists (Figure 12).

Together, these results indicate that the *Lrrk2*^{G2019S} mutation does not impact the production of cytokines in myeloid cells infected with ST, thus the enhanced resistance to ST must be due to a different cellular mechanism.

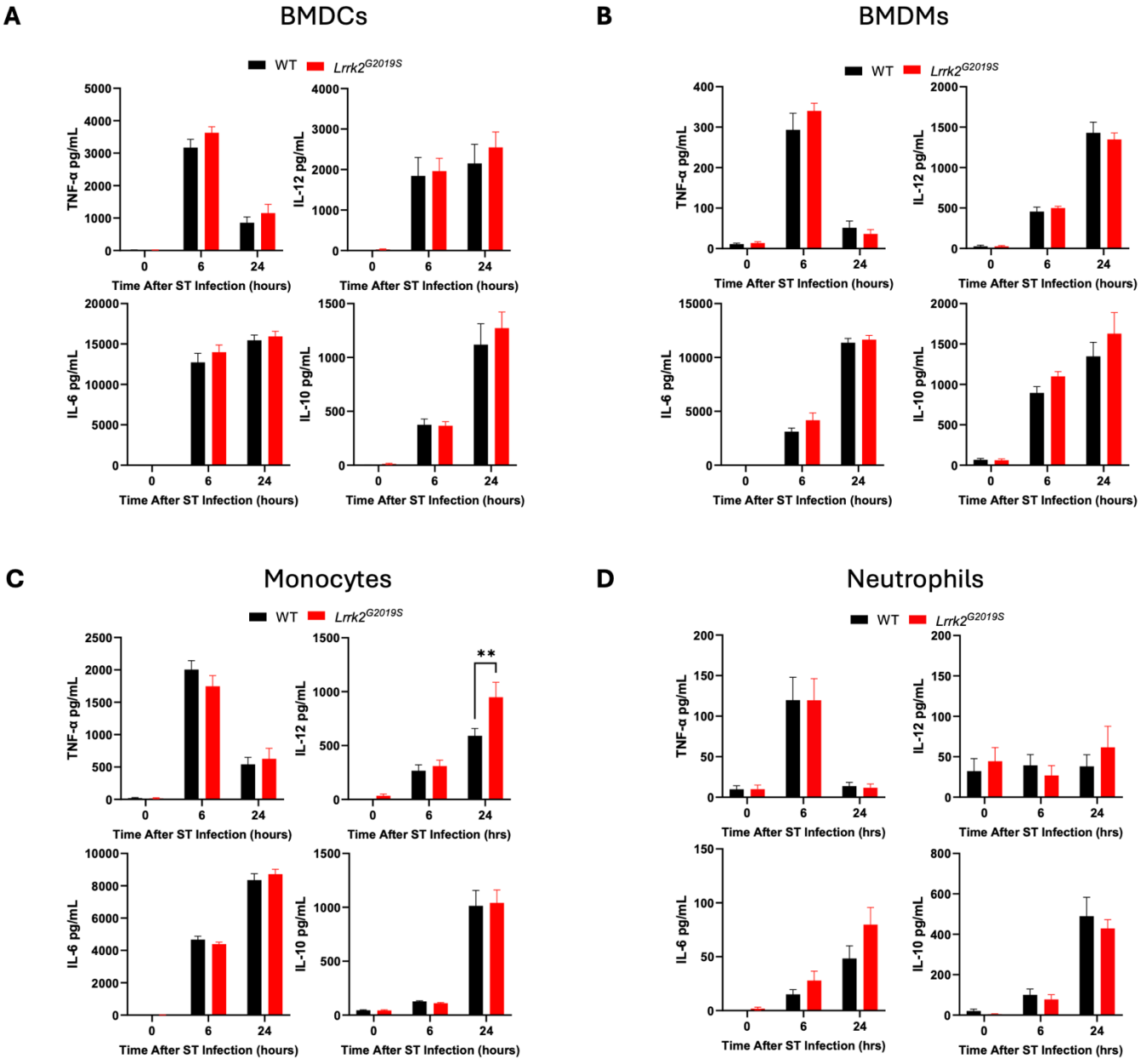
A
BMDCs
WT
Lrrk2G2019S
TNF-α pg/mL
IL-12 pg/mL
IL-6 pg/mL
IL-10 pg/mL
Time After ST Infection (hours)
B
BMDMs
C
Monocytes
**
Time After ST Infection (hrs)
D
Neutrophils

Figure 11. Cytokine secretion by myeloid cells after infection with ST. BMDCs, BMDMs, monocytes, and neutrophils isolated from WT and *Lrrk2*^{G2019S} BM cells were infected with 5 MOI ST-WT. Cell supernatants were collected at 6 and 24 hours after infection. Concentrations of TNFα, IL-10, IL-6, and IL-12 were measured by sandwich ELISA from supernatants of BMDCs (**A**), BMDMs (**B**), monocytes (**C**), and neutrophils (**D**). All graphs depict mean ± SEM (n = 3 (n = 2 for IL-12); two-way ANOVA; **p < 0.01).

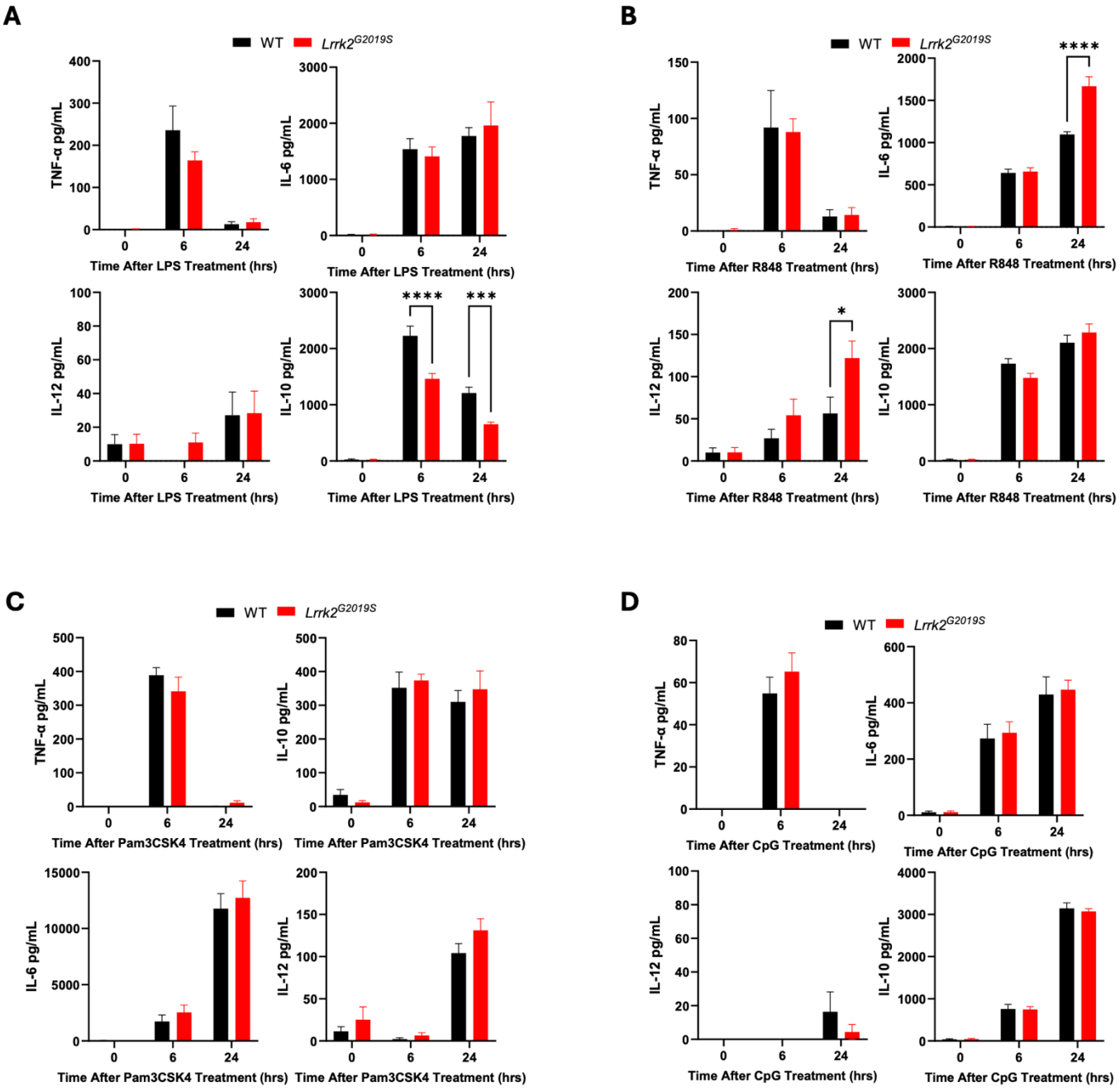
A
WT
Lrrk2G2019S
TNF-α pg/mL
IL-6 pg/mL
IL-12 pg/mL
IL-10 pg/mL
Time After LPS Treatment (hrs)
****
***
B
Time After R848 Treatment (hrs)
*
C
Time After Pam3CSK4 Treatment (hrs)
D
Time After CpG Treatment (hrs)

Figure 12. Cytokine secretion by BMDMs after treatment with TLR agonists. BMDMs differentiated from WT and *Lrrk2*^{G2019S} BM cells were stimulated with various TLR agonists. Cell supernatants were collected at 6 and 24 hours after treatment. Concentrations of TNFα, IL-10, IL-6, and IL-12 were measured by sandwich ELISA following treatment with LPS [100 ng/mL] (**A**), R848 [100 ng/mL] (**B**), Pam3CSK4 [100 ng/mL] (**C**), and CpG [100 ng/mL] (**D**). All graphs depict mean ± SEM (n = 2; two-way ANOVA; *p < 0.05, ***p < 0.001, ****p < 0.001).

3.2.2. *Lrrk2*^{G2019S} mutation does not impact hematopoietic progenitor and myeloid cell death

Cell death is a common outcome during infections and is often a key process that tailors host-pathogen interactions. To determine whether the *p.G2019S* mutation modulates cell death of BM cells following infection with ST, we used a flow cytometry viability stain, Zombie. Zombie is an amine-reactive dye that is non-permeant to live cells, but permeant to cells with compromised membranes (dead cells). We examined the percentage of dead cells (Zombie^{+}) in hematopoietic progenitor and mature myeloid cell populations in BM cells isolated from mice infected with ST (5 dpi). Our results indicated no observable differences in cell death between WT and GS progenitor cell populations (Figure 13A-E). Furthermore, we did not observe any differences in monocyte and neutrophil cell death following *in vivo* infection with ST (Figure 13F & 13G).

Inflammatory cell death following infection has often been thought to be a protective mechanism to fight intracellular pathogens.[90] Pyroptosis, a type of programmed inflammatory cell death, is mediated by caspase-1, which also activates IL-1β.[91] Therefore, we next aimed to determine whether the production of IL-1β may be altered with the *p.G2019S* mutation. Pro-IL-1β is produced in response to activation of PRRs, a step often referred to as priming, but a further PAMP must be encountered to induce the processing and secretion of active IL-1β.[92] Therefore, in order to promote the production of IL-1β during infection with ST, we first primed cells with LPS [10 ng/mL] overnight. The next day, cells were infected with ST-WT. To assess cell death, we used Neutral Red, a cell-based assay of lysosomal activity commonly used as a cell viability assay. We evaluated cell viability after 6 hours of infection with ST-WT in LPS-primed BMDMs and BMDCs. We found that GS BMDMs and BMDCs showed similar levels of cell death compared to WT cells (Figure 14A & 14B). Supernatants were also collected at 3- and

6-hours post-infection with 1 MOI ST-WT, and ELISA was used to evaluate IL-1β secretion by monocytes, neutrophils, BMDMs, and BMDCs. Aligning with our previous findings related to the production of cytokines and cell death, we did not notice any substantial differences in the secretion of IL-1β between WT and GS monocytes, neutrophils, macrophages, or DCs (Figure 13C-F).

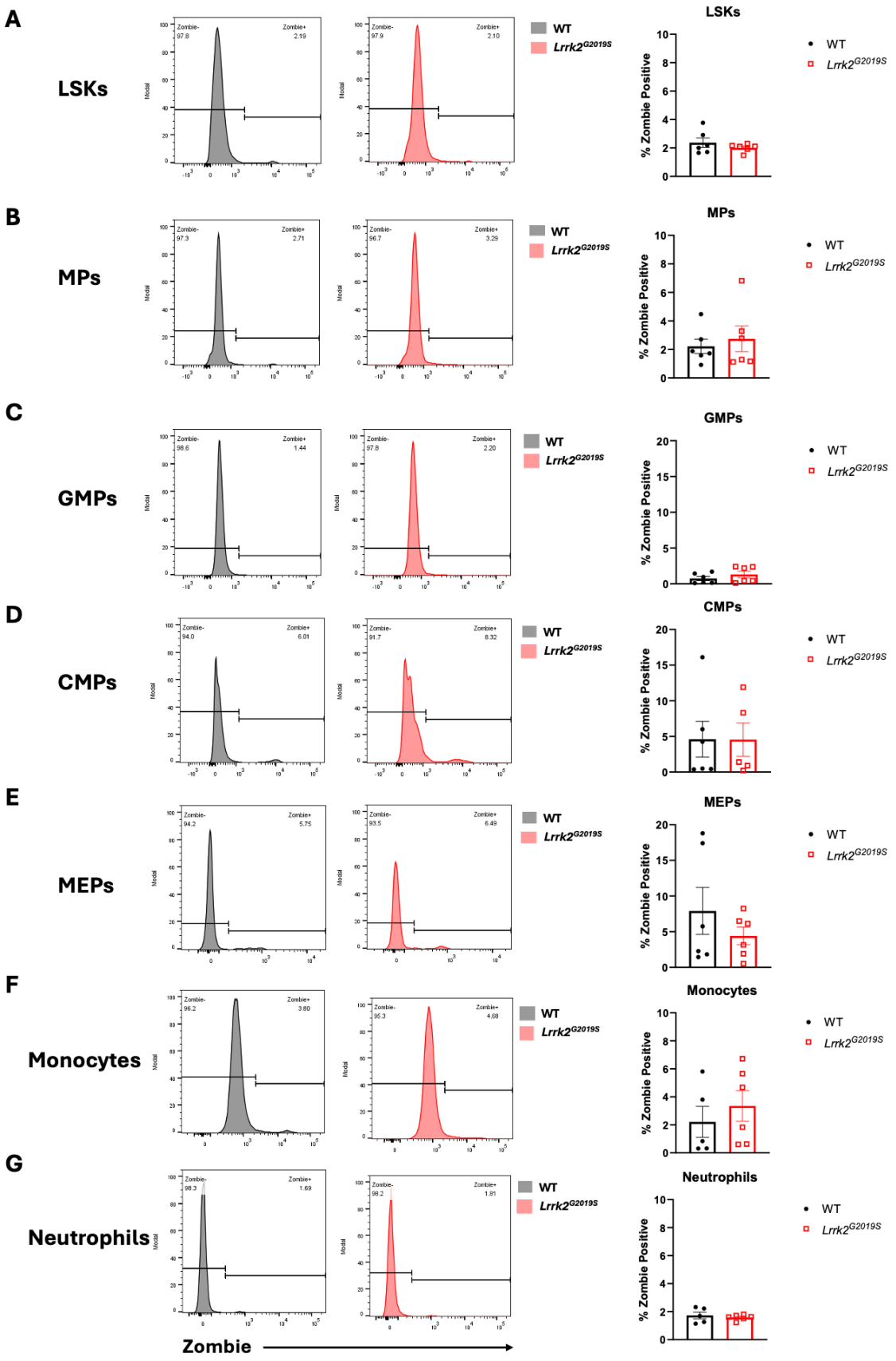
A
LSKs
B
MPs
C
GMPs
D
CMPs
E
MEPs
F
Monocytes
G
Neutrophils
WT
Lrrk2G2019S
% Zombie Positive
Zombie

Figure 13. *Lrrk2*^{G2019S} mutation does not alter hematopoietic progenitor and myeloid cell death in mice infected with ST. 5 dpi with ST, BM cells were isolated from WT and *Lrrk2*^{G2019S} KI mice. Cells were stained with Zombie Viability Dye and cell surface markers to measure the proportion of dead cells in various hematopoietic progenitor and myeloid cell populations. Representative Zombie histograms, and plots of the percentage Zombie^{+} cells are shown for LSK **(A),** MP (**B**), GMP (**C**), CMP (**D**), MEP (**E**), monocyte (**F**), and neutrophil (**G**) cell populations. All graphs depict mean ± SEM (n = 6 for LSKs, MPs, GMPs, CMPs, MEPs; n = 5 for monocytes and neutrophils).

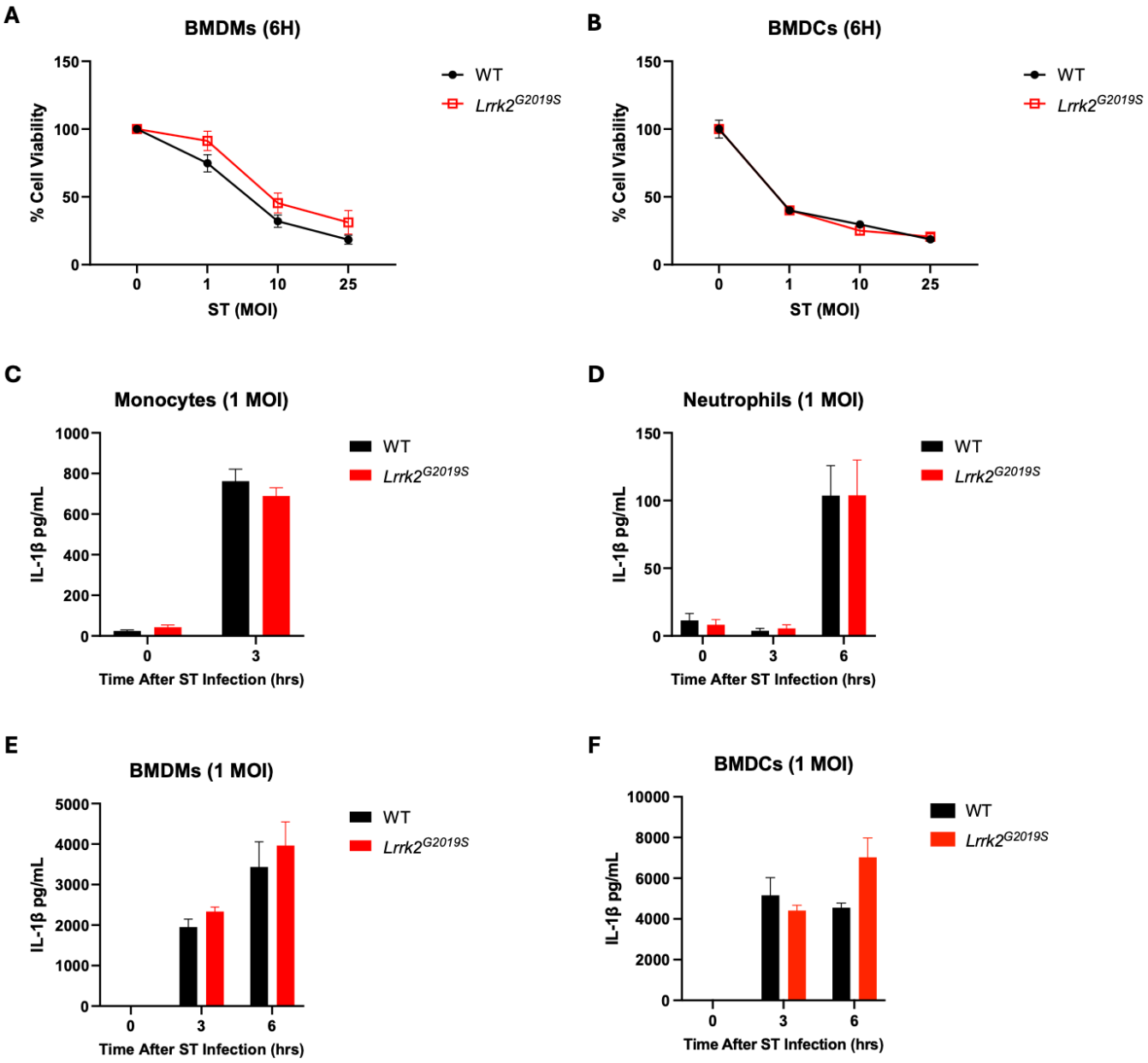
A
BMDMs (6H)
% Cell Viability
150
100
50
0
0
1
10
25
ST (MOI)
WT
Lrrk2G2019S
B
BMDCs (6H)
% Cell Viability
150
100
50
0
0
1
10
25
ST (MOI)
WT
Lrrk2G2019S
C
Monocytes (1 MOI)
IL-1β pg/mL
1000
800
600
400
200
0
0
3
Time After ST Infection (hrs)
WT
Lrrk2G2019S
D
Neutrophils (1 MOI)
IL-1β pg/mL
150
100
50
0
0
3
6
Time After ST Infection (hrs)
WT
Lrrk2G2019S
E
BMDMs (1 MOI)
IL-1β pg/mL
5000
4000
3000
2000
1000
0
0
3
6
Time After ST Infection (hrs)
WT
Lrrk2G2019S
F
BMDCs (1 MOI)
IL-1β pg/mL
10000
8000
6000
4000
2000
0
0
3
6
Time After ST Infection (hrs)
WT
Lrrk2G2019S

Figure 14. *Lrrk2*^{G2019S} mutation does not alter myeloid cell death or production of IL-β in mice infected with ST. (A-B) BMDMs (**A**; n = 3) and BMDCs (**B**; n = 2) cultured from WT and *Lrrk2*^{G2019S} KI mice were primed overnight with LPS [10 ng/mL]. The following day, primed cells were infected with ST-WT for 6 h at various MOIs. Cell viability was assessed by Neutral Red assay. (**C-F)** Monocytes (**C**; n = 3), neutrophils (**D**; n = 2); BMDMs (**E**; n = 3); BMDCs (**F**; n = 1) purified from WT and *Lrrk2*^{G2019S} BM cells were primed overnight with LPS [10 ng/mL] to stimulate the production of pro-IL-1β. The next day, cells were infected with ST-WT and cell supernatants were collected at 3- and 6-hours post infection. The secretion of IL-1β was measured in cell supernatants using sandwich ELISAs. All graphs depict mean ± SEM (unpaired two-tailed t-test; *$p < 0.05$).

3.3. *Lrrk2*^{G2019S} mutation enhances resistance to ST infection in neutrophils

3.3.1. Enhanced LRRK2 kinase activity promotes better control of ST infection in neutrophils

As our results indicated that the *p.G2019S* mutation did not affect the secretion of cytokines or cell death, we subsequently investigated if the enhanced resistance to ST in the BM might be due to a greater intrinsic ability of GS myeloid cells to fight infection. To determine which cell types might be most involved, we isolated BMDCs, BMDMs, monocytes, and neutrophils from WT and GS BM cells. To observe bacterial burden, we infected myeloid cells with 10 MOI ST-Δ*invA*. The mutation in the *invA* gene of ST prevents cell death from occurring, while intracellular replication is not affected. We opsonized the ST-Δ*invA* prior to infection to improve phagocytic uptake of the bacteria. Following infection at various time points, we lysed the cells and plated the cell lysates on LB-agar-streptomycin plates to allow for the selective growth of ST-Δ*invA*. Our results indicated that GS neutrophils show a significant reduction in bacterial burden, compared to WT neutrophils (Figure 15D). However, we did not observe any differences in the bacterial burden of GS monocytes, macrophages, and DCs, compared to WT cells (Figure 15A-C).

To further determine if the enhanced resistance to ST in neutrophils was due to increased LRRK2 kinase activity associated with the *Lrrk2*^{G2019S} mutation, we used another strain of mice that harboured the *Lrrk2*^{D1994S} mutation. The *p.D1994S* mutation of *Lrrk2* leads to a kinase-dead form of LRRK2. Following the same protocol as described above, we noticed that neutrophils purified from *Lrrk2*^{D1994S} mice showed a significant increase in the ST bacterial burden 2 hours post-infection, compared to WT neutrophils (Figure 15E). This result indicates that the reduced bacterial burden observed in GS neutrophils is dependent on increased LRRK2 kinase activity.

Our next goal was to investigate whether the enhanced resistance to infection with ST of GS neutrophils was specific to ST, a Gram-negative intracellular bacterium, or if the results would translate to another infection model. To study this, we used LM, a Gram-positive intracellular bacterium. Similar to infection with ST, LM was opsonized prior to infection, and cells were infected at 10 MOI. After 2 hours of infection, GS neutrophils demonstrated a significant reduction in the LM bacterial burden, compared to WT neutrophils (Figure 15F).

Together, these results indicate that neutrophils might be the myeloid cell type most involved in the improved control of ST in the BM compartment of GS mice. Furthermore, we were able to show that this enhanced resistance was dependent on LRRK2 kinase activity. GS neutrophils appear to have a stronger antimicrobial response, as the enhanced resistance also translated to a model using a different bacterium, LM.

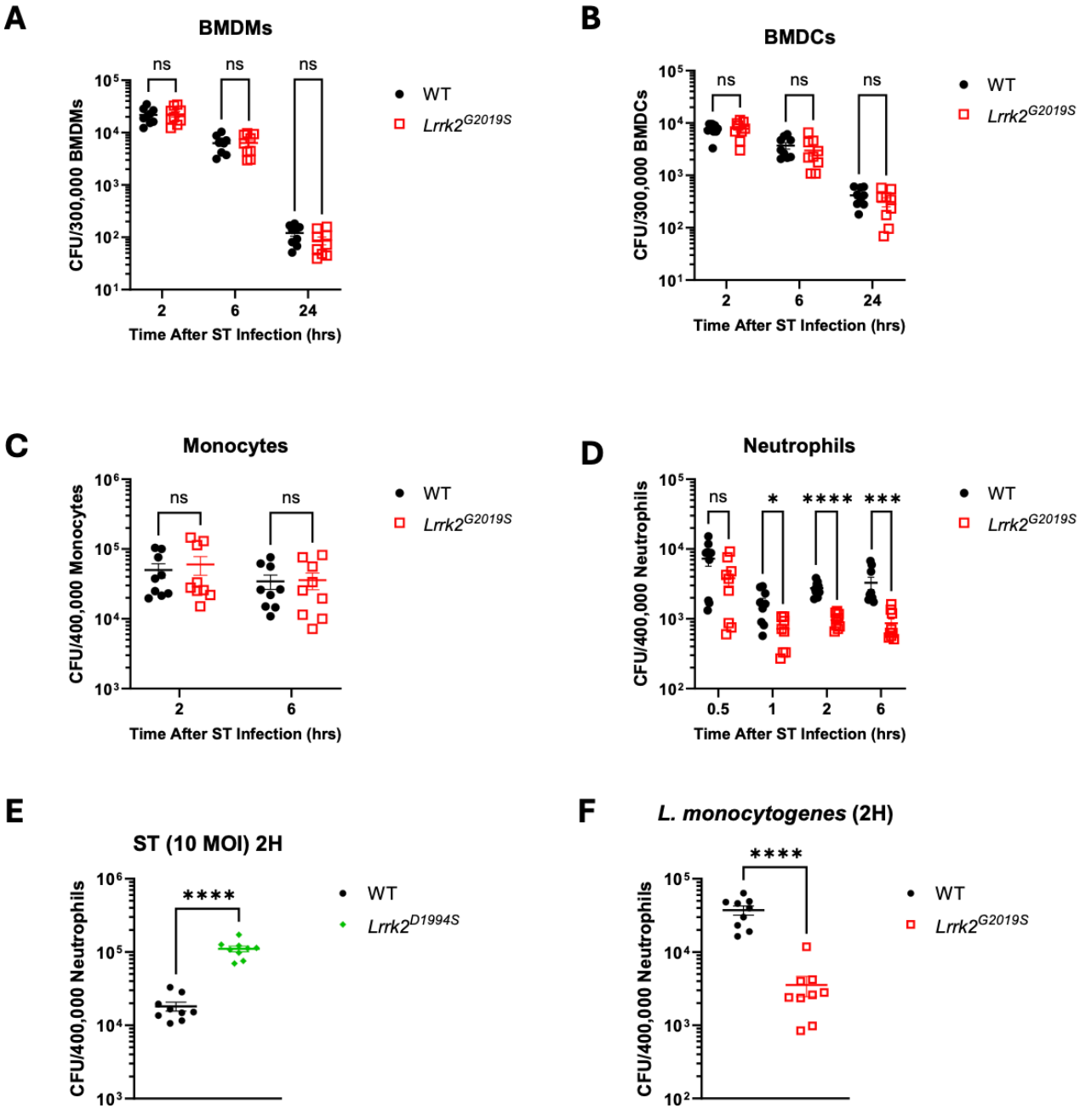
A
BMDMs
ns
ns
ns
CFU/300,000 BMDMs
Time After ST Infection (hrs)
WT
Lrrk2G2019S
B
BMDCs
CFU/300,000 BMDCs
C
Monocytes
CFU/400,000 Monocytes
D
Neutrophils
*
****
***
CFU/400,000 Neutrophils
E
ST (10 MOI) 2H
Lrrk2D1994S
F
L. monocytogenes (2H)

Figure 15. Enhanced LRRK2 kinase activity promotes better control of ST in purified neutrophils. (A-D) BMDMs (**A**), BMDCs (**B**), monocytes (**C**) and neutrophils (**D**) isolated from BM cells of WT and *Lrrk2*^{G2019S} mice were infected with 10 MOI opsonized ST-Δ*invA in vitro*. (**E**) Purified neutrophils from WT and *Lrrk2*^{D1994S} BM cells were infected with 10 MOI ST-Δ*invA in vitro* for 2 hours. (**F)** Purified neutrophils from WT and *Lrrk2*^{G2019S} BM cells were infected with 10 MOI opsonized LM for 2 hours. CFU were counted as a measure of bacterial burden. Data is plotted as mean ± SEM (two-way ANOVA and unpaired two-tailed t-test; *$p < 0.05$, ***$p < 0.001$, ****$p < 0.0001$).

3.3.2. WT and *Lrrk2*^{G2019S} neutrophils show similar levels of phagocytosis

To confirm if the observed difference in bacterial burden between GS and WT neutrophils was due to an enhanced ability of the cells to control infection, and not due to a difference in bacterial uptake, we first evaluated the phagocytic ability of WT and GS neutrophils. To do so, we employed a pHrodo-labelled *E. coli* bioparticle, which can be used to measure the level of phagocytosis via flow cytometry. This is a robust assay, as the fluorescent label on the bioparticle is pH sensitive. As a result, the bioparticles will only become fluorescent once they have reached the low pH of the lysosome (excluding any bacteria that has not entered the cell). Our results indicated that the percentage of actively phagocytosing neutrophils is similar between WT and GS cells (Figure 16A). To confirm these results, we also conducted a CFU experiment, where purified neutrophils were infected with ST-Δ*invA in vitro* and cell lysates were plated 15 minutes following infection to observe bacterial burden. The short infection time allows for an indication of bacterial uptake. Similarly, our results showed no difference in ST CFU at 15 minutes following infection between WT and GS neutrophils (Figure 16B). Together, these results confirmed that the reduced bacterial burden of ST observed in GS neutrophils was not due to phagocytosis, and that other neutrophil effector functions might be involved.

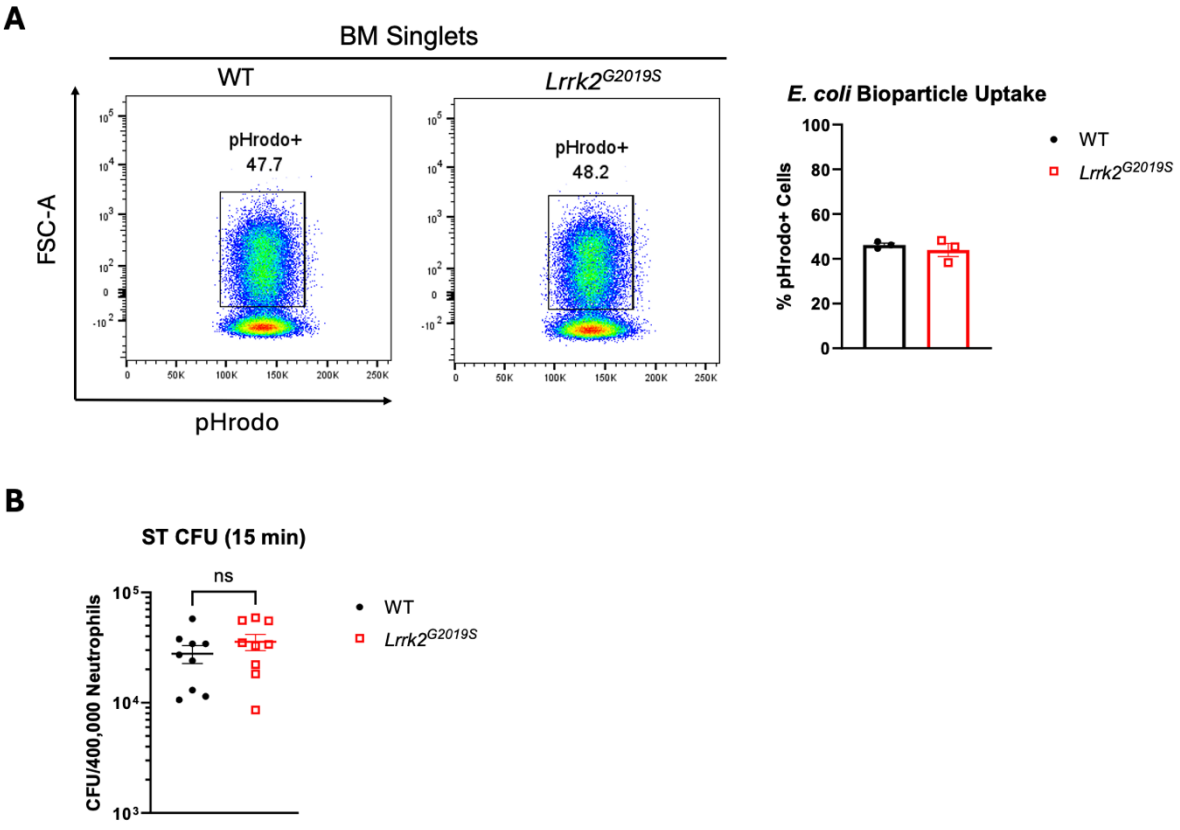
A
BM Singlets
WT
Lrrk2G2019S
pHrodo+
47.7
pHrodo+
48.2
FSC-A
pHrodo
E. coli Bioparticle Uptake
% pHrodo+ Cells
WT
Lrrk2G2019S
B
ST CFU (15 min)
ns
CFU/400,000 Neutrophils
WT
Lrrk2G2019S

Figure 16. WT and *Lrrk2*^{G2019S} neutrophils show similar levels of phagocytosis. (A) WT and *Lrrk2*^{G2019S} neutrophils were incubated with opsonized pHrodo Deep Red *E. coli* bioparticles for 15 minutes and acquired on a flow cytometer. Data was analyzed on FlowJo software. Representative FACS plots and the percentage of phagocytic (pHrodo+) neutrophils are shown. (**B)** WT and *Lrrk2*^{G2019S} neutrophils were infected with 10 MOI opsonized ST-Δ*invA* for 15 minutes. Cells were rinsed 3 times to remove extracellular bacteria. CFU were counted as a measure of bacterial burden. Graphs depict mean ± SEM and were analyzed using two-tailed unpaired t-tests (n = 3).

3.3.3. *Lrrk2*^{G2019S} mutation promotes the production of ROS in myeloid cells

Stimulated neutrophils generate large amounts of ROS, which is an important player in their antibacterial response. As our results indicated that GS and WT neutrophils showed similar levels of phagocytosis, our next goal was to quantify the production of ROS. We used H_2DCFDA, a cell-permeant indicator capable of reacting with several types of reactive oxygen species, to measure the production of ROS in myeloid cells following *in vivo* infection with ST. Our results indicate that at day 5 post-infection with ST-WT, both monocytes and neutrophils from GS mice show a significantly higher fold change (relative to naïve cells) of H_2DCFDA MFI (measured via flow cytometry), compared to WT cells (Figure 17A & 17B).

To more specifically determine the species of ROS involved, we used L-012 and the Amplex Red Assay. L-012 sodium salt is a luminol-based probe that reacts with superoxide anion (O_2^-) to emit luminescence. We infected neutrophils from WT and GS mice with 10 MOI ST-Δ*invA* for 30 minutes, prior to addition of L-012. After adding L-012, we measured the luminescence intensity over a time course, and observed that neutrophils from both WT and GS mice produced higher levels of superoxide anion compared to their uninfected controls. Furthermore, neutrophils from GS mice produced significantly higher levels of superoxide anion than WT neutrophils in response to infection with ST (Figure 17C).

To measure the release of H_2O_2, we used the Amplex Red Assay. We infected neutrophils from WT and GS mice with 10 MOI ST-Δ*invA* for 30 minutes. After infection, we collected cell supernatants which were then used in the Amplex Red Reaction. We did not observe any differences in H_2O_2 production between WT and GS neutrophils following infection with ST (Figure 17D).

Overall, our results suggest that neutrophils from GS mice produce higher levels of ROS, aiding in their ability to fight bacterial infection. Specifically, we were able to demonstrate that neutrophils from GS mice produced higher levels of superoxide anion, but not H_2O_2, following *in vitro* infection with ST.

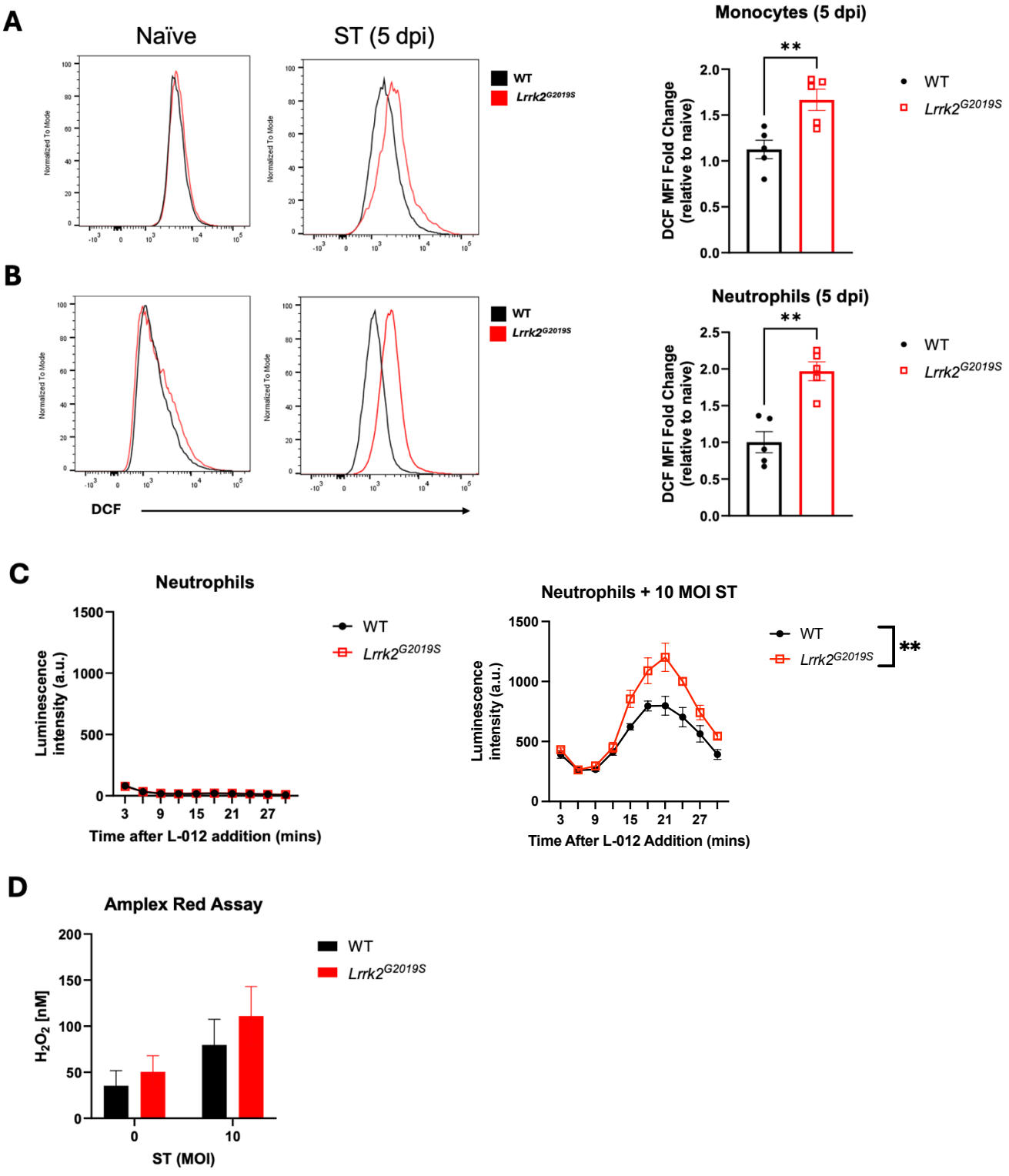
A
Naïve
ST (5 dpi)
Normalized To Mode
WT
Lrrk2G2019S
Monocytes (5 dpi)
**
DCF MFI Fold Change (relative to naive)
B
DCF
Neutrophils (5 dpi)
C
Neutrophils
Luminescence intensity (a.u.)
Time after L-012 addition (mins)
Neutrophils + 10 MOI ST
Time After L-012 Addition (mins)
D
Amplex Red Assay
H2O2 [nM]
ST (MOI)

Figure 17. *Lrrk2*^{G2019S} mutation promotes the production of ROS in myeloid cells following infection with ST. (A-B) BM cells extracted from WT and *Lrrk2*^{G2019S} mice 5 dpi with ST-WT were stained with H_2DCFHDA (DCF), a fluorescent ROS probe, and cell surface antibodies. Cells were acquired on a flow cytometer, and data was analyzed using FlowJo software. Representative DCF MFI histograms and fold increase relative to naïve mice are shown for monocytes **(A)** and neutrophils **(B)** (n = 5). **(C)** Neutrophils purified from WT and *Lrrk2*^{G2019S} BM cells were infected *in vitro* with 10 MOI opsonized ST-Δ*invA* for 30 mins. L-012 sodium salt (a luminal-based probe that reacts with superoxide anions) luminescence was measured using a microplate reader. Representative graphs are shown for control (uninfected) and infected neutrophils (n = 3). (**D**) Neutrophils purified from WT and *Lrrk2*^{G2019S} BM cells were infected with 10 MOI opsonized ST-Δ*invA* for 30 mins. Cell supernatants were collected in phenol red-free R8 and used in the Amplex Red Assay to assess the production of H_2O_2 (n = 4). Graphs depict mean ± SEM and were analyzed using two-tailed unpaired t-tests or two-way ANOVA (**p < 0.01).

3.3.4. *Lrrk2*^{G2019S} mutation promotes the transcription of genes involved in the production of ROS in neutrophils

To better determine the mechanisms behind the higher levels of ROS observed in GS neutrophils following infection with ST, we conducted RT-qPCRs to observe the mRNA levels of genes involved in both the production and detoxification of ROS.

As we observed higher production of superoxide anion in GS neutrophils, relative to WT neutrophils, our goal was to measure the transcription of genes responsible for encoding NADPH oxidase, the enzyme responsible for superoxide anion production. NADPH oxidase is made up of several components (Figure 2). The core component consists of gp91^{phox} and p22^{phox}, which are encoded by *Cybb* and *Cyba*, respectively. The activating subunits consist of p67^{phox}, p47^{phox}, and p40^{phox}, which are encoded by *Ncf2*, *Ncf1*, and *Ncf4*, respectively. Our results indicate that GS neutrophils show relatively higher transcription of *Cyba*, *Cybb*, and *Ncf2* at various timepoints of infection with 10 MOI ST- Δ*invA*, relative to WT neutrophils (Figure 18A, 18B, 18D). Although *Ncf1* and *Ncf4* do not show any significant differences between WT and GS neutrophils, there appears to be a slight increase in mRNA transcript levels of these genes in neutrophils from GS mice (Figure 18C and 18E). Interestingly, we also noticed that GS neutrophils had significantly higher *Nox1* mRNA transcripts, a gene that encodes another member of the NADPH oxidase family, at basal levels compared to WT neutrophils. However, this transcription was downregulated following infection with ST (Figure 18F). The high basal levels of *Nox1* might act to ensure a state of readiness for rapid response to infection, while its downregulation post-infection could act as a protective mechanism to maintain a balanced immune response. No differences were observed in the transcription of NOX3 or DUOX2, other proteins involved in NADPH-dependent production of ROS (Figure 18F).

After our results indicated higher transcription of genes involved in the production of ROS, we next sought to determine if the *Lrrk2*^{G2019S} mutation might impact the mRNA levels of genes involved in the detoxification of ROS. In addition to measuring genes encoding catalase, superoxide dismutase (SOD) 1 and 2, we also measured genes downstream of the nuclear factor erythroid 2-related factor-antioxidant response element (Nrf2-ARE) pathway. The Nrf2-ARE transcriptional pathway plays an important role in the regulation of genes that control the expression of proteins critical in the detoxification and elimination of ROS.[93] We did not observe any significant differences in the transcription of genes involved in the detoxification of ROS between WT and GS mice following infection with ST (Figure 18G).

Finally, we investigated a set of genes encoding several antibacterial peptides. *Mpo* encodes myeloperoxidase, which is commonly used by neutrophils to destroy invading pathogens by catalyzing the conversion of H_2O_2 to hypochlorous acid and other strong oxidants.[94] *Elane* encodes neutrophil elastase, a serine protease that also aids in the killing of pathogens.[95] *Lcn2* encodes Lipocalin-2, a protein capable of attenuating bacterial growth by preventing bacterial iron acquisition.[96] Transcript levels of *Mpo* and *Elane* were similar between WT and GS neutrophils, both at a basal level and following a 2 hour infection with 10 MOI ST-Δ*invA* (Figure 18F). The transcription of *Lcn2* appeared to be higher at a basal level in GS neutrophils, and was significantly upregulated following infection with ST, compared to WT neutrophils (Figure 18F).

Overall, our findings suggest that the *Lrrk2*^{G2019S} mutation possibly leads to enhanced levels of ROS during infection with ST through the upregulation of several genes involved in the production of ROS. However, the hyperactive kinase activity does not appear to impact the detoxification of ROS.

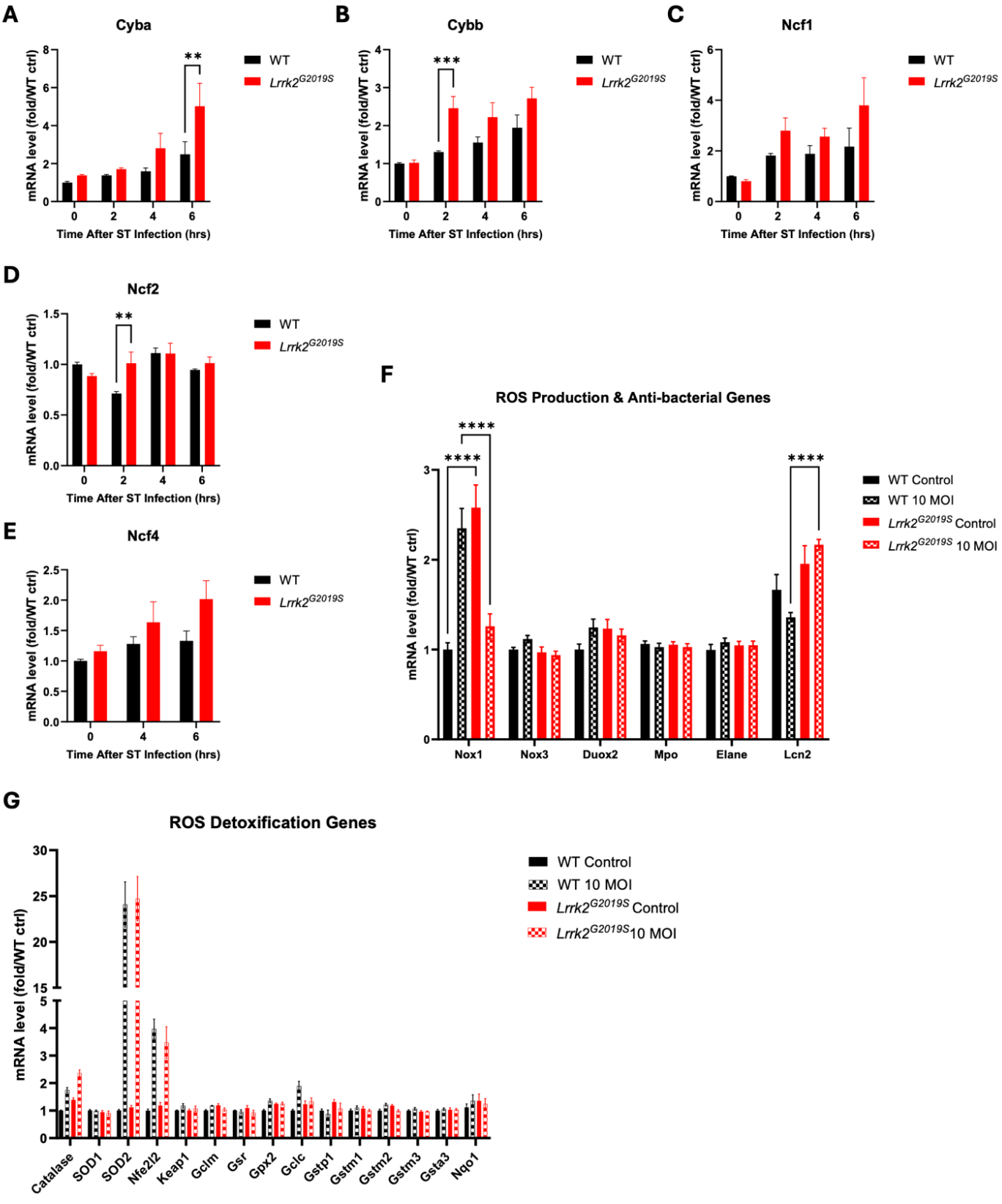
A
Cyba
mRNA level (fold/WT ctrl)
Time After ST Infection (hrs)
WT
Lrrk2G2019S
**
B
Cybb
***
C
Ncf1
D
Ncf2
E
Ncf4
F
ROS Production & Anti-bacterial Genes
****
WT Control
WT 10 MOI
Lrrk2G2019S Control
Lrrk2G2019S 10 MOI
Nox1
Nox3
Duox2
Mpo
Elane
Lcn2
G
ROS Detoxification Genes
Catalase
SOD1
SOD2
Nfe2l2
Keap1
Gclm
Gsr
Gpx2
Gclc
Gstp1
Gstm1
Gstm2
Gstm3
Gsta3
Nqo1

Figure 18. *Lrrk2*^{G2019S} mutation promotes the transcription of genes involved in the production of ROS in neutrophils following infection with ST. Neutrophils purified from WT and *Lrrk2*^{G2019S} BM cells were infected *in vitro* with 10 MOI opsonized ST-Δ*invA*. RNA was extracted from cells using the RNeasy RNA Extraction Kit. mRNA levels were determined by quantitative RT-PCR using GAPDH for normalization. mRNA levels were determined by Δ(ΔCt) method and are reported as fold change relative to WT untreated neutrophils. Transcript levels of *Cyba* (**A**), *Cybb* (**B**), *Ncf1* (**C**), *Ncf2* (**D**), and *Ncf4* (**E**) were measured at 2-6 hours after infection with ST. Transcript levels of a selection of genes involved in the production and detoxification of ROS, as well as genes that encode antimicrobial peptides were measured at 2 hours post-infection with ST (**F & G**). Graphs depict mean ± SEM and were analyzed using two-way ANOVAs (n = 3; **p < 0.01; ***p < 0.001, ****p < 0.0001).

3.3.5. Inhibition of ROS abrogates the enhanced *Lrrk2*^{G2019S}-mediated control of ST infection in neutrophils

As our results indicated that GS neutrophils demonstrated higher production of ROS compared to WT neutrophils, our next aim was to confirm that this effect was responsible for the enhanced control of ST observed in GS neutrophils. To do so, we purified neutrophils from WT and GS mice, and treated the neutrophils with various inhibitors of ROS for an hour prior to infection with 10 MOI opsonized ST-Δ*invA*. The inhibitors were also supplied throughout the duration of the 2-hour infection. *N*-acetyl-L-cysteine (NAC), an antioxidant that acts by increasing the cellular pool of free radical scavengers, reduced the difference in bacterial burden between WT and GS neutrophils, leading to no significant differences between the two genotypes in the presence of NAC (Figure 19A). Meanwhile, MitoTEMPO, a mitochondria-targeted antioxidant, also appeared to slightly return bacterial burden of GS neutrophils to WT levels, but a difference nevertheless remained (Figure 19B). Furthermore, when neutrophils were treated with apocynin, an inhibitor of NADPH-oxidases, the enhanced clearance of ST in GS neutrophils was lost in a dose-dependent manner (Figure 19C). We also tested sivelestat, an inhibitor of neutrophil elastase. We did not observe any impact of neutrophil elastase inhibition on the bacterial burden of GS neutrophils, suggesting that neutrophil elastase is likely not a key player in the reduced ST bacterial burden observed in GS neutrophils (Figure 19D).

Together, our results indicate that increased production of ROS in *Lrrk2*^{G2019S} neutrophils contributes to the reduced bacterial burden observed, compared to WT neutrophils.

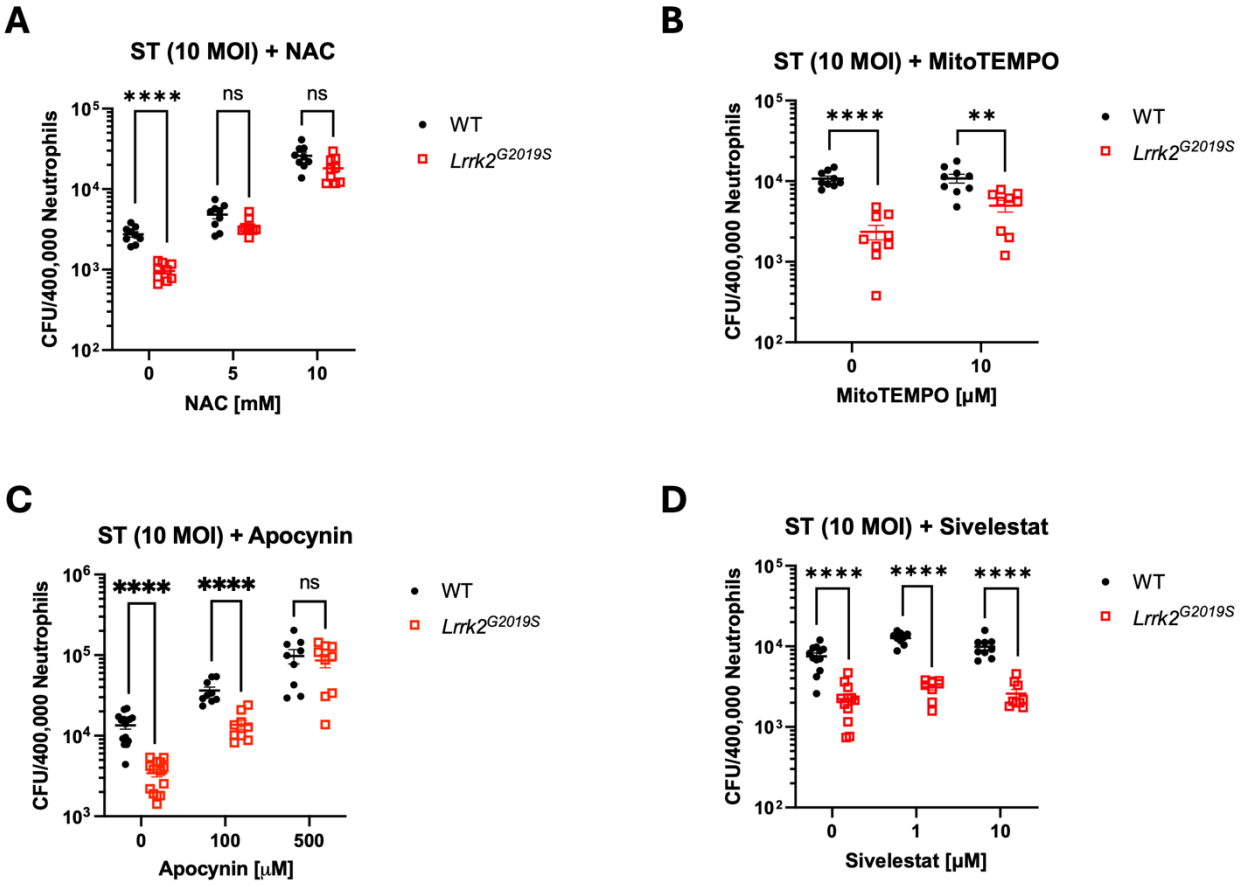
A
ST (10 MOI) + NAC
CFU/400,000 Neutrophils
10^5
10^4
10^3
10^2
****
ns
ns
0
5
10
NAC [mM]
WT
Lrrk2G2019S
B
ST (10 MOI) + MitoTEMPO
CFU/400,000 Neutrophils
10^5
10^4
10^3
10^2
****
**
0
10
MitoTEMPO [µM]
WT
Lrrk2G2019S
C
ST (10 MOI) + Apocynin
CFU/400,000 Neutrophils
10^6
10^5
10^4
10^3
****
****
ns
0
100
500
Apocynin [µM]
WT
Lrrk2G2019S
D
ST (10 MOI) + Sivelestat
CFU/400,000 Neutrophils
10^5
10^4
10^3
10^2
****
****
****
0
1
10
Sivelestat [µM]
WT
Lrrk2G2019S

Figure 19. ROS inhibition abrogates the enhanced control of ST in *Lrrk2*^{G2019S} neutrophils. Neutrophils purified from WT and *Lrrk2*^{G2019S} BM cells were infected *in vitro* with 10 MOI opsonized ST-Δ*invA* for 2H. One hour prior to, and during infection, cells were treated with *N*-acetyl-L-cysteine (NAC) **(A),** MitoTEMPO **(B),** apocynin **(C)** or sivelestat **(D).** Graphs depict mean ± SEM and were analyzed using two-way ANOVAs (n = 3; **p < 0.01, ****p < 0.0001).

4. DISCUSSION

LRRK2 is a multi-domain protein kinase implicated in various cellular processes, such as autophagy, mitochondrial function, and endocytosis, with significant roles in both the central nervous system and the immune system.[97] LRRK2 first came to prominent attention when it was discovered that mutations in the *Lrrk2* gene were associated with autosomal dominant inherited PD. Among these mutations, the *p.G2019S* mutation, located within the protein kinase domain, is one of the most common genetic determinants of PD.[98] GWAS have further linked mutations in *Lrrk2* to CD and leprosy – both of which heavily involve the immune system.[75,83,84] LRRK2 is highly expressed in immune tissues and cells, and this expression is regulated by immune stimulation.[72,73] LRRK2 has also been biochemically linked to several pathways involved in immune and inflammatory responses.[71] There are contrasting reports between the effects of LRRK2 kinase activity during different bacterial infections, with LRRK2 kinase activity enhancing the restriction of some bacteria, and increasing the susceptibility to infection for others.[72,86,88] The agonistic *Lrrk2*^{G2019S} mutation has previously been shown to promote better control of infection with ST in mice; however, the underlying mechanisms and cell types that promote better bacterial clearance remain to be elucidated. We hypothesized that *Lrrk2*^{G2019S} mutation modulates the expansion and function of myeloid cells, which confers better control of ST in mice.

4.1. Impact of *Lrrk2*^{G2019S} mutation on the bone marrow compartment during infection with ST

Previous work has suggested that *Lrrk2*^{G2019S} mutation promotes better control of systemic infection with ST in mice.[72] Shutinoski and colleagues were able to show a significant reduction in the bacterial burden in spleens of *Lrrk2*^{G2019S} mice in comparison to WT mice following an

intravenous challenge with ST.[72] Liu et al. further demonstrated that *Lrrk2*$^{-/-}$ mice had significantly higher ST bacterial loads in the spleen, peritoneal cavity, and blood following intraperitoneal injection.[86] Since it has been shown that LRRK2 expression is relatively high in the BM compartment and immune cells, both critical aspects of the host response to infection, we aimed to determine whether the *Lrrk2*^{G2019S} mutation would also enhance resistance to infection with ST in the BM compartment. We observed that BM cells from *Lrrk2*^{G2019S} mice showed a significant reduction in the ST bacterial burden compared to WT mice (Figure 4A) following a systemic infection with ST, supporting the idea that the cells in the BM compartment may be responsible for the enhanced bacterial control that is observed in *Lrrk2*^{G2019S} mice.

Hematopoiesis is a critical process that occurs in the BM to generate and replenish the blood. As our results indicated a protective role for *Lrrk2*^{G2019S} in the BM compartment, we then wondered if the *Lrrk2*^{G2019S} mutation might modulate hematopoiesis in the BM at a steady state. Our results indicate that the overall BM cell numbers, HSPC, and mature myeloid cell numbers are similar between WT and *Lrrk2*^{G2019S} naïve mice (Figure 7 & Figure 8). These results are similar to findings from Park et al., who also showed no differences in the number of peripheral myeloid cells between WT rats and rats harbouring the human *Lrrk2*^{G2019S} gene; however, they did demonstrate lower numbers of BM myeloid progenitors using colony-forming assays in *Lrrk2*^{G2019S} transgenic rats at a steady state.[99]

It is well established that systemic infections evoking inflammatory signals can give rise to emergency hematopoiesis. During this process, pathogens can be sensed by PRRs on HSPCs, triggering induced mobilization of HSPCs to replenish consumed short-lived mature hematopoietic immune effector cells, enhancing the overall host defense.[21] Although we observed similar hematopoietic cell numbers at a steady state between WT and *Lrrk2*^{G2019S} mice,

we then wondered if the *Lrrk2*^{G2019S} mutation might promote emergency hematopoiesis following systemic infection with ST. Indeed, we report significantly higher BM cell numbers in *Lrrk2*^{G2019S} mice, compared to WT mice, at 5 days-post infection with ST (Figure 9A). We also observed a significantly greater fold increase (relative to naïve mice) of LSKs in *Lrrk2*^{G2019S} mice, compared to WT mice (Figure 9B). Additionally, the *p.G2019S* mutation promoted maintenance of myeloid cells, especially neutrophils, during infection with ST (Figure 10), indicating that hyperactive LRRK2 kinase activity acts to promote hematopoietic cell expansion in response to infection with ST. Although we did not notice differences in the fold change (relative to naïve mice) of MPs, hematopoiesis is a transient process during infection, and the *Lrrk2*^{G2019S} mutation may influence MP numbers at a different stage of infection. As previously reviewed by Manz et al., *de novo* generation of neutrophils is especially important during systemic infection, and neutropenia is often associated with considerable lethality from complications relating to infection.[100] This supports the idea that the increased maintenance of neutrophil cell numbers observed in *Lrrk2*^{G2019S} mice likely plays a significant role in the enhanced bacterial clearance during systemic infection with ST. Importantly, Moehle et al. were able to demonstrate that the *Lrrk2*^{G2019S} mutation results in an increase in the myeloid cell chemotactic response, both *in vitro* and *in vivo* in response to thioglycolate injections in the peritoneum in rats.[101] This suggests that in addition to showing greater hematopoietic expansion, *Lrrk2*^{G2019S} mutant cells may also be more efficient at homing to sites of infection, and this idea needs to be further investigated in the *Salmonella* infection model.[101]

Our results align with previous findings in an acute and chronic colitis model where *Lrrk2*^{G2019S} transgenic rats displayed increased myeloid cell numbers relative to control rats.[99] Further supporting this, another study found an overall increase in leukocytes in the colon during

colitis of *Lrrk2*^{G2019S} mice, compared to WT mice.[102] In a model more similar to our study, Park et al. also demonstrated significantly higher levels of myeloid cell numbers in the blood of *Lrrk2*^{G2019S} transgenic rats in a systemic inflammation model induced with LPS injection, compared to control rats.[99] Using ST to induce peritoneal inflammation, Liu and colleagues demonstrated that *Lrrk2*$^{-/-}$ mice showed a significant reduction in total peritoneal cells and neutrophils from peritoneal fluid after infection.[86] Together, our results along with findings from previous studies suggest that LRRK2 kinase activity might be an important regulator of hematopoiesis during the inflammatory response to infection, but the exact mechanisms remain to be determined.

LRRK2 is involved in many important cell signalling mechanisms, including the MAPK pathway, which is known to regulate hematopoiesis and myeloid cell maturation.[103–106] However, the current understanding of the impact of LRRK2 on MAPK signalling is debated in the literature. For example, White et al. demonstrated that the phosphorylation of some proteins involved in the MAPK pathway is reduced in cell extracts from patients with G2019S-associated PD, relative to healthy controls.[107] Despite this, the kinase domain of LRRK2 shows close similarity to MAPKKKs (MAPK kinase kinases), implicating a possible function of LRRK2 within the MAPK cascades.[108] Through *in vitro* kinase assays, LRRK2 has indeed been found to phosphorylate different components of the MAPK pathway, including MAPK kinase 3/6 (MKK3/6) and MKK4/7, and the *Lrrk2*^{G2019S} mutation showed significantly higher phosphorylation of MKK6 compared to WT LRRK2.[109] Therefore, aberrant regulation of MAPK signaling pathways due to abnormal LRRK2 activity could potentially play a role in the myeloid cell responses to inflammation and infection. Further studies investigating these effects may

enhance our understanding of the molecular mechanisms through which *Lrrk2*^{G2019S} promotes better control of infection.

4.2. *Lrrk2*^{G2019S} mutation improves the intrinsic ability of neutrophils to control infection with ST

Although we had established that the *Lrrk2*^{G2019S} mutation showed enhanced resistance against ST in the BM of systemically infected mice, we strove to determine which specific BM cell types were most responsible for this protection. As our data indicated that LRRK2 expression was higher in myeloid (CD11b^{+}) versus non-myeloid (CD11b^{-}) cells (Figure 6D), we focused our studies on the myeloid compartment, specifically BMDMs, BMDCs, monocytes, and neutrophils. Our results indicated that the *p.G2019S* mutation did not have any impact on the secretion of cytokines by myeloid cells in response to infection with ST or stimulation with various TLR agonists (Figures 11 & 12). This finding suggests that instead, myeloid cells may be intrinsically better at controlling infection with ST. Our data aligns with findings from previous studies that also showed *Lrrk2*^{G2019S} mutation did not alter cytokine secretion following LPS stimulation in murine macrophages.[72,101] However, it is important to note that other studies have shown increased TLR-stimulated production of cytokines in human monocytes and macrophages with the *Lrrk2*^{G2019S} mutation.[110]

Furthermore, we evaluated HSPC and myeloid cell death following *in vivo* and *in vitro* infection with ST. In host defence, inflammatory cell death can act as a protective mechanism by eliminating infected cells and alerting the host through danger signals and inflammatory mediators.[90] We did not observe any impact of the *p.G2019S* mutation on hematopoietic and myeloid cell death following infection with ST (Figures 13 & 14). Our results are contradictory to findings by Weindel et al., that showed *Lrrk2*^{G2019S} macrophages had significantly greater

levels of cell death in response to infection with ST.[89] Weindel et al. also reported lower levels of IL-1β secretion in *Lrrk2*^{G2019S} macrophages (while we reported no differences); however, this was using an Mtb infection model.[89] Conversely, another study indicated a protective role for LRRK2 during ferroptosis (an iron-dependent regulated cell death pathway) in RAW macrophages, highlighting that the role of LRRK2 in immune cell death is not clear.[111]

Interestingly, we found that isolated *Lrrk2*^{G2019S} neutrophils showed a significant reduction in the bacterial burden of ST following *in vitro* infection (Figure 15D), while no differences were observed in purified monocytes, or differentiated BMDMs or BMDCs (Figure 15 A-C). These results indicate that neutrophils may be primarily responsible for the increased resistance of *Lrrk2*^{G2019S} mice to infection with ST. To further test that these results were dependent on the kinase activity of LRRK2, we purified neutrophils from *Lrrk2*^{D1994S} mice. The *p.D1994S* mutation of *Lrrk2* results in a kinase inactive form of LRRK2. Here we observed that the bacterial burden of the *Lrrk2*^{D1994S} neutrophils was significantly higher than that of WT neutrophils following infection with ST (Figure 15E), confirming that the enhanced resistance of *Lrrk2*^{G2019S} neutrophils was due to increased kinase activity. Furthermore, we wondered if the effects we observed were specific to ST, or whether the hyperactive LRRK2 kinase activity was promoting a more general antibacterial response. To test this, we infected WT and *Lrrk2*^{G2019S} neutrophils with LM, and found that our results were consistent between ST and LM infection (Figure 15F), indicating that increased LRRK2 kinase activity promotes an enhanced antibacterial response in isolated neutrophils. This result strengthened our previous finding that the *Lrrk2*^{G2019S} mutation promoted greater neutrophil expansion following *in vivo* infection with ST, suggesting that *Lrrk2*^{G2019S} mice do not only have higher neutrophil cell numbers, but that these neutrophils also possess an intrinsic ability to mediate better control of bacterial infection.

4.2.1. *Lrrk2*^{G2019S} mutation promotes the production of ROS in neutrophils

With the knowledge that the *Lrrk2*^{G2019S} mutation results in enhanced resistance to ST in neutrophils, compared to the other myeloid cell types investigated, we next aimed to determine what molecular mechanism(s) might be involved. We initially wondered if the differences in CFU observed may be due to impaired phagocytic ability of *Lrrk2*^{G2019S} cells; however, our results robustly demonstrate that isolated WT and *Lrrk2*^{G2019S} neutrophils show similar levels of phagocytosis (Figure 16). Similarly, Moehle et al. have previously reported that LPS-stimulated WT and *Lrrk2*^{G2019S} macrophages show similar levels of phagocytosis of zymosan beads.[101] Conflicting results have been reported by Kim et al., who demonstrated that G2019S-KI microglia and BMDMs displayed increased engulfment of either zymosan beads or *E. coli* bioparticles both at a basal level and in a TLR-dependent manner.[112]

We observed no differences in the production of cytokines in neutrophils with the *p.G2019S* mutation, and in fact, the overall level of cytokines was much lower compared to other myeloid cell types tested. This is in line with the understanding in the literature that although neutrophils have the ability to produce cytokines following *in vitro* activation, neutrophils make fewer molecules of a given cytokine than monocytes/macrophages or lymphocytes do on a per-cell basis.[113,114] Depending on the cytokine, neutrophils are thought to possess 10-20 times less RNA than monocytes or lymphocytes, contributing towards the reduced production observed.[114] In addition to production of cytokines, neutrophils employ several mechanisms for effective bacterial clearance, such as the production of ROS, release of antimicrobial proteins and enzymes, and the formation of NETs. Importantly, the oxidative burst is the first line of defense against environmental pathogens, and neutrophils are one of the highest producers of ROS in the immune system.[50] ROS can further augment the overall antimicrobial response of neutrophils by

activating the release of granules, inducing the generation of NETs, and stimulating the production of pro-inflammatory cytokines.[50] With this in mind, we sought to determine whether the *p.G2019S* mutation of *Lrrk2* may promote increased production of ROS by ST-infected neutrophils. We first noticed that in BM cells isolated from mice that were infected *in vivo* with ST, *Lrrk2*^{G2019S} mice demonstrated higher production of ROS in both monocytes and neutrophils (Figure 17A & 17B). Our *in vivo* experiments utilized H_2DCFHDA, a probe commonly used to measure ROS levels via flow cytometry; however, it is not specific to particular ROS species, and it is recommended to be restricted to an initial assessment of a change in cellular redox state.[115] Therefore, to more specifically target which ROS species might be most involved, we used both L-012, a luminescent probe that reacts with superoxide anions, and the Amplex Red Assay, which measures H_2O_2 production. Interestingly, our results indicated that *Lrrk2*^{G2019S} purified neutrophils showed greater luminescence with L-012 in response to infection with ST but did not show any differences in H_2O_2 production (Figure 17C & 17D). Unlike H_2DCFHDA fluorescence, which is already present at high levels in myeloid cells without infection, L-012 luminescence is low in naïve cells, and significantly upregulated following infection. This finding highlights the important role of superoxide anions in the antibacterial response of myeloid cells. Overall, our findings suggest that neutrophils harbouring the *Lrrk2*^{G2019S} mutation produce significantly higher levels of ROS following systemic *in vivo* infection with ST, and specifically, higher levels of superoxide anions after *in vitro* infection with ST.

Oxidative stress is a key player in the degeneration of dopaminergic neurons in PD, and therefore, with the *p.G2019S* mutation being one of the most common genetic determinants of PD, the role of LRRK2 in the production of ROS has been extensively studied. Heo et al. demonstrated that LRRK2 is able to increase intracellular ROS levels and that the *p.G2019S*

mutation further enhances this effect in dopaminergic neurons.[116] Furthermore, mutations in LRRK2 that result in increased kinase activity, in particular the *p.G2019S* mutation, were shown to promote enhanced phosphorylation of peroxiredoxin 3 in a neuroblastoma cell line.[117] As peroxiredoxin 3 is an important detoxifying and reducing enzyme in the mitochondria, the $Lrrk2^{G209S}$ mutation led to greater ROS levels in the neuroblastoma cells.[117] Helton and colleagues recently showed that inhibition of the dimerization of LRRK2 was sufficient to decrease its kinase activity and inhibit the production of ROS in primary cortical neurons.[118]

The investigation into the role of LRRK2 in the production of ROS has not been limited to neurons. With the recent emphasis on the involvement of the immune system in the development of PD, and the knowledge surrounding the role of LRRK2 in the immune system, many studies have further evaluated the impact of LRRK2 on the production of ROS in immune cells. Recently, Weindel et al. found that $Lrrk2^{G2019S}$ BMDMs produced significantly higher levels of cellular ROS and mitochondrial superoxide following LPS treatment.[89] Further evidence, and closely related to our work, Shutinoski et al. demonstrated that both heterozygous $Lrrk2^{G2019S/WT}$ and homozygous $Lrrk2^{G2019S}$ BMDMs showed significantly higher production of ROS after infection with ST.[72] On the other hand, *Lrrk2* knock-out RAW 264.7 macrophage cells show significantly lower levels of ROS following LPS stimulation.[119] Taken together, these studies support our findings that increased LRRK2 kinase activity via the $Lrrk2^{G2019S}$ mutation is sufficient to induce greater production of ROS in response to infection with ST.

After discovering that neutrophils harbouring the $Lrrk2^{G2019S}$ mutation produced greater levels of ROS following infection with ST, we next worked to uncover the underlying mechanisms behind the increased ROS levels. It was possible that increased LRRK2 kinase

activity was either promoting the production of ROS, or inhibiting mechanisms that are engaged in the detoxification of ROS.

The Nrf2-ARE pathway acts to inhibit the progression of inflammation by controlling the expression of genes whose protein products are involved in the detoxification and elimination of reactive oxidants.[93] Previous studies have shown that the brains of *Lrrk2*-transgenic mice have decreased expression of Nrf2 and Nrf2 target genes compared to control mice, and that the knockdown of *Lrrk2* in neuroblastoma cells results in increased expression of Nrf2, suggesting that LRRK2 may act to increase ROS levels by inhibiting the ROS detoxification pathways.[120,121] We measured the transcript levels of genes encoding Keap1, Nrf2, and several downstream genes under the control of Nrf2. Our results indicated that at steady-state, and following infection with ST, there were no differences in the transcript levels of these genes between WT and *Lrrk2*^{G2019S} neutrophils (Figure 18G), suggesting that *Lrrk2*^{G2019S} mutation may not impact ROS detoxification in neutrophils, but might instead act to increase the production of ROS.

Stimulated neutrophils are intense physiological producers of superoxide radicals. Since the production of superoxide primarily occurs via NADPH oxidases in neutrophils, we wondered whether the *Lrrk2*^{G2019S} mutation results in greater transcription of NOX complexes.[122] The classical NOX found in neutrophils, NOX2, consists of several subunits, including the two membrane subunits (gp91^{phox} and p22^{phox}), three cytosolic subunits (p47^{phox}, p67^{phox}, and p40^{phox}) and the G-protein Rac.[123] In response to various stimuli, such as microbial products or cytokines, p47^{phox} (*Ncf1*), p67^{phox} (*Ncf2*), and p40^{phox} (*Ncf4*) associate in the cytosol and translocate to the cell membrane to interact with gp91^{phox} (*Cybb*) and p22^{phox} (*Cyba*), leading to the formation of the active NOX enzyme complex.[124] Meanwhile, Rac GTPases bind to NOX2 at the catalytic core, inducing the electron transfer and generation of superoxide anions.[124] NOX2 and its

components are critical during infection with ST in mice. In fact, *Cybb*$^{-/-}$ mice are hypersusceptible to infection with ST and high bacterial burden in the spleens of such mice were correlated with less ST killing in neutrophils and inflammatory monocytes.[125] As well, macrophages from *gp91*$^{-/-}$ mice exert significantly less antimicrobial activity to ST than WT control macrophages.[126] Interestingly, our results indicated that *Lrrk2*^{G2019S} neutrophils show significantly higher transcript levels of *Cyba*, *Cybb*, and *Ncf2* at various time points following infection with ST (Figure 18A, 18B, 18D). Although not significant, *Lrrk2*^{G2019S} neutrophils also appear to have slightly increased *Ncf1* and *Ncf4* transcript levels (Figure 18C, 18E). Together, these results indicate that the increased *Lrrk2* kinase activity acts to promote the transcription of the various components of the NOX complex. This likely contributes to the increased production of ROS levels that we observed in *Lrrk2*^{G2019S} myeloid cells.

To confirm that the increased production of ROS was indeed contributing to the observed resistance against infection with ST in *Lrrk2*^{G2019S} neutrophils, we employed several ROS scavengers/inhibitors. Our results suggest that in the presence of NAC, which acts as a ROS scavenger and precursor for glutathione biosynthesis, the *Lrrk2*^{G2019S}-mediated protection from ST in neutrophils was abrogated, and the bacterial burden returned to levels similar to that of WT neutrophils (Figure 19A). Furthermore, using apocynin, an inhibitor of NADPH oxidase that is thought to prevent the translocation of p47^{phox} from the cytosol to the membrane and prevent the assembly of the NOX enzyme, we also observed a loss of protection that was previously seen in *Lrrk2*^{G2019S} neutrophils (Figure 19C). The effect of apocynin appears to be dose-dependent, as the agonistic *Lrrk2* mutation remained protective at a lower concentration of apocynin. This may be due to the robust effect that the enhanced LRRK2 kinase activity has on increasing the production of ROS, thus requiring a higher concentration of apocyinin to effectively inhibit ROS

in the presence of *Lrrk2*^{G2019S} mutation. It is important to note that the ROS inhibitors and scavengers we used increased the bacterial burden of both WT and *Lrrk2*^{G2019S} neutrophils, compared to the control (no inhibitor present) samples. We suggest that this is due to an overall decrease in cellular ROS, which has important antibacterial effects, and thus an impaired ability of the cells to fight infection.

Despite our results providing a clear explanation for the increased ROS levels and enhanced protection against infection with ST observed in *Lrrk2*^{G2019S} neutrophils, the mechanisms underlying the upregulated transcription of NOX subunits remains to be elucidated. Several possible mechanisms can be postulated. In addition to LRRK2 being involved with the MAPK pathway, LRRK2 has also been implicated to affect the NF-κB pathway, which is one of the dominant pathways of gene transcription in immune cells. Several studies have shown that *Lrrk2* knock-down or genetic deletion in microglia reduced NF-κB transcriptional activity.[127,128] Moreover, Dzamko et al. showed that *Lrrk2*^{G2019S} carriers exhibit higher levels of peripheral NF-κB-dependent inflammatory cytokines compared to control subjects, highlighting that LRRK2 is likely involved in promoting pro-inflammatory NF-κB signalling.[129] Importantly, NF-κB is capable of regulating ROS through inducing the transcription of genes that are involved in both the detoxification of ROS and in the production of ROS. Specifically, transcription of the gp91^{phox} (*Cybb*) subunit has been shown to be controlled by NF-κB both in microglia and fibroblasts.[130] It would be interesting to see if similar regulation occurs in neutrophils, and whether NF-κB might be able to regulate the expression of other NOX2 subunits. Furthermore, using ChIP-Atlas, we were able to determine that that transcription factor PU.1 (*Spi1*) is associated with all the components of NOX2 in murine neutrophils, and several studies have shown that PU.1 is essential for promoter activity in NOX subunits.[131–133] Interestingly, in

addition to the function of PU.1 in NOX subunit transcription, this transcription factor is also a key regulator of hematopoietic cell differentiation. Although no studies, to our knowledge, have investigated the relationship between PU.1 and LRRK2, there are several ways that LRRK2 may interact with PU.1. Previous work has shown that the phosphorylation of PU.1 is important for the regulation of several hematopoietic and myeloid genes, which can enhance its capacity to activate the transcription of genes.[134,135] As LRRK2 is a kinase, and *Lrrk2*^{G2019S} mutation results in a hyperactive kinase, a route for future exploration could be to investigate a potential connection between LRRK2 kinase activity and PU.1 phosphorylation, possibly explaining both increased hematopoietic expansion and NOX2 transcription during infection with ST, as observed in our experiments. Additionally, Bonadies et al. demonstrated that NF-κB is able to activate PU.1 expression, and Etzrodt et al. were able to show that NF-κB signalling in response to TNF appears to regulate transcription of PU.1 in HSCs.[136,137] As previously discussed, LRRK2 has been thought to be involved in NF-κB signalling, introducing yet another way in which LRRK2 might be able to have a downstream effect on PU.1 regulation. However, our results did not reveal any impact of the *p.G2019S* mutation on the transcription of cytokines which are primarily driven by the NF-κB pathway, highlighting that the impact of LRRK2 on the production of ROS may be related to a separate mechanism.

Interestingly, Keeney et al. recently demonstrated that both nigrostriatal dopamine neurons and microglia from PD patients had significantly higher NOX2 activation compared to controls, and that NOX2 activation appeared to increase the LRRK2 kinase activity.[138] Therefore, it is possible that there could be a positive feedback loop occurring in our model, where hyperactive LRRK2 increases NOX levels, and the greater NOX activity further exacerbates LRRK2 kinase activity; however, further studies will need to be conducted.

In addition to the production of ROS, neutrophils also store several antimicrobial peptides, which are released from granules and into NETs following activation. One of these peptides, neutrophil elastase, is a protease that aids in the destruction of engulfed bacteria and is thus an important part of neutrophils' ability to control infection. As our results indicated *Lrrk2*^{G2019S} neutrophils showed enhanced resistance to infection with ST, we wondered if increased LRRK2 kinase activity may also affect neutrophil elastase. We measured the transcription of *Elane* (the gene that encodes neutrophil elastase) both prior to and after infection with ST but did not notice any significant differences between WT and *Lrrk2*^{G2019S} neutrophils (Figure 18F). As well, we used a common inhibitor of neutrophil elastase, sivelestat, but noticed that even in the presence of sivelestat, the bacterial burden in *Lrrk2*^{G2019S} neutrophils remained significantly lower than that of WT (Figure 19D), suggesting that neutrophil elastase is likely not a key player involved in the enhanced control of ST observed in *Lrrk2*^{G2019S} neutrophils. Collectively, our findings suggest that the *p.G2019S* mutation acts to promote the production of ROS in neutrophils, through enhancing the transcription of NADPH oxidase. Our results further indicate that the increased levels of ROS are critical for the reduced bacterial burden observed in *Lrrk2*^{G2019S} neutrophils, compared to WT cells.

5. CONCLUSION

The work presented in this thesis reveal novel insights into the mechanisms underlying the enhanced resistance of *Lrrk2*^{G2019S} KI mice to infection with ST. We have revealed that the *p.G2019S* mutation promotes better control of ST in the BM compartment. There was no impact of the *p.G2019S* mutation on hematopoietic progenitor and myeloid cell populations in naïve mice. However, the *Lrrk2*^{G2019S} mice showed enhanced HSC expansion and improved maintenance of mature myeloid cells, especially neutrophils, during infection with ST.

Further experiments revealed that the *p.G2019S* mutation did not impact the production of cytokines in myeloid cells following infection with ST. We also showed that WT and *Lrrk2*^{G2019S} mice had similar levels of hematopoietic progenitor and myeloid cell death following *in vivo* infection with ST. Using an *in vitro* method to promote inflammatory cell death during infection with ST, we did not observe any differences in the secretion of IL-1β or macrophage and DC death.

Our results also revealed that neutrophils, but not monocytes, macrophages, or DCs, showed a significant reduction in the bacterial burden of ST following *in vitro* infection. We confirmed that enhanced control of ST was due to the increased LRRK2 kinase activity in *Lrrk2*^{G2019S} neutrophils using a kinase dead *Lrrk2* mutant. Additionally, we discovered that the *p.G2019S* mutation was not only promoting better control of ST, but also of LM, in neutrophils. We were able to further show that the reduced bacterial burden was not due to a difference in phagocytosis between WT and *Lrrk2*^{G2019S} neutrophils. Instead, we successfully demonstrated that the *p.G2019S* mutation promotes the production of ROS in myeloid cells following *in vivo* infection with ST. More specifically, our results revealed that the *Lrrk2*^{G2019S} mutation enhances the production of superoxide anions in neutrophils but does not impact the production of H_2O_2.

Further supporting these results, we showed that the *p.G2019S* mutation promoted the transcription of genes encoding NADPH oxidase, the primary producer of superoxide anions. We did not observe any differences in the transcription of genes involved in the detoxification of ROS. Finally, our results confirmed that the increased production of ROS in *Lrrk2*^{G2019S} neutrophils is a key mechanism involved in the enhanced control of ST infection. We showed that in the presence of several inhibitors of ROS, the bacterial burden of *Lrrk2*^{G2019S} neutrophils returns to the level of WT neutrophils.

Overall, the results of this thesis provide a deeper understanding of the impact of *Lrrk2*^{G2019S} mutation on the BM compartment and innate immune response, and how it contributes to better control of ST (Figure 20). As the *p.G2019S* mutation has been associated with PD, it is conceivable that this mutation may function to augment the inflammatory response contributing to PD pathogenesis.

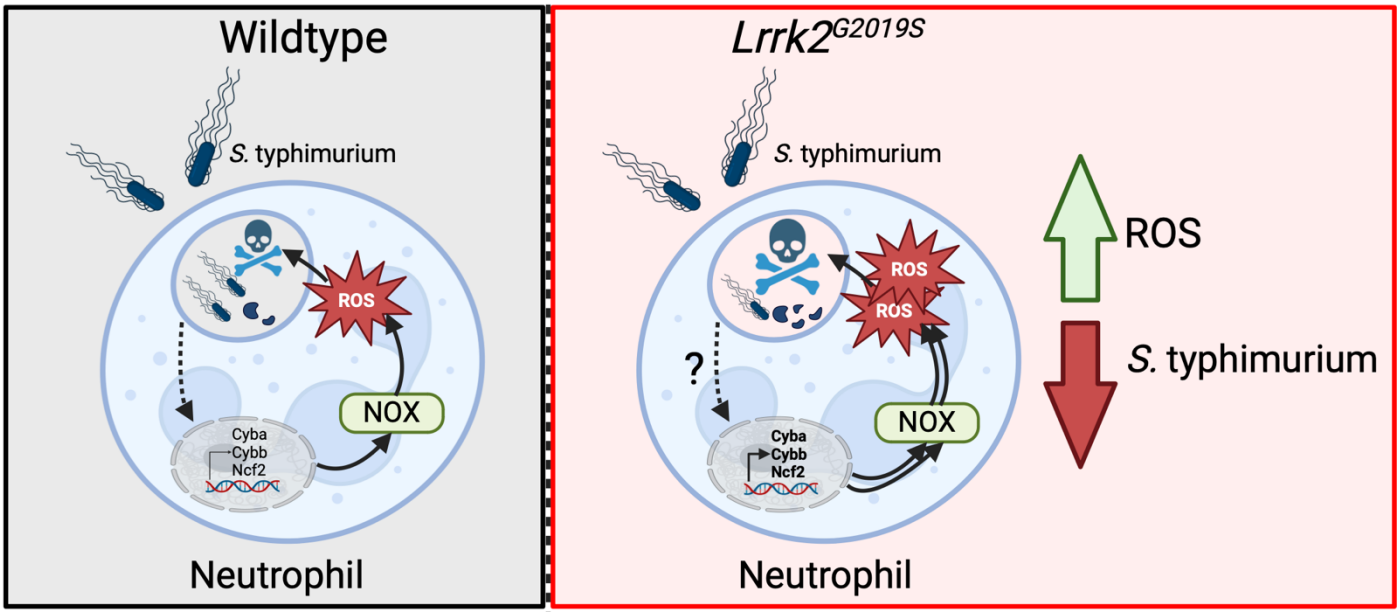
Wildtype
S. typhimurium
ROS
NOX
Cyba
Cybb
Ncf2
Neutrophil
Lrrk2G2019S
S. typhimurium
ROS
ROS
?
NOX
Cyba
Cybb
Ncf2
Neutrophil
ROS
S. typhimurium

Figure 20. Model of the impact of the *Lrrk2*^{G2019S} mutation during infection with ST in neutrophils. Of all myeloid cells tested *in vitro*, the *Lrrk2*^{G2019S} mutation only reduced the bacterial burden of ST in neutrophils. *Lrrk2*^{G2019S} neutrophils showed enhanced transcription of genes encoding components of the NADPH oxidase enzyme, leading to higher levels of ROS. The increased ROS levels are critical for the enhanced resistance to infection with ST observed in *Lrrk2*^{G2019S} neutrophils.

6. REFERENCES

1. Delves, P. J. & Roitt, I. M. The Immune System. *N Engl J Med* **343**, 37–49 (2000).
2. McComb, S., Thiriot, A., Akache, B., Krishnan, L. & Stark, F. Introduction to the Immune System. in *Immunoproteomics* (eds. Fulton, K. M. & Twine, S. M.) vol. 2024 1–24 (Springer New York, New York, NY, 2019).
3. Tomar, N. & De, R. K. A Brief Outline of the Immune System. in *Immunoinformatics* (eds. De, R. K. & Tomar, N.) vol. 1184 3–12 (Springer New York, New York, NY, 2014).
4. Hoggatt, J. & Pelus, L. M. Hematopoiesis. in *Brenner's Encyclopedia of Genetics* 418–421 (Elsevier, 2013). doi:10.1016/B978-0-12-374984-0.00686-0.
5. Rosenbauer, F. & Tenen, D. G. Transcription factors in myeloid development: balancing differentiation with transformation. *Nat Rev Immunol* **7**, 105–117 (2007).
6. Mitroulis, I., Kalafati, L., Hajishengallis, G. & Chavakis, T. Myelopoiesis in the Context of Innate Immunity. *J Innate Immun* **10**, 365–372 (2018).
7. Wu, L. & Liu, Y.-J. Development of Dendritic-Cell Lineages. *Immunity* **26**, 741–750 (2007).
8. Boes, K. M. & Durham, A. C. Bone Marrow, Blood Cells, and the Lymphoid/Lymphatic System. in *Pathologic Basis of Veterinary Disease* 724-804.e2 (Elsevier, 2017). doi:10.1016/B978-0-323-35775-3.00013-8.
9. *Molecular Biology of the Cell*. (Garland Science, New York, 2002).
10. Akashi, K., Traver, D., Miyamoto, T. & Weissman, I. L. A clonogenic common myeloid progenitor that gives rise to all myeloid lineages. *Nature* **404**, 193–197 (2000).
11. Marshall, J. S., Warrington, R., Watson, W. & Kim, H. L. An introduction to immunology and immunopathology. *Allergy Asthma Clin Immunol* **14**, 49 (2018).

12. *Autoimmunity: From Bench to Bedside*. (Center for Autoimmune Diseases Research, School of Medicine and Health Sciences, El Rosario University, Bogota, Colombia, 2013).
13. Megha, Kb., Joseph, X., Akhil, V. & Mohanan, Pv. Cascade of immune mechanism and consequences of inflammatory disorders. *Phytomedicine* **91**, 153712 (2021).
14. Mogensen, T. H. Pathogen Recognition and Inflammatory Signaling in Innate Immune Defenses. *Clin Microbiol Rev* **22**, 240–273 (2009).
15. Li, D. & Wu, M. Pattern recognition receptors in health and diseases. *Sig Transduct Target Ther* **6**, 291 (2021).
16. Zhang, J.-M. & An, J. Cytokines, Inflammation, and Pain. *International Anesthesiology Clinics* **45**, 27–37 (2007).
17. Hamilton, J. A. Colony-stimulating factors in inflammation and autoimmunity. *Nat Rev Immunol* **8**, 533–544 (2008).
18. Hughes, C. E. & Nibbs, R. J. B. A guide to chemokines and their receptors. *The FEBS Journal* **285**, 2944–2971 (2018).
19. *Immunobiology: The Immune System in Health and Disease ; [Animated CD-ROM Inside]*. (Garland Publ. [u.a.], New York, NY, 2001).
20. Rosales, C. & Uribe-Querol, E. Phagocytosis: A Fundamental Process in Immunity. *BioMed Research International* **2017**, 1–18 (2017).
21. Wang, J., Erlacher, M. & Fernandez-Orth, J. The role of inflammation in hematopoiesis and bone marrow failure: What can we learn from mouse models? *Front. Immunol.* **13**, 951937 (2022).
22. Paudel, S., Ghimire, L., Jin, L., Jeansonne, D. & Jeyaseelan, S. Regulation of emergency granulopoiesis during infection. *Front. Immunol.* **13**, 961601 (2022).

23. Mitchell, A. J., Roediger, B. & Weninger, W. Monocyte homeostasis and the plasticity of inflammatory monocytes. *Cellular Immunology* **291**, 22–31 (2014).

24. Shi, C. & Pamer, E. G. Monocyte recruitment during infection and inflammation. *Nat Rev Immunol* **11**, 762–774 (2011).

25. Serbina, N. V., Jia, T., Hohl, T. M. & Pamer, E. G. Monocyte-Mediated Defense Against Microbial Pathogens. *Annu. Rev. Immunol.* **26**, 421–452 (2008).

26. Jakubzick, C. *et al.* Minimal Differentiation of Classical Monocytes as They Survey Steady-State Tissues and Transport Antigen to Lymph Nodes. *Immunity* **39**, 599–610 (2013).

27. Westman, J., Grinstein, S. & Marques, P. E. Phagocytosis of Necrotic Debris at Sites of Injury and Inflammation. *Front. Immunol.* **10**, 3030 (2020).

28. Mawhinney, M., Kulle, A. & Thanabalasuriar, A. From infection to repair: Understanding the workings of our innate immune cells. *WIREs Mechanisms of Disease* **14**, e1567 (2022).

29. Davies, L. C., Jenkins, S. J., Allen, J. E. & Taylor, P. R. Tissue-resident macrophages. *Nat Immunol* **14**, 986–995 (2013).

30. Epelman, S., Lavine, K. J. & Randolph, G. J. Origin and Functions of Tissue Macrophages. *Immunity* **41**, 21–35 (2014).

31. Hashimoto, D. *et al.* Tissue-Resident Macrophages Self-Maintain Locally throughout Adult Life with Minimal Contribution from Circulating Monocytes. *Immunity* **38**, 792–804 (2013).

32. Chang, C.-F. *et al.* Divergent Functions of Tissue-Resident and Blood-Derived Macrophages in the Hemorrhagic Brain. *Stroke* **52**, 1798–1808 (2021).

33. Shapouri-Moghaddam, A. *et al.* Macrophage plasticity, polarization, and function in health and disease. *Journal Cellular Physiology* **233**, 6425–6440 (2018).

34. Hourani, T. *et al.* Label-free macrophage phenotype classification using machine learning methods. *Sci Rep* **13**, 5202 (2023).

35. Atri, C., Guerfali, F. & Laouini, D. Role of Human Macrophage Polarization in Inflammation during Infectious Diseases. *IJMS* **19**, 1801 (2018).

36. Yunna, C., Mengru, H., Lei, W. & Weidong, C. Macrophage M1/M2 polarization. *European Journal of Pharmacology* **877**, 173090 (2020).

37. Song, L., Dong, G., Guo, L. & Graves, D. T. The function of dendritic cells in modulating the host response. *Molecular Oral Microbiology* **33**, 13–21 (2018).

38. Théry, C. & Amigorena, S. The cell biology of antigen presentation in dendritic cells. *Current Opinion in Immunology* **13**, 45–51 (2001).

39. Clark, G. J. *et al.* The role of dendritic cells in the innate immune system. *Microbes and Infection* **2**, 257–272 (2000).

40. Tai, Y., Wang, Q., Korner, H., Zhang, L. & Wei, W. Molecular Mechanisms of T Cells Activation by Dendritic Cells in Autoimmune Diseases. *Front. Pharmacol.* **9**, 642 (2018).

41. Rosales, C. Neutrophil: A Cell with Many Roles in Inflammation or Several Cell Types? *Front. Physiol.* **9**, 113 (2018).

42. Burn, G. L., Foti, A., Marsman, G., Patel, D. F. & Zychlinsky, A. The Neutrophil. *Immunity* **54**, 1377–1391 (2021).

43. Gierlikowska, B., Stachura, A., Gierlikowski, W. & Demkow, U. Phagocytosis, Degranulation and Extracellular Traps Release by Neutrophils—The Current Knowledge, Pharmacological Modulation and Future Prospects. *Front. Pharmacol.* **12**, 666732 (2021).

44. DeLeo, F. R. & Allen, L.-A. H. Phagocytosis and neutrophil extracellular traps. *Fac Rev* **9**, (2020).

45. Eichelberger, K. R. & Goldman, W. E. Manipulating neutrophil degranulation as a bacterial virulence strategy. *PLoS Pathog* **16**, e1009054 (2020).

46. Stock, A. J., Kasus-Jacobi, A. & Pereira, H. A. The role of neutrophil granule proteins in neuroinflammation and Alzheimer's disease. *J Neuroinflammation* **15**, 240 (2018).

47. Lent-Schochet, D. & Jialal, I. Chronic Granulomatous Disease. in *StatPearls* (StatPearls Publishing, Treasure Island (FL), 2024).

48. Segal, A. W. HOW NEUTROPHILS KILL MICROBES. *Annu. Rev. Immunol.* **23**, 197–223 (2005).

49. McCann, S. & Roulston, C. NADPH Oxidase as a Therapeutic Target for Neuroprotection against Ischaemic Stroke: Future Perspectives. *Brain Sciences* **3**, 561–598 (2013).

50. Nguyen, G. T., Green, E. R. & Mecsas, J. Neutrophils to the ROScue: Mechanisms of NADPH Oxidase Activation and Bacterial Resistance. *Front. Cell. Infect. Microbiol.* **7**, 373 (2017).

51. Chen, T. *et al.* Receptor-Mediated NETosis on Neutrophils. *Front. Immunol.* **12**, 775267 (2021).

52. LaRock, D. L., Chaudhary, A. & Miller, S. I. Salmonellae interactions with host processes. *Nat Rev Microbiol* **13**, 191–205 (2015).

53. Broz, P., Ohlson, M. B. & Monack, D. M. Innate immune response to Salmonella typhimurium, a model enteric pathogen. *Gut Microbes* **3**, 62–70 (2012).

54. Santos, R. L. *et al.* Animal models of infections: enteritis versus typhoid fever. *Microbes and Infection* **3**, 1335–1344 (2001).

55. Fàbrega, A. & Vila, J. Salmonella enterica Serovar Typhimurium Skills To Succeed in the Host: Virulence and Regulation. *Clin Microbiol Rev* **26**, 308–341 (2013).

56. Foster, J. W. & Hall, H. K. Inducible pH homeostasis and the acid tolerance response of Salmonella typhimurium. *J Bacteriol* **173**, 5129–5135 (1991).

57. Coburn, B., Grassl, G. A. & Finlay, B. B. *Salmonella* , the host and disease: a brief review. *Immunol Cell Biol* **85**, 112–118 (2007).

58. Ohl, M. E. & Miller, S. I. Salmonella: A Model for Bacterial Pathogenesis. *Annu. Rev. Med.* **52**, 259–274 (2001).

59. Mastroeni, P., Grant, A., Restif, O. & Maskell, D. A dynamic view of the spread and intracellular distribution of Salmonella enterica. *Nat Rev Microbiol* **7**, 73–80 (2009).

60. Knuff, K. & Finlay, B. B. What the SIF Is Happening—The Role of Intracellular Salmonella-Induced Filaments. *Front. Cell. Infect. Microbiol.* **7**, 335 (2017).

61. Steele-Mortimer, O. The Salmonella-containing vacuole—Moving with the times. *Current Opinion in Microbiology* **11**, 38–45 (2008).

62. Naseer, N. *et al.* Human NAIP/NLRC4 and NLRP3 inflammasomes detect Salmonella type III secretion system activities to restrict intracellular bacterial replication. *PLoS Pathog* **18**, e1009718 (2022).

63. Usmani, A., Shavarebi, F. & Hiniker, A. The Cell Biology of LRRK2 in Parkinson's Disease. *Mol Cell Biol* **41**, e00660-20 (2021).

64. Tong, Y. *et al.* R1441C mutation in LRRK2 impairs dopaminergic neurotransmission in mice. *Proc. Natl. Acad. Sci. U.S.A.* **106**, 14622–14627 (2009).

65. Chang, E. E. S. *et al.* LRRK2 mutant knock-in mouse models: therapeutic relevance in Parkinson's disease. *Transl Neurodegener* **11**, 10 (2022).

66. Kang, U. & Marto, J. A. Leucine-rich repeat kinase 2 and Parkinson's disease. *Proteomics* **17**, 1600092 (2017).

67. Li, J.-Q., Tan, L. & Yu, J.-T. The role of the LRRK2 gene in Parkinsonism. *Mol Neurodegeneration* **9**, 47 (2014).

68. Ahmadi Rastegar, D. & Dzamko, N. Leucine Rich Repeat Kinase 2 and Innate Immunity. *Front. Neurosci.* **14**, 193 (2020).

69. Zhang, D., Lin, J. & Han, J. Receptor-interacting protein (RIP) kinase family. *Cell Mol Immunol* **7**, 243–249 (2010).

70. Zhang, P. *et al.* Crystal structure of the WD40 domain dimer of LRRK2. *Proc. Natl. Acad. Sci. U.S.A.* **116**, 1579–1584 (2019).

71. Wallings, R. L. & Tansey, M. G. LRRK2 regulation of immune-pathways and inflammatory disease. *Biochemical Society Transactions* **47**, 1581–1595 (2019).

72. Shutinoski, B. *et al. Lrrk2* alleles modulate inflammation during microbial infection of mice in a sex-dependent manner. *Sci. Transl. Med.* **11**, eaas9292 (2019).

73. Hakimi, M. *et al.* Parkinson's disease-linked LRRK2 is expressed in circulating and tissue immune cells and upregulated following recognition of microbial structures. *J Neural Transm* **118**, 795–808 (2011).

74. Gardet, A. *et al.* LRRK2 Is Involved in the IFN-γ Response and Host Response to Pathogens. *J.I.* **185**, 5577–5585 (2010).

75. Hui, K. Y. *et al.* Functional variants in the *LRRK2* gene confer shared effects on risk for Crohn's disease and Parkinson's disease. *Sci. Transl. Med.* **10**, eaai7795 (2018).

76. Fava, V. M. *et al.* A Missense LRRK2 Variant Is a Risk Factor for Excessive Inflammatory Responses in Leprosy. *PLoS Negl Trop Dis* **10**, e0004412 (2016).

77. the NIDDK IBD Genetics Consortium *et al.* Genome-wide association defines more than 30 distinct susceptibility loci for Crohn's disease. *Nat Genet* **40**, 955–962 (2008).

78. Tan, E.-K. *et al.* Parkinson disease and the immune system — associations, mechanisms and therapeutics. *Nat Rev Neurol* **16**, 303–318 (2020).

79. Singleton, A. B., Farrer, M. J. & Bonifati, V. The genetics of P arkinson's disease: Progress and therapeutic implications. *Movement Disorders* **28**, 14–23 (2013).

80. Luzon-Toro, B., de la Torre, E. R., Delgado, A., Perez-Tur, J. & Hilfiker, S. Mechanistic insight into the dominant mode of the Parkinson's disease-associated G2019S LRRK2 mutation. *Human Molecular Genetics* **16**, 2031–2039 (2007).

81. Ren, C. *et al.* G2019S Variation in LRRK2: An Ideal Model for the Study of Parkinson's Disease? *Front. Hum. Neurosci.* **13**, 306 (2019).

82. Xavier, R. J. & Podolsky, D. K. Unravelling the pathogenesis of inflammatory bowel disease. *Nature* **448**, 427–434 (2007).

83. Franke, A. *et al.* Genome-wide meta-analysis increases to 71 the number of confirmed Crohn's disease susceptibility loci. *Nat Genet* **42**, 1118–1125 (2010).

84. Zhang, F.-R. *et al.* Genomewide Association Study of Leprosy. *N Engl J Med* **361**, 2609–2618 (2009).

85. Fava, V. M. *et al.* Pleiotropic effects for Parkin and LRRK2 in leprosy type-1 reactions and Parkinson's disease. *Proc. Natl. Acad. Sci. U.S.A.* **116**, 15616–15624 (2019).

86. Liu, W. *et al.* LRRK2 promotes the activation of NLRC4 inflammasome during Salmonella Typhimurium infection. *Journal of Experimental Medicine* **214**, 3051–3066 (2017).

87. Zhang, Q. *et al.* Commensal bacteria direct selective cargo sorting to promote symbiosis. *Nat Immunol* **16**, 918–926 (2015).

88. Härtlova, A. *et al.* LRRK2 is a negative regulator of *Mycobacterium tuberculosis* phagosome maturation in macrophages. *The EMBO Journal* **37**, e98694 (2018).

89. Weindel, C. G. *et al.* Mitochondrial ROS promotes susceptibility to infection via gasdermin D-mediated necroptosis. *Cell* **185**, 3214-3231.e23 (2022).

90. Yang, Y., Jiang, G., Zhang, P. & Fan, J. Programmed cell death and its role in inflammation. *Military Med Res* **2**, 12 (2015).

91. Den Hartigh, A. B. & Fink, S. L. Pyroptosis Induction and Detection. *CP in Immunology* **122**, e52 (2018).

92. Lopez-Castejon, G. & Brough, D. Understanding the mechanism of IL-1β secretion. *Cytokine & Growth Factor Reviews* **22**, 189–195 (2011).

93. Nguyen, T., Nioi, P. & Pickett, C. B. The Nrf2-Antioxidant Response Element Signaling Pathway and Its Activation by Oxidative Stress. *Journal of Biological Chemistry* **284**, 13291–13295 (2009).

94. Frangie, C. & Daher, J. Role of myeloperoxidase in inflammation and atherosclerosis (Review). *Biomed Rep* **16**, 53 (2022).

95. Thulborn, S. J. *et al.* Neutrophil elastase as a biomarker for bacterial infection in COPD. *Respir Res* **20**, 170 (2019).

96. Wang, Q. *et al.* Lipocalin 2 Protects Against Escherichia coli Infection by Modulating Neutrophil and Macrophage Function. *Front Immunol* **10**, 2594 (2019).

97. Wallings, R., Manzoni, C. & Bandopadhyay, R. Cellular processes associated with LRRK 2 function and dysfunction. *The FEBS Journal* **282**, 2806–2826 (2015).

98. Healy, D. G. *et al.* Phenotype, genotype, and worldwide genetic penetrance of LRRK2-associated Parkinson's disease: a case-control study. *The Lancet Neurology* **7**, 583–590 (2008).

99. Park, J. *et al.* Parkinson disease–associated *LRRK2 G2019S* transgene disrupts marrow myelopoiesis and peripheral Th17 response. *J Leukoc Biol* **102**, 1093–1102 (2017).

100. Manz, M. G. & Boettcher, S. Emergency granulopoiesis. *Nat Rev Immunol* **14**, 302–314 (2014).

101. Moehle, M. S. *et al.* The G2019S LRRK2 mutation increases myeloid cell chemotactic responses and enhances LRRK2 binding to actin-regulatory proteins. *Hum. Mol. Genet.* **24**, 4250–4267 (2015).

102. Cabezudo, D., Tsafaras, G., Van Acker, E., Van Den Haute, C. & Baekelandt, V. Mutant LRRK2 exacerbates immune response and neurodegeneration in a chronic model of experimental colitis. *Acta Neuropathol* **146**, 245–261 (2023).

103. Geest, C. R. & Coffer, P. J. MAPK signaling pathways in the regulation of hematopoiesis. *Journal of Leukocyte Biology* **86**, 237–250 (2009).

104. Hsu, C.-L., Kikuchi, K. & Kondo, M. Activation of mitogen-activated protein kinase kinase (MEK)/extracellular signal–regulated kinase (ERK) signaling pathway is involved in myeloid lineage commitment. *Blood* **110**, 1420–1428 (2007).

105. Miranda, M., McGuire, T. & Johnson, D. Importance of MEK-1/-2 signaling in monocytic and granulocytic differentiation of myeloid cell lines. *Leukemia* **16**, 683–692 (2002).

106. Štefková, K. *et al.* MAPK p38alpha Kinase Influences Haematopoiesis in Embryonic Stem Cells. *Stem Cells International* **2019**, 1–16 (2019).

107. White, L. R., Toft, M., Kvam, S. N., Farrer, M. J. & Aasly, J. O. MAPK-pathway activity, Lrrk2 G2019S, and Parkinson's disease. *J. Neurosci. Res.* **85**, 1288–1294 (2007).

108. Mata, I. F., Wedemeyer, W. J., Farrer, M. J., Taylor, J. P. & Gallo, K. A. LRRK2 in Parkinson's disease: protein domains and functional insights. *Trends in Neurosciences* **29**, 286–293 (2006).

109. Gloeckner, C. J., Schumacher, A., Boldt, K. & Ueffing, M. The Parkinson disease-associated protein kinase LRRK2 exhibits MAPKKK activity and phosphorylates MKK3/6 and MKK4/7, *in vitro*. *Journal of Neurochemistry* **109**, 959–968 (2009).

110. Ahmadi Rastegar, D. *et al.* Effect of LRRK2 protein and activity on stimulated cytokines in human monocytes and macrophages. *npj Parkinsons Dis.* **8**, 34 (2022).

111. Oun, A. *et al.* LRRK2 protects immune cells against erastin-induced ferroptosis. *Neurobiology of Disease* **175**, 105917 (2022).

112. Kim, K. S. *et al.* Regulation of myeloid cell phagocytosis by LRRK2 via WAVE2 complex stabilization is altered in Parkinson's disease. *Proc. Natl. Acad. Sci. U.S.A.* **115**, (2018).

113. Tecchio, C., Micheletti, A. & Cassatella, M. A. Neutrophil-Derived Cytokines: Facts Beyond Expression. *Front. Immunol.* **5**, (2014).

114. Cassatella, M. A. Neutrophil-Derived Proteins: Selling Cytokines by the Pound. in *Advances in Immunology* vol. 73 369–509 (Elsevier, 1999).

115. Murphy, M. P. *et al.* Guidelines for measuring reactive oxygen species and oxidative damage in cells and in vivo. *Nat Metab* **4**, 651–662 (2022).

116. Heo, H. Y. *et al.* LRRK2 enhances oxidative stress-induced neurotoxicity via its kinase activity. *Experimental Cell Research* **316**, 649–656 (2010).

117. Angeles, D. C. *et al.* Mutations in *LRRK2* increase phosphorylation of peroxiredoxin 3 exacerbating oxidative stress-induced neuronal death. *Hum. Mutat.* **32**, 1390–1397 (2011).

118. Helton, L. G. *et al.* Allosteric Inhibition of Parkinson's-Linked LRRK2 by Constrained Peptides. *ACS Chem. Biol.* **16**, 2326–2338 (2021).

119. Oun, A. *et al.* Characterization of Lipopolysaccharide Effects on LRRK2 Signaling in RAW Macrophages. *IJMS* **24**, 1644 (2023).

120. Sarkar, A. & Singh, M. P. A Complex Interplay of DJ-1, LRRK2, and Nrf2 in the Regulation of Mitochondrial Function in Cypermethrin-Induced Parkinsonism. *Mol Neurobiol* **61**, 953–970 (2024).

121. Kawakami, F. *et al.* Nrf2 Expression Is Decreased in LRRK2 Transgenic Mouse Brain and LRRK2 Overexpressing SH-SY5Y Cells. *Biological & Pharmaceutical Bulletin* **46**, 123–127 (2023).

122. Winterbourn, C. C., Kettle, A. J. & Hampton, M. B. Reactive Oxygen Species and Neutrophil Function. *Annu. Rev. Biochem.* **85**, 765–792 (2016).

123. Rastogi, R., Geng, X., Li, F. & Ding, Y. NOX Activation by Subunit Interaction and Underlying Mechanisms in Disease. *Front. Cell. Neurosci.* **10**, (2017).

124. Bode, K., Hauri-Hohl, M., Jaquet, V. & Weyd, H. Unlocking the power of NOX2: A comprehensive review on its role in immune regulation. *Redox Biology* **64**, 102795 (2023).

125. Burton, N. A. *et al.* Disparate Impact of Oxidative Host Defenses Determines the Fate of Salmonella during Systemic Infection in Mice. *Cell Host & Microbe* **15**, 72–83 (2014).

126. Vazquez-Torres, A., Jones-Carson, J., Mastroeni, P., Ischiropoulos, H. & Fang, F. C. Antimicrobial Actions of the Nadph Phagocyte Oxidase and Inducible Nitric Oxide Synthase in Experimental Salmonellosis. I. Effects on Microbial Killing by Activated

Peritoneal Macrophages in Vitro. *The Journal of Experimental Medicine* **192**, 227–236 (2000).

127. Kim, B. *et al.* Impaired Inflammatory Responses in Murine Lrrk2-Knockdown Brain Microglia. *PLoS ONE* **7**, e34693 (2012).

128. Russo, I. *et al.* Leucine-rich repeat kinase 2 positively regulates inflammation and down-regulates NF-κB p50 signaling in cultured microglia cells. *J Neuroinflammation* **12**, 230 (2015).

129. Dzamko, N., Rowe, D. B. & Halliday, G. M. Increased peripheral inflammation in asymptomatic leucine-rich repeat kinase 2 mutation carriers. *Movement Disorders* **31**, 889–897 (2016).

130. Anrather, J., Racchumi, G. & Iadecola, C. NF-κB Regulates Phagocytic NADPH Oxidase by Inducing the Expression of gp91. *Journal of Biological Chemistry* **281**, 5657–5667 (2006).

131. Anderson, K. L., Smith, K. A., Pio, F., Torbett, B. E. & Maki, R. A. Neutrophils Deficient in PU.1 Do Not Terminally Differentiate or Become Functionally Competent. *Blood* **92**, 1576–1585 (1998).

132. Li, S.-L., Valente, A. J., Zhao, S.-J. & Clark, R. A. PU.1 Is Essential for p47 Promoter Activity in Myeloid Cells. *Journal of Biological Chemistry* **272**, 17802–17809 (1997).

133. Suzuki, S. *et al.* PU.1 as an essential activator for the expression of gp91 ^{phox} gene in human peripheral neutrophils, monocytes, and B lymphocytes. *Proc. Natl. Acad. Sci. U.S.A.* **95**, 6085–6090 (1998).

134. Gross, S. A., Zheng, J. H., Le, A. T., Kerzic, P. J. & Irons, R. D. PU.1 phosphorylation correlates with hydroquinone-induced alterations in myeloid differentiation and cytokine-

dependent clonogenic response in human CD34+ hematopoietic progenitor cells. *Cell Biol Toxicol* **22**, 229–241 (2006).

135. Lodie, T. A. *et al.* Stimulation of macrophages by lipopolysaccharide alters the phosphorylation state, conformation, and function of PU.1 via activation of casein kinase II. *J Immunol* **158**, 1848–1856 (1997).
136. Etzrodt, M. *et al.* Inflammatory signals directly instruct PU.1 in HSCs via TNF. *Blood* **133**, 816–819 (2019).
137. Bonadies, N. *et al.* PU.1 is regulated by NF-κB through a novel binding site in a 17 kb upstream enhancer element. *Oncogene* **29**, 1062–1072 (2010).
138. Keeney, M. T. *et al.* NADPH oxidase 2 activity in Parkinson's disease. *Neurobiology of Disease* **170**, 105754 (2022).

CURRICULUM VITAE

Kate Hurley

EDUCATION

2022 – 2024 **MSc,** Microbiology and Immunology
Supervisor: Dr. Subash Sad
University of Ottawa

2018 – 2022 **Bachelor of Medical Sciences,** Honors Specialization in Interdisciplinary Medical Sciences and Scholar's Electives Program, with distinction
Western University

HONOURS & AWARDS

2024	NSERC Canada Graduate Scholarship (CGS-M) ($17,500)
2023	Award of Excellence in Graduate Studies
2023	Society for Neuroscience Trainee Professional Development Award ($1,000)
2023	Queen Elizabeth II Graduate Scholarship in Science and Technology ($15,000)
2022	Faculty of Medicine Special Merit Scholarship ($6,000)
2021	Parkinson's Foundation Summer Student Fellowship ($4,000)
2021	Dean's Undergraduate Research Opportunity Scholarship ($6,000)
2018	Governor General's Bronze Academic Medal
2018 – 2022	Western University Continuing Admission Scholarship ($10,000)
2018 – 2022	Dean's Honours List
2020	Social Innovation Pitch Competition Winner
2020	Youth Impact Challenge Semi-Finalist

RESEARCH EXPERIENCE

2022 – present **Graduate Student,** University of Ottawa
- Supervisor: Dr. Subash Sad
- Research focus: Investigating the impact of Lrrk2^{G2019S} mutation on the innate immune system

2022 **Summer Research Student,** Canadian Nuclear Laboratories
- Supervisor: Dr. Yi Wang
- Research focus: Impact of radiation injury on the gastrointestinal system

2019 – 2021 **Undergraduate Research Assistant,** Robarts Research Institute
- Supervisor: Dr. Sean Cregan
- Research focus: Investigating the underlying cellular mechanisms contributing to cell death in Parkinson's disease

2019 **Summer Research Student,** Ottawa Hospital Research Institute
- Supervisor: Dr. John Bell
- Research focus: Improving the efficacy of oncolytic viral therapy

PUBLICATIONS

Hurley K, Cao M, Huang H, Wang Y. (2023). Targeted Alpha Therapy (TAT) with Single-Domain Antibodies (Nanobodies). *Cancers, 15*(13), 3493. https://doi.org/10.3390/cancers15133493

Hurley K, Clow R, Jadhav A, Azzam EI, Wang Y (2023). Mitigation of Acute Radiation Syndrome (ARS) with human umbilical cord blood. *Int J Radiat Biol,* 1-18. https://doi.org/10.1080/09553002.2023.2277372

CONFERENCE PRESENTATIONS

Hurley K, Rijal D, El Hamra R, Bhan A, Yadav S, Brandt W, Ariana A, Schlossmacher M, Sad S. Investigating the role of Leucine-rich repeat kinase 2 (LRRK2) on innate immunity. *Poster presentation at Canadian Society for Immunology 2024.*

Hurley K, Schlossmacher M, Sad S. Investigating the impact of Parkinson's disease-associated mutation, *Lrrk2*^{G2019S}, on innate immunity. *Poster presentation at Society for Neuroscience 2023.*

Demmings M, **Hurley K**, Cregan S. Activating transcription factor 4 inhibits mTOR signalling to trigger PUMA-dependent neuronal apoptosis in models of Parkinson's disease. *Poster presentation at Canadian Association for Neuroscience 2021.*

LEADERSHIP & VOLUNTEER EXPERIENCE

2021 – present **Volunteer Mentor,** Big Brothers Big Sisters
- Provide comfort and support to mentees through the adversities they face by engaging in one-on-one weekly meetings

2022 – present **Meal Assistant and Volunteer Visitor,** Perley Health
- Volunteer at a long-term care center, providing personalized dining support and fostering meaningful connections with residents through one-on-one visits

2022 - present **Tutor,** Go2Grad Tutors
- Develop lesson plans and provide individualized tutoring lessons in chemistry, biology, and math to high school and undergraduate students

2023 **Graduate Student Mentor,** DEGREE Shadowing Program
- Shared insights into graduate school to undergraduate students and provided an opportunity for the students to shadow my work in the laboratory environment

2022 - 2023 **Graduate Student Mentor,** IgNITE Medical Case Competition
- Support and guide teams of high school and undergraduate students through the development of a novel scientific project for a medical-related case competition

2019 – 2022 **Co-founder,** Discovery Days Western
- Co-founded initiative to provide free and accessible career-based workshops to underprivileged children and youth in the London community

2020 – 2022 **Executive Member,** Universities Allied for Essential Medicines
- Co-authored report highlighting Western University's current global health initiatives and a strategic plan for future developments, ultimately advocating for equitable licensing policies for accessible medicine

2020 – 2022 **Volunteer Tutor,** Smart Steps Western
- Provided weekly, complimentary tutoring services to underprivileged youth in the London community

2019 – 2022 **Mentor,** Scholar's Electives Mentorship Program
- Offered mentorship to incoming students of the Scholar's Electives program, while fostering a feeling of belonging to the university and connecting them with appropriate resources

2019 – 2020 **Workshop Facilitator,** Let's Talk Science Western
- Planned and facilitated fun, interactive science-based workshops for school-aged children

2019 – 2020 **Volunteer Caregiver,** Merrymount Family Support & Crisis Center
- Supported and worked with the Crisis Residential program to provide care to children who stay overnight at the center during times of family crisis

2019 – 2020 **Committee Member,** Juvenile Diabetes Camp (Rotaract)

- Assisted in planning a safe and enjoyable camp experience for children with Type I Diabetes

2018 – 2019 **Executive Member,** Elgin Hall Resident's Council

- Planned and organized activities to help build a stronger community amongst students in university residences